Michigan Technological University

Michigan Technological University

Digital Commons @ Michigan Tech

Dissertations, Master's Theses and Master's Reports

2017

Effect of spark advance and fuel on knocking tendency of spark ignited engine

Abhay S. Joshi
Michigan Technological University, abhayjos@mtu.edu

Follow this and additional works at: https://digitalcommons.mtu.edu/etdr

  Part of the Automotive Engineering Commons, and the Heat Transfer, Combustion Commons

EFFECT OF SPARK ADVANCE AND FUEL ON KNOCKING TENDENCY OF SPARK IGNITED ENGINE

By

Abhay S Joshi

A REPORT

Submitted in partial fulfillment of the requirements for the degree of

MASTER OF SCIENCE

In

Mechanical Engineering

MICHIGAN TECHNOLOGICAL UNIVERSITY

2017

This report has been approved in partial fulfillment of the requirements for the Degree of MASTER OF SCIENCE in Mechanical Engineering.

Department of Mechanical Engineering – Engineering Mechanics

Report Advisor: *Dr. Scott A. Miers*

Committee Member: *Mr. Jeremy J. Worm*

Committee Member: *Dr. David D. Wanless*

Department Chair: *Dr. William W. Predebon*

ACKNOWLEDGMENTS

I will like to thank Dr. Scott Miers for the encouragement, support and guidance during the entire duration of this study. I will like to thank my committee member Prof. Worm and Dr. Wanless for taking the time out of their schedule to review my report. I will also like to thank Behdad Afkhami for helping and guiding me whenever needed.

Also, an acknowledgment is given to the support of this study from the faculty and staff of the Department of Mechanical Engineering and Engineering Mechanics for their support.

Table of Contents

List of Figures

LIST OF TABLES

Abstract

Knock, in spark ignition engine is the combustion caused by the autoignition of the fuel-air mixture. It is the phenomenon that limits engine performance and thermal efficiency. Knock also has an adverse effect on emissions and fuel economy. Engine designers target engines with maximum power and torque output without compromising on fuel economy. Engine downsizing is the method generally adopted. The main goal of engine downsizing is to achieve better fuel economy while increasing the power and torque output of the engine. Better fuel economy is achieved by reducing the displaced volume which in turn means a much higher brake mean effective pressure. It is common for downsized engines to have BMEP values higher than 20 bar. As a comparison, this value reduces to about 15 bar without downsizing for the same power output. To compensate for the reduced volume, boosting devices like turbochargers or superchargers are incorporated. This increased pressure leads to a higher temperature of the compressed mixture. As a result, the self-ignition temperature is attained quicker than expected which promotes the occurrence of knock. When targeting high engine outputs at lower speeds, sustained knocking events can prove to cause catastrophic engine damage. The need to understand the phenomenon of knock as completely as possible is extremely important. Elimination of knock will prove to be vital for further engine development.

The major factors affecting knock are the octane rating of the fuel, spark timing, compression ratio of the engine, the percentage of exhaust gas re-circulation employed and lambda value. This report studies the effect of changing the fuel octane rating and spark timing on intensity of knock. The report briefly introduces knock, theories of its occurrence, detection methods and control techniques. Three fuels, E10 87, E0 91 and E15 91 were tested on a spark ignited, liquid cooled, two-cylinder carbureted engine. The fuels were selected as they represent a range of octane ratings usually available for daily use. In-cylinder pressure and crankcase vibrations are the two parameters used for knock detection. Each fuel was tested for a set of three spark timings set 10 CAD apart.

With an increase in spark advance, the knocking intensity increases when all other engine operating parameters are maintained constant. From the comparison of results for E0 91 and E15 91 fuels it can be concluded that the knock intensity decreases with an increase in ethanol content when all other engine operating conditions, including fuel octane rating and spark advance, were kept unchanged. Finally, the comparison of results from E0 91 and E10 87 fuels exhibit mixed effects of rise in ethanol levels and drop in octane rating on the knock intensity. While, for lower loads, the effect of increase in octane rating dominates resulting in lower knock intensity for E0 91, for higher loads the increase in ethanol content seems to have an upper hand resulting in lower knock intensity for E10 87 fuel.

1   Introduction

Identification and control of knock is an important parameter in the process of engine development. Important engine parameters like fuel consumption, exhaust emissions, noise, power density and durability are directly or in-directly affected by engine knock. With the rising fuel prices and emission norms getting stringent day-by-day, the goal for designing a modern engine is to provide the maximum possible thermal efficiency and power density with the cleanest possible emissions. The thermal efficiency can be increased largely by compressing the air-fuel mixture to a higher value. Intake boosting is a solution for increasing the power density. This trend in compression ratio is shown in Figure 1.1.
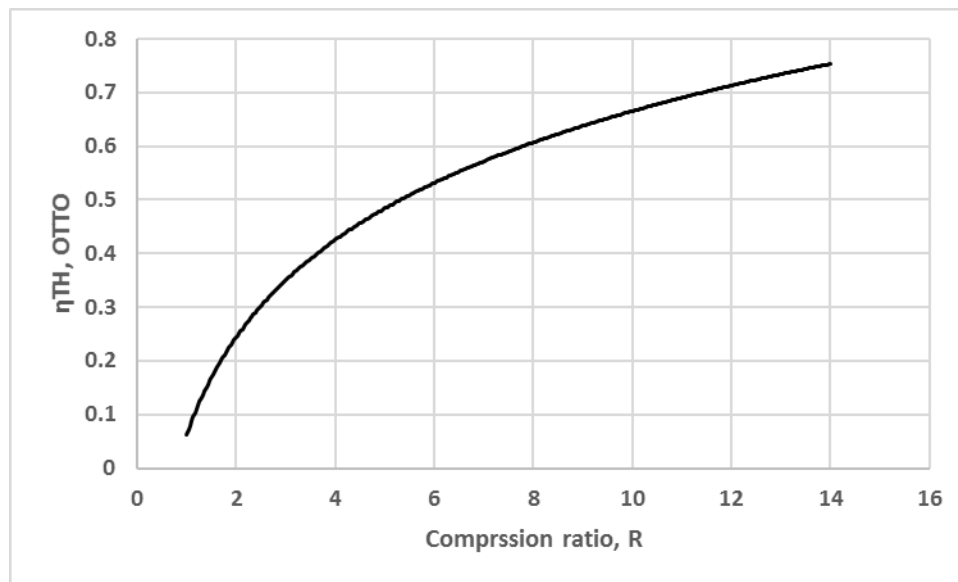
Figure 1.1: Variation of thermal efficiency with compression ratio [1]

Under both these conditions, the pressure in the combustion chamber will increase thereby creating conditions conducive for knock. In other words, the thermal efficiency and power density limits of a modern engine are largely limited by knock. Engine combustion research has been done both in academia and industry for decades. However, the relation between important parameters like knock index and fuel chemistry, pressure oscillations and heat transfer and auto ignition and flame front propagation are not completely explained. The work in the field of knock is mainly focused on understanding the relation between pre-ignition and knock, sources of pre-ignition and the influence of fuel properties on knock initiation. A thorough understanding of knock and an accurate method of knock prediction helps the engine designers develop engines that have better fuel economy, lower emissions and higher thermal efficiency.

Spark ignition engine combustion is a process that can be categorized into two types namely the normal combustion (non-knocking) and the abnormal (knocking) combustion. Under normal operating conditions, the combustion proceeds solely due to the developing flame front. It starts

with the initiation of the spark at the spark plug and proceeds to the opposite wall of the combustion chamber through the air-fuel mixture. In case of abnormal combustion, the unburnt gas in the combustion chamber ignites before the propagating flame reaches the unburned zone. This happens when the temperature and pressure of the unburnt mixture reaches the self-ignition value. As a result, shock waves are generated which reflect within the combustion chamber causing a ringing sound. This is known as knock.

Ability to control or reduce knock will also reduce the physical damage to the engine like melting of piston, gasket leaks, cylinder bore scuffing, spark plug fragmentation, exhaust valve melt and piston ring cracks. As a result, the longevity of the engine will improve significantly. Many advances have been made towards controlling and reducing knock. Complete elimination of knock is not practically possible but the goal of all researches in the field is to identify knock and reduce it to a minimum.

Some of the major factors affecting knock are compression ratio, intake air temperature, spark plug location, piston and head design, fuel octane number and spark timing. Out of these, the effect of fuel octane number and spark timing on knocking tendency in a spark ignition engine was studied in this report.

2   Literature Review

2.1   Background

There has been extensive research; both by theoretical and analytical means and on metal engines, with the ultimate goal of reducing engine knock to a bare minimum. In general, two theories were studied to explain the occurrence of knock.

1. Autoignition
2. Detonation

The ignition of the air and fuel mixture in region of the combustion chamber that is on the opposite end of the spark plug before the spark ignited flame reaches the zone is referred to as autoignition. The ignited volume is referred to as end gas. When the pressure and temperature of this part of the combustion chamber reaches a value higher than the autoignition point of the end gas, at its present condition, the volume ignites spontaneously. This ignition may start at a single location or at multiple locations within the end gas volume. Autoignition leads to high pressure waves that oscillate within the combustion chamber at sonic velocities. As they bounce from one wall of the combustion chamber to another, a pinging sound is generated. This pinging sound is known as knock.

According to Internal combustion engine fundamentals by Heywood [1], the theory of detonation credits the occurrence of knock to the high-speed propagation of the flame front. The flame propagates from the spark plug to the opposite end of the combustion chamber. Under knocking conditions, the flame front travels at sonic velocities and engulfs the end gas at a much faster rate as compared to normal operation. This results in rapid release of energy causing a shock wave. The wave will oscillate within the combustion chamber which may result in the chamber vibrating at its natural frequency. The impact of the shock wave is for a short duration but is of a high magnitude.

Of the two theories, the auto-ignition theory isa more widely accepted theory for knock initiation.

2.2   Advanced techniques for knock detection

With advances made in the field of high speed photography, it is now possible to capture the progress of a flame inside the cylinder. This makes it easier to visualize the events occurring in the cylinder as the flame proceeds. Many researchers have conducted tests using such high-speed photography. The major techniques used are:

- ICCD camera [4]

- Laser induced fluorescence (LIF) measurement [4]
- High speed video camera [4]
- UV visible natural emission spectroscopy [4]
- Chemiluminescence of radical species measurement [4]

Figure 2.1 shows a comparison between a normal and a knocking engine cycle for an optical engine as a part of the study done by Zhi Wang, Hui Liu and Rolf D Reitz [4]. It also shows the corresponding cylinder pressures and crank angles. Images a-g represents a normal combustion cycle whereas images A – G shows a knocking cycle. The brighter portion of the figures represents the propagating flame front while the unburnt gas mixture is shown by the darker area. The bright spots in the unburnt section are the hotspots. These are localized high temperature regions in the unburnt gas mixture and are prone to auto ignition. The highlighted zone on the pressure trace represents the crank angle and in-cylinder pressure values when the images were captured.
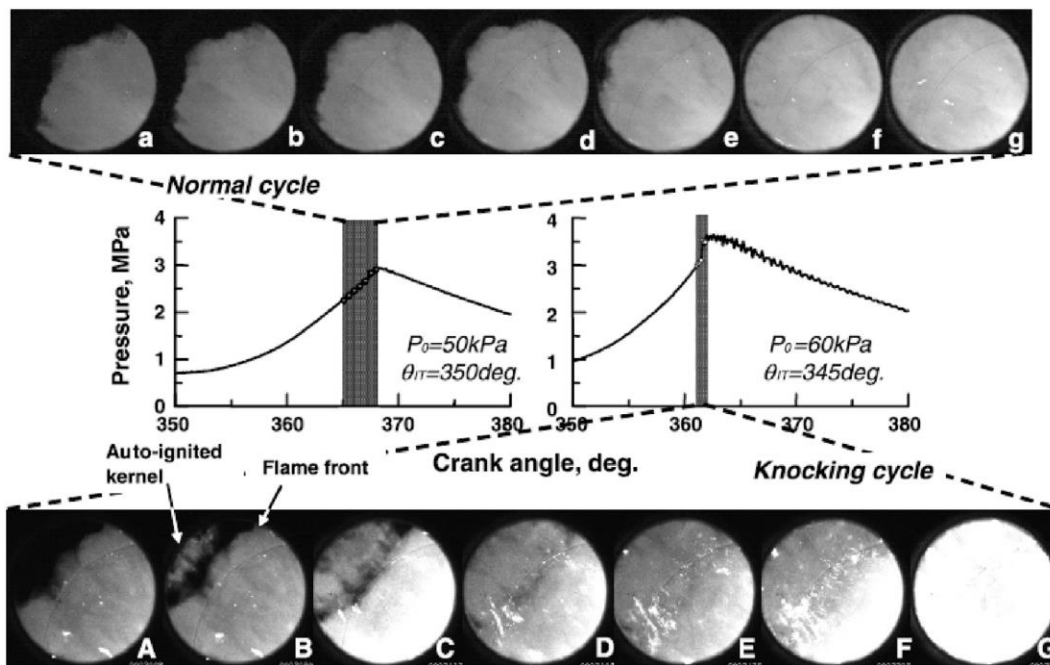
Figure 2.1: Series of high speed direct images and related cylinder pressure for normal and knocking engine cycle [4]

For the normal combustion cycle, the flame is shown propagating in the expected manner. No formation of hot spots is observed at any stage during the process. The unburnt gasses ignite only on coming in contact with the propagating flame front. This is also evident from the corresponding pressure trace. The cylinder pressure rises steadily with the crank rotation. A max cylinder pressure value is achieved and pressure starts reducing gradually. No fluctuations or abnormal rise or drop is shown in the pressure values.

In contrast, the knocking cycle is shown to follow a different trend. The first images of both the cycles are similar. No hotspots are identified and the flame is propagating across the cylinder in the expected manner. The second image (B) shows the formation of a brighter zone within the unburnt gas region. These are the auto ignited regions leading to knocking combustion. The auto ignited region gets hotter and expands as the cycle progresses and finally engulfs the entire region. This is also evident from the pressure trace. The trace undergoes a steep rise in pressure during the period corresponding to the time interval between images A and B. This is followed by fluctuations in pressure values mainly resulting from the formation and expansion of hotspots.

Figure 2.2 shows the combustion parameters for a typical engine knock cycle as presented by Zhi Wang, Hui Liu and Rolf D Reitz [4]. The figure 2.2 shows the trends followed by in-cylinder pressure that is measured using a piezo-electric pressure transducer, pressure oscillations captured by a knock sensor, unburnt gas temperature and heat release rate calculated according to first law of thermodynamics versus crank angle. In this case, the 0 CAD does not stand for the top dead center. For this particular configuration, the TDC lies at about 25 CAD. For calculation of temperature of unburnt gasses, the process of compression of end gasses is assumed to be adiabatic. A 60° window of crank angle is considered. Besides the legends on the figure, the following the abbreviations are used.

- $CA_{ko:}$ Crank angle at knock onset
- $P_{ko:}$ In-cylinder pressure at knock onset
- P_{max}: Maximum cylinder pressure
- ΔP: Difference between knock onset pressure and maximum pressure values

The entire knocking combustion process represented in the Figure 2.2 can be divided into two parts: flame propagation phase and the auto ignition phase. The flame propagation phase initiates at the spark plug and continues till the knock onset angle. During this phase the pressure trace follows the expected trend gradually increasing as the cycle progresses. The temperature of the unburnt gasses also rises steadily. This is due to the compression and combustion occurring in the cylinder. The heat release rate (HRR) gradually increases. There is a minor drop in the HRR just prior to the CA_{ko}. This can be attributed to the downward motion of the piston and heat transfer across the cylinder walls. The pressure oscillations, measured by the knock sensor, are of a low magnitude since there are minor pressure fluctuations during this stage. The auto ignition phase begins at the CAko and continues thereafter. The combustion parameters during this phase show a completely different trend. The pressure rises suddenly to reach the peak value and continues to oscillate with diminishing amplitude. The heat release rate shows a sudden drop in trend. Also, the pressure oscillations, captured by the knock sensor are of a higher magnitude. This represents higher fluctuations in pressure at this stage.
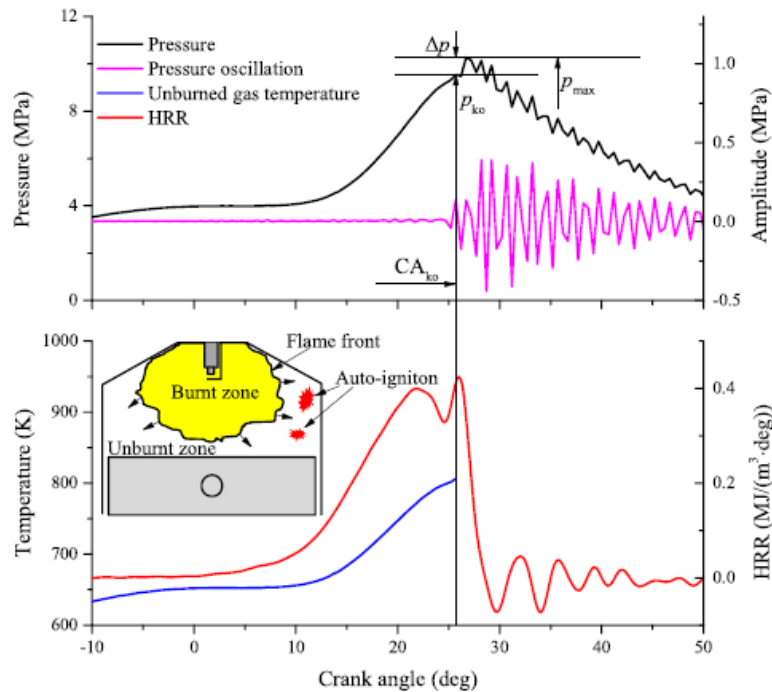
Figure 2.2: Combustion parameters of engine knock cycle [4]

2.3   Effects of knock

The major effect of knock is the physical damage caused to the engine. Knocking combustion, in SI engines, leads to high frequency pressure oscillations in the combustion chamber. These oscillations can damage different components of the engine. The Figure 2.3 shows damage to some of the engine components because of knock.

Figure A & H shows the damage done to the piston. The side of the piston along with the rings can be shown to have melted. Figure B shows damage done to the cylinder wall. Figures C & D represent similar physical damage done to the spark plug. Figure E shows a damaged cylinder gasket. Figures F & G show physical damages done to the cylinder head and the exhaust valve.

As shown from the figures, no component in the engine combustion chamber is unaffected by knock. This makes the understanding and control of knock even more important.
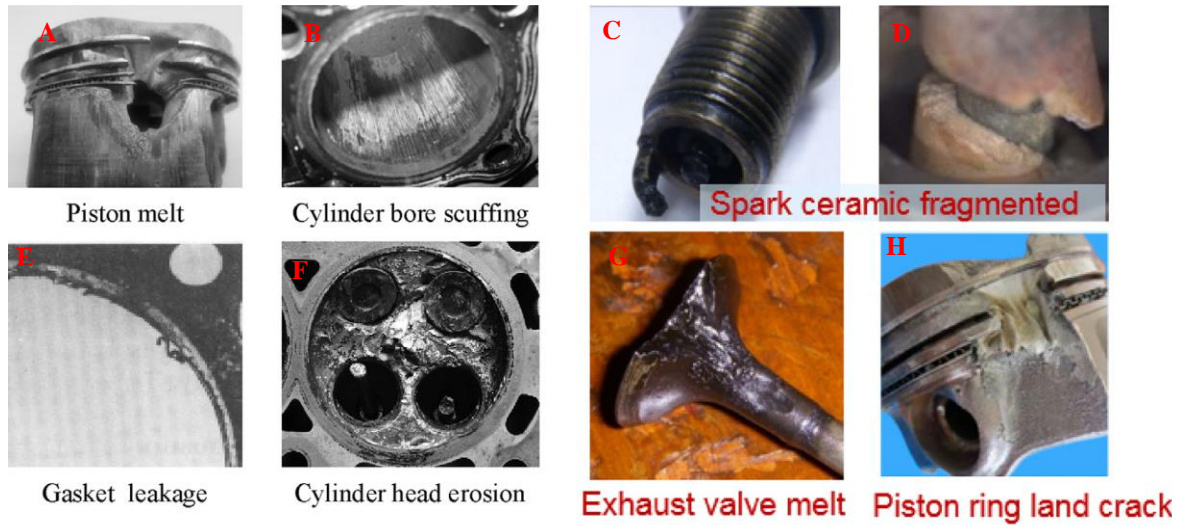
Figure 2.3: Typical damage caused by engine knock [4]

2.4 Detection of knock

In order to reduce the knocking tendency of the engine, it is necessary to study the methods of knock detection. There are two major techniques used for knock detection in engines.

2.4.1 In-cylinder pressure

The in-cylinder pressure method for knock detection involves direct study of combustion as it occurs in the combustion chamber. Piezo-electric pressure transducers are used for cylinder pressure measurement. The quartz crystals used in these transducers have a high frequency response and small size. They are light in weight and do not consume any power. The major disadvantage associated with their use is the variability introduced in the data as a result of thermal shock. Under stable operating conditions, the accuracy of piezo electric transducer can be very high with errors of less than 1% [2]. But this performance is affected due to exposure to continuous variations in temperature resulting from combustion. This variation in temperature causes the young's modulus and resonant frequency of the quartz crystal and distortion of the diaphragm. This phenomenon is known as thermal shock. A 50 kPa variation in pressure has been measured as a result of thermal shock [2]. Figure 2.4 shows the variation in pressure caused as a result of thermal shock and its correlation with transducer surface temperature. This is a part of research conducted by Seokhwan Lee and Choongsik Bae at Korea Advanced Institute of Science and Technology on a 2400 cc, four-cylinder gasoline engine. As shown from Figure 2.4, the absolute difference in measured pressure is observed to vary directly with the change in temperature. At about 45 CAD, a temperature change of 12°C leads to a change of 0.8 bar in the pressure readings.
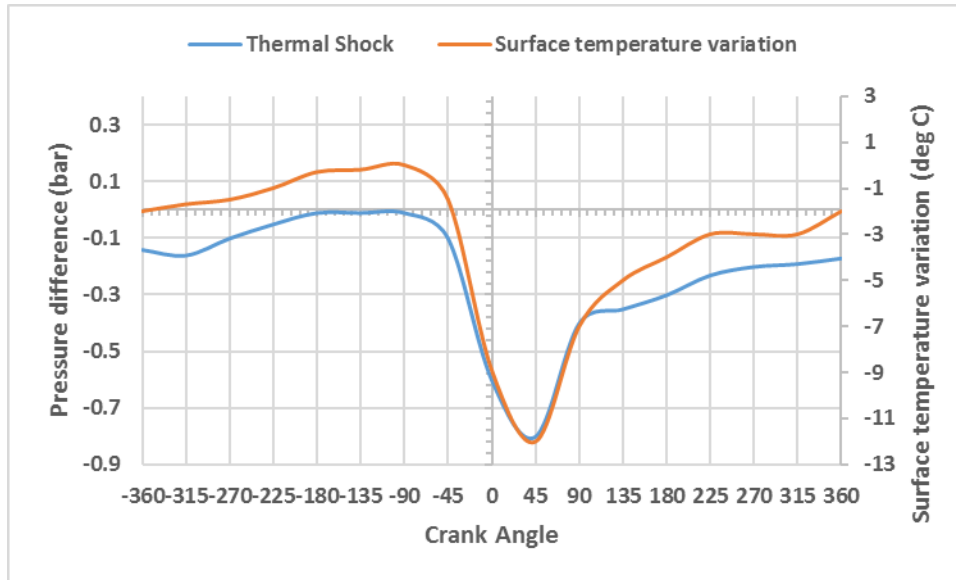
Figure 2.4: Correlation between variation in temperature and thermal shock [2]

This makes the location of the transducer in the combustion chamber important. There are multiple factors on which the choice of an in-cylinder pressure transducer mounting location depends. During the combustion stroke, when the piston is near TDC, all of the mass of the working fluid is inside the piston bowl and the clearance volume. So, the location of the transducer should be such that it has access to this mass when the piston is at TDC. The deposition of fuel on the sensing element of the transducer can cause measurement errors and lead to inaccurate data. To avoid this, the transducer should be located such that the fuel jet does not impinge on its surface as well as the diaphragm [3]. Andre V. Buneo and his team conducted a study in this field. An AVL GM 12 D pressure transducer was mounted in the port for spark plug as shown in Figure 2.5. A mean pressure value for 56 cycles was calculated and a scatter of the points was plotted to judge the repeatability of the tests. Figure 2.6 shows this scatter for the said location of the pressure transducer.
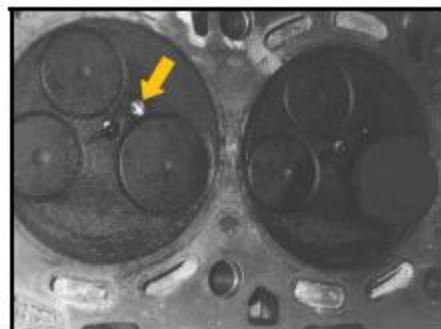
Figure 2.5: Pressure transducer mounting location [3]

Two points, C1 (beginning of exhaust stroke) and B2 (during the compression stroke) are randomly selected along the cycle. The point C1 signifies a location where transducer is under combustion thermal loads while point B2 signifies a point where transducer is cooled after gas exchange. The scatter of the points with respect to the diagonal of the plot shows a good repeatability of the recorded data. Higher scatter along the X-axis in Figure 2.6 signifies a higher short-term drift. An equal scatter of points along x and y axes indicates a negligible short-term drift. A small drift in data is expected due to the varying nature of combustion cycles. It can be concluded that the said location of pressure transducer in the cylinder is suitable for accurate pressure data. A similar location is implemented for this study.
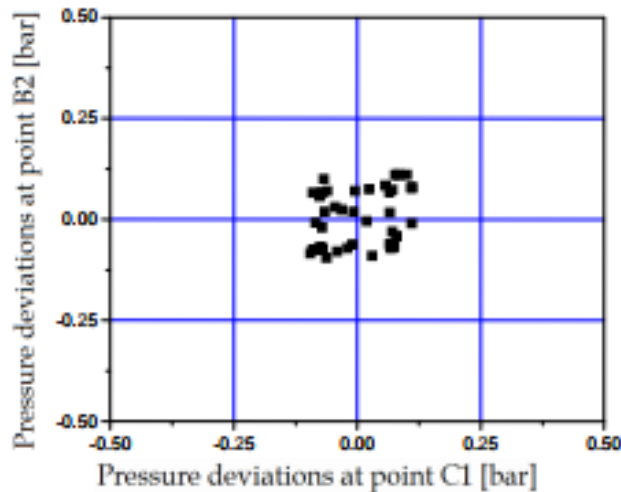
Figure 2.6: Deviation of pressure reading with respect to mean value [3]

According to a study conducted by Andrew L Randolph from the General Motors Research Laboratory [6], out of the three configurations tested, namely flush mount, remote mount with a single slot and remote mount with multiple slots, the last configuration gave the most accurate results. Figure 2.7 represents the three configurations and the cross sections of the adaptors used respectively. In case of flush mount, there was no external adapter used. A single slot adapter was found to provide significant thermal shock protection. However, designing of this adapter is critical. Care must be taken to make sure that pressure distortions resulting from excess pressure drops or acoustic resonances are avoided. If resonance occurs, variability of the signal approaches that obtained in case of flush mounting without an adapter thereby rendering the use of the adapter ineffective. The use of multi slot adapter was found to reduce thermal shock. As a result, the cyclic variability in IMEP, bulk burn duration and final mass burned calculations also reduced by about 50 % as compared to results from flush mounting. The reduction in thermal shock and reduction in variability of the results made the multi slot design most accurate.
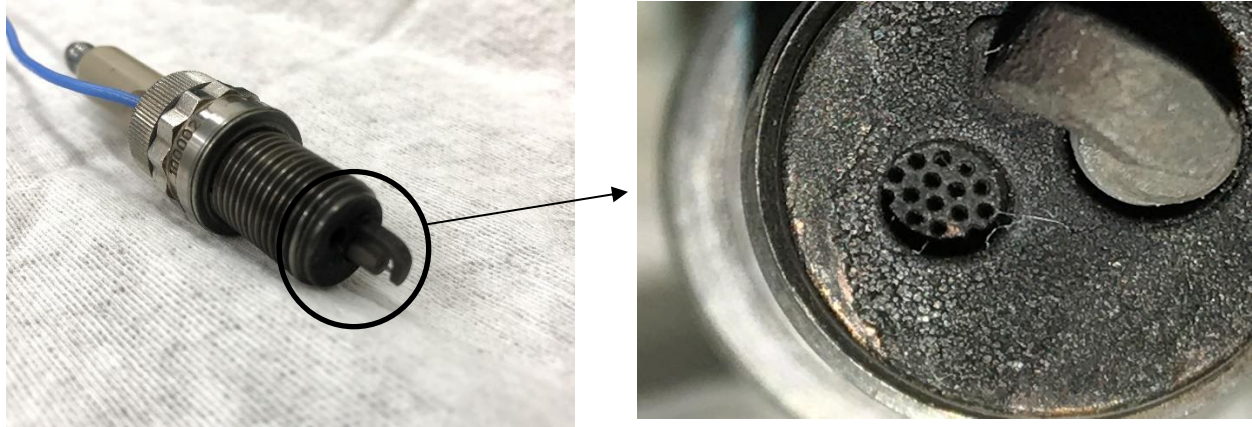
Figure 2.7: Multi hole flame arrestor

This pressure data is correlated to crank angle typically using an encoder mounted on the crank shaft. The result is a pressure against crank angle curve. A window typically of 40 CAD is set after top dead center for compression stroke. The pressure data is collected over this window and a parameter called knock intensity is calculated. Knock intensity is defined as the rate of change of pressure within a knock window for a particular cycle. The pressure data so collected is measured with crank angle degrees as a reference. If the speed of the engine is known for that cycle, the crank angle degrees can be converted to time domain using Equation 2.1.

$$t = \frac{CAD}{RPM*6}$$ Equation 2.1

   where t: time (sec)

      CAD: length of knock window (deg) (in this case 40)

      RPM: engine speed (RPM)

Once the time required by the crank shaft to cover the knock window is known, the knock intensity can be calculated using Equation 2.2. $KI = \sum_{T=0}^{t} (P_{i+1} - P_{i})$ [11]   Equation 2.2

$$KI = \sum_{T=0}^{t} (P_{i+1} - P_{i})\ [11]$$ Equation 2.2

   where: KI = knock intensity

      t = time (sec)

      T = time required for crankshaft to cover the knock window calculated in equation 2.1 (sec)

P = cylinder pressure (bar)

i = crank angle degrees

Using this equation, the knock intensity for a cycle is calculated. A threshold value for knock intensity is established based on the engine design and operating conditions. If the calculated KI value for a cycle exceeds this threshold, the cycle is considered as a knocking cycle.

According to the research conducted by Arsham J Shahlari and Jaal B Gandhi [8], among all the metrics available of knock intensity evaluation, it is most reliably indicated by time or frequency domain integration of pressure oscillation energy. This method for knock onset detection is known as threshold value exceeded (TVE) method, in which a cycle is a knocking cycle if the band pass filtered pressure signal exceeds a predetermined threshold value. The filter is a Butterworth filter of order 3 or 4. The lower cutoff frequency is generally set at 4 kHz. Since the cutoff frequency must be normalized by the Nyquist frequency, there is a limit of upper cutoff frequency. This must be lower than half the frequency at which data was logged. The disadvantage of this method is that it is late in knock detection by a few crank angle degrees since the threshold must be set high enough to avoid false detection of knock. This is corrected by subtracting a fixed number of degrees from the crank angle at which knock onset was detected using this technique. In this method, the threshold value is commonly set at 100 kPa, beyond which the cycles are considered knocking cycles [8]. Although the 100 kPa limit was used by Shahlari and Gandhi in their study [8], they did provide a justification for the magnitude of the knock limit (100 kPa).

The major disadvantage of this method is the cost of the components involved. Also since the pressure transducers are mounted inside the combustions chamber, they are in direct contact with the high pressure, high temperature products. This influences the life span of the sensor.

2.4.2 Cylinder block vibrations

This method involves detection of knock based on vibrations of the engine. It requires a measuring device, typically an accelerometer, to be mounted on the engine. The accelerometer picks up normal vibrations during valve opening and closing and combustion. When knocking occurs, pressure waves are generated with high peak to peak variations. These waves reflect from one wall to another within the combustion chamber. This movement of the pressure waves can generate sound within the audible range. This also causes the engine block to vibrate. These vibrations are recorded and processed using the accelerometer for knock detection.

The major advantage of this method is the low cost and durability of the components involved because the measurement is performed outside the combustion chamber.

2.5 Control Strategies

The occurrence of knock is attributed to the auto-ignition of end gases before the propagating flame front reaches this zone. The following are some of the methods used for controlling the occurrence of knock in a spark-ignition engine.

2.5.1 Delayed spark timing

This is the most common method employed to avoid knocking of the engine. Retarding the spark timing will cool the end gas and reduce its pressure thereby increase the time required for auto ignition. This method is employed in modern vehicles to avoid knock. A knock sensor is mounted on the combustion chamber to detect the pressure oscillations. This signal is fed to the ECU and based on the intensity of the vibrations, the ECU is programmed to detect knock in the engine. In this case, the spark timing is retarded by the ECU when knock is detected. This process continues back and forth until the vibrations are reduced to an acceptable level. However, this method has some disadvantages. Retardation of spark means the engine will not be working at an optimized condition. This may result in lower torque and power output. Also, the engine will operate at a lower thermal efficiency due to un-optimized combustion phase. The engine performance also deteriorates due to reduction in mean temperature and pressure of the combustion chamber.

2.5.2 Exhaust gas re-circulation (EGR)

EGR is another technique used to reduce knock in modern engines. The exhaust gas is cooled before it is introduced into the cylinder. This cooled exhaust gas does not undergo combustion. The cooled exhaust gas soaks up the heat from the compressed mixture which reduces the combustion temperature and more fuel is consumed. Investigation conducted by Zhi Wang and his team [4] shows that introduction of EGR results in a rich combustion mixture which enhances the flame propagation speed. As a result of reduction in combustion temperature and increase in flame propagation speed, introduction cooled EGR has proved effective in reducing the knocking tendency of the engine. Studies have shown that every percent addition in EGR has results equivalent to 0.5 octane number increase [4]. Also, the introduction of EGR has the potential to boost the performance of the engine.

The literature gave an overview about the phenomenon of knock, its effects, detection methods and control strategies. An accelerometer was mounted on the cylinder head to record vibrations. Considering the ideal position of transducer mounting, for this study, a transducer integrated into the spark plug is used. It is mounted in the chamber such that it is exposed to the high-pressure condition but there will not be any fuel impingement. A band pass filter, similar to the one discussed in the literature review, is used to analyze data and identify knock. Since this study involved the detection of knock, no control strategies were implemented.

Effect of spark advance and fuel properties on knock will be studied further in this report. For the fuel properties, the change in octane number and change in ethanol content was studied

separately. Three spark advances were tested for three different fuels with varying octane numbers and ethanol contents.

3 Experimental Setup

The block diagram in Figure 3.1 shows the location and signal path for major components of this study. Not all instruments used are shown below but are described in this section.
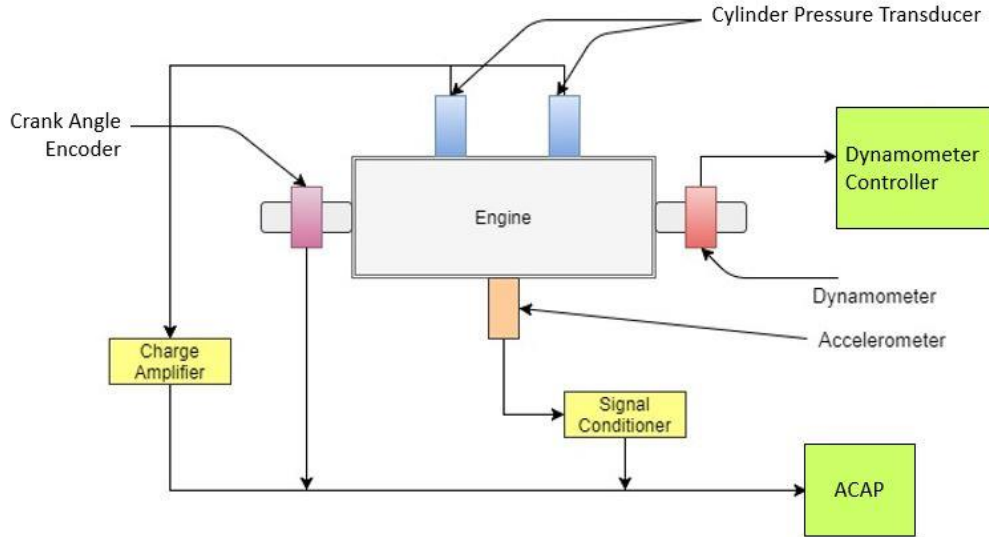
Figure 3.1: Block diagram for test setup

The engine used for this study was a spark ignited, twin-cylinder, liquid cooled, Kohler LH690.

Table 3.1: Kohler LH 690 engine specifications

Manufacturer	Kohler
Engine Model	LH 690
Displacement	674 cc
Max. Power @ RPM	17.9 kW @ 3600 rpm
Max. Torque @ RPM	58.2 Nm @ 2400 rpm
Bore	80 mm
Stroke	67 mm
Fuel Delivery	Carburetor
Cooling System	Liquid cooled
Lambda Control	Open loop

To load the engine, a Land-and-Sea DYNOmite 9" toroid water brake dynamometer was installed directly onto the crankshaft of the engine. The engine speed was controlled electronically through the Land-and-Sea software. On the dynamometer, a servo valve controlled the amount of water going into the water brake based on the engine speed set by the user. The torque on the engine was measured using a strain gauge mounted on the torque arm of the dynamometer. Data was collected at 1500 rpm, 1800 rpm and 2100 rpm with two torque points of 15 Nm and 25 Nm at every speed. The loads are equivalent to 4 bar and 6.4 bar IMEP respectively. Refer Table 7.1 for detailed test matrix.

Figure 3.2: Engine setup showing 9" water brake dynamometer

Being a carbureted engine and without an ECU, it is not possible to change the spark timing without modifications. Figure 3.3 shows the position of the ignition coil in relation to the flywheel. The spark is initiated when the magnet on the fly wheel passes by the two solid state ignition coils. The spark timing was modified by physically moving the ignition coil thereby changing the time when magnet passed by it. An aluminum plate was fabricated to hold the ignition coil for one cylinder as shown in Figure 3.4. The plate had a slot along which the two mounting bolt for the coil were guided. Measurements in steps of five degrees were made on the plate to facilitate the accurate positioning of the coil. Using this setup, the coil can be set within a degree of tolerance. While the coil for cylinder 2 had this arrangement, the coil of cylinder 1 was

kept at stock spark timing of 40° bTDC. This allowed evaluation of the effect of change in spark timing on the performance of cylinder 2.
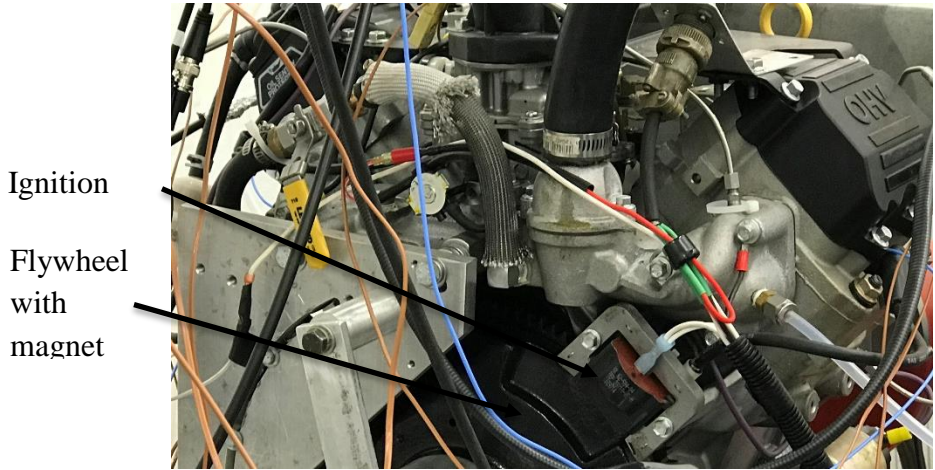
Figure 3.3: Ignition coil and flywheel position
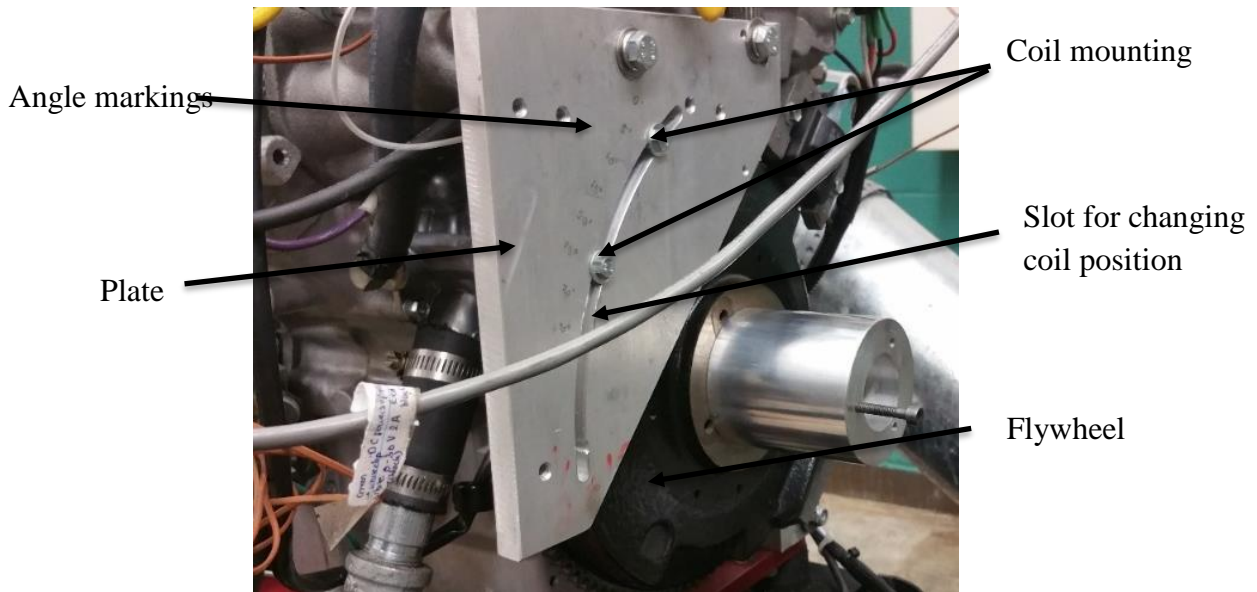
Figure 3.4: Setup for changing spark advance for cylinder 2

An ACAP system was used for high speed combustion data acquisition. The following table gives the details of the system and the modules used for this study.

Table 3.2: Modules used in ACAP

Module Number	Description
6001	CAMAC CC
1104CM	4 channel charge amplifier
EMPTY	
1642	Knock module
2904 A	Spincoder timer/counter
2860	4 CH / 1 MS/s digitizer
2860	4 CH / 1 MS/s digitizer
4012 A	TRAQ 1 system controller
5008	8192 K memory module
4325	TRAQ RTP

Parameters logged using this system were in-cylinder pressures from both cylinders and accelerometer readings. The ACAP system was also used to calculate knock intensity and peak to peak pressure variation during a knock event.

Being used in an event triggered mode, ACAP requires an encoder to know the position of the crank at every data point. A rotary encoder manufactured by Encoder Products was used for this study. It outputs 720 pulses per revolution meaning a pulse is generated every 0.5° of crank rotation. This generated the triggers for ACAP to record data. The encoder was connected to ACAP using BNC connections. There are three pulses generated A, B and Z from the encoder. A and B pulses are generated every 0.5° and signify the direction of rotation of the engine. For this study, only the A pulse was used since the engine rotates in one direction. The Z pulse was generated once every 360 degrees and signified the end of a rotation cycle. The encoder was mounted on a specially designed aluminum attachment fixed on the flywheel. The shaft of this attachment rotates at the same speed as the crankshaft. The design of this attachment can be found in the appendix for reference.

Table 3.3: Encoder specifications

Manufacturer	Encoder products
Model	260 with flex arm
Input voltage	4.75 – 28 VDC
Output (A/B)	2/CAD
Index (Z)	1/rev
Max shaft speed	7500 rpm

The in-cylinder pressure was measured using piezo-electric pressure transducers mounted in special spark plugs. Each cylinder was fitted with a spark plug pressure transducer setup. The Figure 3.5 shows the structure of the piezo electric pressure transducer integrated with the spark plug used for this study.
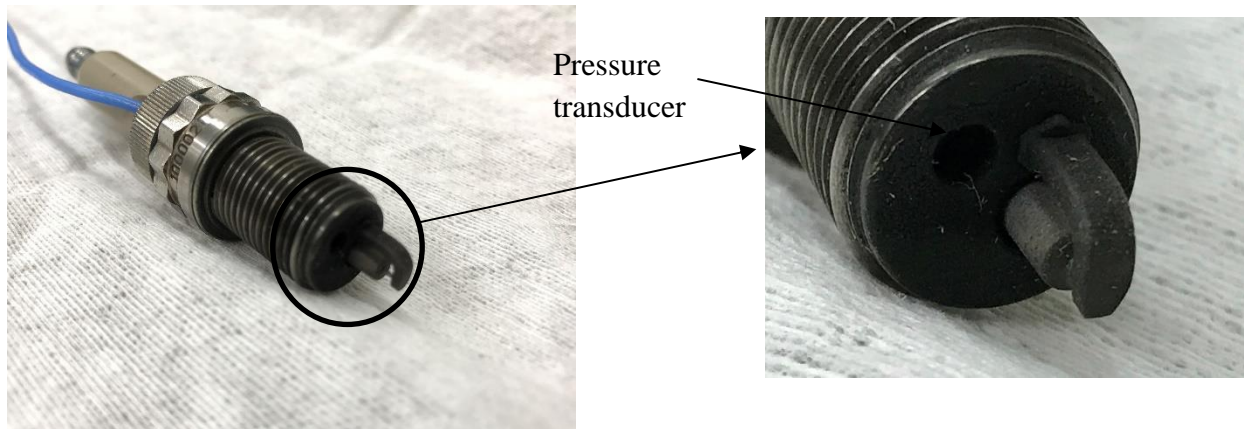
Figure 3.5: Structure of the spark plug with integrated pressure transducer

No special modifications were required for the mounting since the spark plugs of the stock size were available. The data is passed through a digital amplifier and then to the ACAP system for processing. Table 3.4 gives the details.

Table 3.4: In-cylinder pressure transducer specifications

Manufacturer	AVL
Model (spark plug)	ZF43F7LPRT
Model (pressure transducer)	GH13Z-24

Flame arrestor	Yes
Sensitivity	16 pC/bar
Range	0 – 250 bar
Thermal Shock error	± 3 bar

An accelerometer was used to measure the vibrations of the engine block, to study the correlation with the pressure signal. The knock event was confirmed using the accelerometer data. The accelerometer was mounted on the cylinder head of second cylinder as shown in Figure 3.6. It was connected to a charge amplifier and then to ACAP. The acquisition of the accelerometer data was event based, where the data was recorded every 0.5° crank rotation and not based on time. Table 3.5 gives the specifications for the accelerometer and Table 3.6provide the charge amplifier specifications used for this experiment.
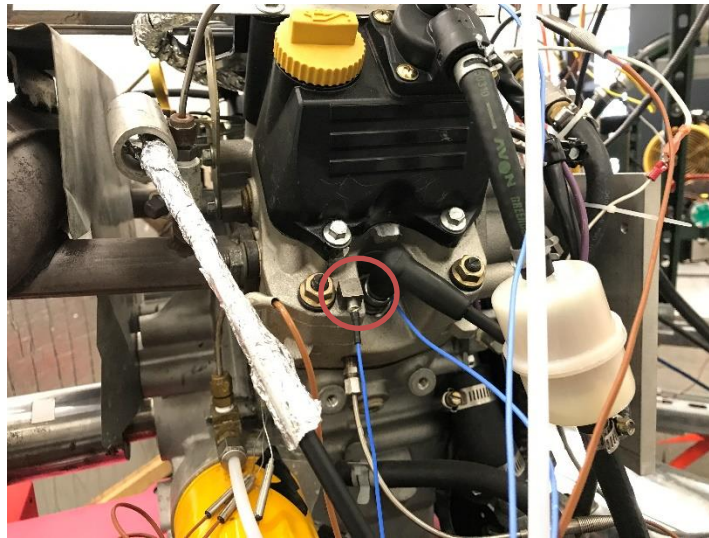
Figure 3.6: Mounting location for accelerometer

Table 3.5: Accelerometer specifications

Manufacturer	PCB Piezotronics
Model	356 A11
Voltage sensitivity	1.02 mV/ (ms^{-2})
Frequency range	Z: 2-10000 Hz X, Y: 2 – 7000 Hz

Excitation voltage	18 – 30 VDC
Sensing element	Ceramic

Table 3.6: Accelerometer charge amplifier specifications

Manufacturer	PCB Piezotronics
Model	480 B21
Excitation voltage	25 -29 VDC
Frequency range	0.15 – 100000 Hz
Temperature range	0 – 50 C
DC power	30 – 40 VDC

Ungrounded, k-type thermocouples and slow-speed pressure transducers were used to measure various temperatures and pressures at the following locations, as shown in Table 3.7. This data was acquired using Land-and-Sea DYNOmax software.

Table 3.7: Thermocouples locations

Location	Specification
Carburetor Inlet	K-type
Coolant In Global	K-type
Coolant Out Global	K-type
Exhaust Port 1	K-type
Exhaust Port 2	K-type
Oil	K-type
Exhaust fan	K-type
Fuel cart	K-type

Low speed pressure transducers are used to measure and log pressure values at five locations which are vital in judging the performance of the engine. Table 3.8 shows the locations of the pressure measurement and the measurement range of the pressure transducer for that location.

Table 3.8: Pressure transducer location and measurement ranges

Location	Range
Carburetor inlet pressure	0 – 2.06 bar
Fuel pressure before fuel pump	0 – 2.06 bar
Fuel pressure after fuel pump	0 – 2.06 bar
Intake manifold pressure	0 – 3.45 bar
Oil pressure	0 – 6.9 bar

The required fuel pressure at carburetor was generated using a fuel pump mounted on the engine, in addition to a fuel supply pump at the fuel cart. The fuel pressure at carburetor was maintained within a pre-determined range of 1.17 bar to 1.24 bar.

For this study, three speeds of 1500 rpm, 1800 rpm and 2100 rpm were tested. For every speed point, two loads of 15 Nm and 25 Nm were tested. Three spark advances of 0°, 10° and 20° were considered along with three fuels namely E0 91, E15 91 and E10 87. Refer to appendix section 7.1 for detailed test matrix. The change in spark advance will yield the effects on knocking tendency which can be studied considering the stock configuration of 0° spark advance as standard for comparison. The comparison of results from E0 91 and E15 91 will show the effect of change in ethanol content on knocking intensity of the engine. Also, the results from E0 91 and E10 87 would show the combined effect of increase in ethanol content and decrease in octane rating on knock. This will have conflicting results since the increase in ethanol content and decrease in octane rating will have opposite effects on the knocking tendency of the engine. In both these cases, E0 91 will be considered as baseline case and comparison will be done accordingly.

4 Results and Discussion

In this section, the effect of ethanol content, octane number and spark advance on knocking tendency of the engine is discussed. The combustion data was collected using ACAP while Land and Sea was used for gathering non-combustion related values. The non-combustion values were logged for a period of 180 seconds. This period is considered sufficient to verify the stable operation of an engine at a test point.

The engine was tested for three fuels E0 91, E15 91, and E10 87. Here, E0, E15 and E10 indicate the volume percentage content of ethanol in the fuel while 91 and 87 are the (R+M)/2 octane ratings of the fuels used. The ignition coil was moved by 0°, 10° and 20° with respect to the stock configuration to test the engine at a baseline case and two advanced spark timings. For every condition, three speed points of 1500 rpm, 1800 rpm and 2100 rpm and two brake torque points of 15 Nm and 25 Nm were tested. The detailed test matrix for this study is included in appendix 7.1 at the end of this report.

To compare the effect of octane number and ethanol content on knocking tendency, the discussion was divided into two sub-sections. The first sub-section studied the effect of ethanol content and the second sub-section studied the effect of octane number. To avoid bias caused by ethanol content, E0 91 fuel was considered as baseline fuel and compared to other cases.

4.1 Engine Stability

This section discusses the parameters of the engine which can be considered to determine the stable operation of the engine.

Table 4.1 shows the statistics of lambda values with advance in spark timing. The statistics considered here do not take into account the individual speed/load points.

Table 4.1: Average value of lambda

	Spark Advance		
Fuel	**0**	**10**	**20**
E0 91	0.91 ± 0.1	0.88 ± 0.1	0.87 ± 0.08
E15 91	0.99 ± 0.1	0.94 ± 0.1	0.93 ± 0.08
E10 87	0.93 ± 0.08	0.9 ± 0.1	0.91 ± 0.1

The lambda values presented in the table are measured using a wide-band lambda sensor mounted in the exhaust pipe of the engine. Being a carbureted engine, accurate control of lambda values was not possible.

The raw data for lambda variation can be referred to in the appendix section 7.2. Figure 7.1 show the variation of lambda values for all tests with respect to time.

Table 4.1 shows the variation of exhaust gas temperatures for cylinder 2 with advances in spark timing. The statistics considered here do not take into account the individual speed/load points.

Table 4.2: Average value of exhaust gas temperatures for cylinder 2

	Spark Advance		
Fuel	0	10	20
E0 91	630°C ± 50	584°C ± 70	574°C ± 70
E15 91	658°C ± 80	614°C ± 77	619°C ± 85
E10 87	634°C ± 70	594°C ± 70	592°C ± 70

A stable exhaust gas temperature indicates stable operation of the engine. The temperature ranges are expected to change with load and spark advance. This trend is followed for all cases. The exhaust gas temperatures for all cases vary between a minimum of 574°C to a maximum of 658°C. The variation of exhaust gas temperature with time for all cases can be found in Figure 7.4, Figure 7.5, and Figure 7.6 in appendix section 7.2.

One of the factors affecting knock is the cylinder wall temperature. A higher wall temperature will encourage knocking while knock will be reduced at lower wall temperatures. To compare knocking tendencies of the engine under different conditions, it is necessary that the wall temperatures be comparable to one another. Table 4.3 shows the variation of coolant out temperatures with changes to spark timing. The statistics considered here do not take into account the individual speed/load points.

Table 4.3: Average value of coolant temperatures

	Spark Advance		
Fuel	0	10	20
E0 91	85°C ± 9	85°C ± 12	84°C ± 11

| E15 91 | 87°C ± 9 | 88°C ± 8 | 90°C ± 10 |
| E10 87 | 88°C ± 7 | 85°C ± 8 | 88°C ± 10 |

The heat exchanger used for this test was designed for an engine producing about 90 kW. The tested engine only produced 9 kW. This made it difficult to control the temperature of the coolant. An attempt was made to maintain the temperature of the coolant between 84°C to 88°C. The end temperature of every test is dependent on the speed and load point being tested. The temperatures were within acceptable limits with a minimum of 84°C and maximum of 90°C. The variation of coolant temperature with time is presented in Figure 7.7, Figure 7.8, and Figure 7.9 in appendix section 7.2.

Oil temperature also provides an indication of the overall stability of the engine. Ideally, the oil temperature is higher than the coolant temperature at the same load. However, oil takes a longer time to heat up to a steady-state value.

Table 4.4: Average value of oil temperatures shows the variation of coolant out temperatures with advance in spark timing. The statistics considered here do not take into account the individual speed/load points.

Table 4.4: Average value of oil temperatures

Spark Advance			
Fuel	0	10	20
E0 91	85°C ± 12	87°C ± 15	86°C ± 15
E15 91	87°C ± 12	90°C ± 9	94°C ± 12
E10 87	90°C ± 12	89°C ± 12	92°C ± 12

For this study, the oil temperatures were expected to bear the same trends, be comparable to each other and should not undergo sudden changes. The average values of oil temperatures are comparable to each other with a maximum value of 94°C and a minimum of 85°C. The gradients in oil temperatures depend on the speed and load conditions being tested and are shown to be consistent across fuels and spark advances. The variations in oil temperature have a direct effect on the frictional losses in the engine, and thus the indicated work will vary, for the same brake work. The variation of oil temperature against time can be found in Figure 7.10, Figure 7.11, and Figure 7.12 for all conditions in appendix section 7.2.

The quantity of fuel consumed in the engine varies with speed and load points. The fuel pressure at the carburetor inlet impacts the quantity of fuel delivered to the engine as well. For this study, it was necessary that the fuel pressure values be comparable to one another since a change in quantity of fuel will significantly affect the knocking tendency.

Table 4.5 shows the change in the average fuel pressure at carburetor inlet as the spark timing was varied. The statistics considered here do not take into account the individual speed/load points.

Table 4.5: Average fuel pressure at carburetor inlet

Fuel	Spark Advance		
	0	10	20
E0 91	1.2 bar ± 0.02	1.21 bar ± 0.01	1.22 bar ± 0.03
E15 91	1.2 bar ± 0.03	1.22 bar ± 0.03	1.25 bar ± 0.01
E10 87	1.22 bar ± 0.02	1.24 bar ± 0.02	1.25 bar ± 0.01

The values of the fuel pressure are comparable to one another with a maximum value of 1.26 bar and a minimum of 1.2 bar. The variation in fuel pressure values with time for all cases can be found in Figure 7.16, Figure 7.17, and Figure 7.18 in appendix section 7.2.

Table 4.6, Table 4.7, and Table 4.8 show the average values for crank angles at 50% mass fraction burned (CA50) at all test points for E0 91, E15 91, and E10 87 fuels, respectively. The CA50 crank angles were advanced with an advance in spark timing at all test points and fuels. Also, the CA50 values vary with changes to the speed and load test points.

Table 4.6: Average CA50 for E0 91 fuel

Test Point	Spark Advance		
	0	10	20
1500 RPM / 15 Nm	19.8	15.06	7.61
1500 RPM / 25 Nm	14.22	4.17	-2.34
1800 RPM / 15 Nm	20.51	14.10	4.17
1800 RPM / 25 Nm	17.13	8.25	-0.04
2100 RPM / 15 Nm	20.44	12.64	7.14

Test Point			
2100 RPM / 25 Nm	16.67	7.28	0.63

Table 4.7: Average CA50 for E15 91 fuel

Test Point	Spark Advance		
	0	10	20
1500 RPM / 15 Nm	20.14	13.35	7.30
1500 RPM / 25 Nm	15.88	4.7	-1.97
1800 RPM / 15 Nm	21.04	14.39	8.03
1800 RPM / 25 Nm	17.75	7.75	1.18
2100 RPM / 15 Nm	20.87	13.81	8.69
2100 RPM / 25 Nm	17.78	7.48	1.11

Table 4.8: Average CA50 for E10 87 fuel

Test Point	Spark Advance		
	0	10	20
1500 RPM / 15 Nm	20.12	12.61	6.24
1500 RPM / 25 Nm	13.57	3	-2.67
1800 RPM / 15 Nm	20.71	11.54	7.15
1800 RPM / 25 Nm	17.18	5.65	0.02
2100 RPM / 15 Nm	21.2	10.94	5.91
2100 RPM / 25 Nm	16.70	5.86	1.3

Table 4.9, Table 4.10, and Table 4.11 show the average values for burn duration (D10-90) at all test points for E0 91, E15 91, and E10 87 fuels, respectively. The burn duration values decreased with an advance in spark timing and also changed due to the specific test point values.

Table 4.9: Average burn duration (D10-90) for E0 91 fuel

Test Point	Spark Advance		
	0	10	20
1500 RPM / 15 Nm	37.14	34	27.19
1500 RPM / 25 Nm	30.05	22.01	15.24
1800 RPM / 15 Nm	36.59	33.19	27.15
1800 RPM / 25 Nm	33.1	26.54	18.67
2100 RPM / 15 Nm	37.79	31.70	25.92
2100 RPM / 25 Nm	32.55	25.27	18.38

Table 4.10: Average burn duration (D10-90) for E15 91 fuel

Test Point	Spark Advance		
	0	10	20
1500 RPM / 15 Nm	37.44	32.38	26.43
1500 RPM / 25 Nm	31.97	21.85	15.42
1800 RPM / 15 Nm	37.73	33.39	27.76
1800 RPM / 25 Nm	33.78	25.86	19.72
2100 RPM / 15 Nm	37.18	32.30	27.62
2100 RPM / 25 Nm	33.77	25.41	18.93

Table 4.11: Average burn duration (D10-90) for E10 87 fuel

Test Point	Spark Advance		
	0	10	20
1500 RPM / 15 Nm	37.26	31.73	25.72
1500 RPM / 25 Nm	29.32	20.14	14.7
1800 RPM / 15 Nm	38.12	31.13	26.8
1800 RPM / 25 Nm	32.89	21.62	18.61
2100 RPM / 15 Nm	36.98	29.67	24.46
2100 RPM / 25 Nm	32.19	23.7	19.47

The cycle-to-cycle variation in the operation of an engine can be judged by the coefficient of variation (COV) of indicated mean effective pressure (IMEP). The COV values are calculated for every cycle using Equation 4.1.

$$COV\ (IMEP) = \frac{\sigma(IMEP)}{\mu(IMEP)}$$
Equation 4.1

where $\sigma : standard\ deviation$

$\mu :$ mean value

The combustion quality of a cycle can be judged using the COV of IMEP parameter. For this study, the maximum value of COV of IMEP was maintained below 10%, which was possible for the carbureted engine.

Table 4.12,

Table 4.13, and Table 4.14 show the average values for COV of IMEP at all test points for E0 91, E15 91, and E10 87 fuels, respectively.

The COV of IMEP values are well within the maximum range for all cases with a maximum value of 4.7 % and a minimum of 0.7 %. The variation of COV of IMEP values with time can be found in Figure 7.13, Figure 7.14, and Figure 7.15 in appendix section 7.2.

Table 4.12: Average COV of IMEP for E0 91 fuel

Test Point	Spark Advance		
	0	10	20
1500 RPM / 15 Nm	4.15	4.10	1.4
1500 RPM / 25 Nm	1.09	0.59	1.47
1800 RPM / 15 Nm	4.11	2.48	1.30
1800 RPM / 25 Nm	1.64	0.75	1.08
2100 RPM / 15 Nm	3.3	2.24	0.99
2100 RPM / 25 Nm	1.70	0.69	1.02

Table 4.13: Average COV of IMEP for E15 91 fuel

Test Point	Spark Advance		
	0	10	20
1500 RPM / 15 Nm	3.5	2.35	1.03
1500 RPM / 25 Nm	2.82	0.62	1.23
1800 RPM / 15 Nm	4.41	2.39	1.13
1800 RPM / 25 Nm	3.25	0.72	1.02
2100 RPM / 15 Nm	4.54	2.49	1.23
2100 RPM / 25 Nm	2.43	1.05	0.85

Table 4.14: Average COV of IMEP for E10 87 fuel

Test Point	Spark Advance		
	0	10	20
1500 RPM / 15 Nm	4.45	2.16	1.25
1500 RPM / 25 Nm	1.06	0.88	1.43
1800 RPM / 15 Nm	3.89	2.25	1.17
1800 RPM / 25 Nm	1.85	0.67	1.11
2100 RPM / 15 Nm	3.41	1.8	0.95
2100 RPM / 25 Nm	1.80	0.6	0.86

4.2 Characterization of Knock

For this study, an in-cylinder pressure transducer and a cylinder head mounted accelerometer were used for detection of knock. The raw signals from the transducers and the accelerometer were recorded and processed for knock detection.

A knock window was determined in terms of crank angles to be 0 degrees after top dead center (dATDC) to 40 dATDC based on the literature reviewed in section 2.4.1. Raw pressure data for this window was passed through a bandpass filter. The lower and upper cut-off frequencies for the filter were set at 4 kHz and 8.9 kHz respectively. The lower cutoff frequency was selected based on the study conducted by Arsham Shahlari and Dr. Gandhi, which was previously reviewed in section 2.4.1. The upper cutoff frequency was based on the engine speed, since data was collected using encoder triggers and not time trigger, and was kept constant at the lowest value to avoid discrepancies. A third-order Butterworth bandpass filter was used for this analysis. A third-order filter was chosen to avoid excessive attenuation of the signal that comes with an increase in filter order. The first 10 values of the filtered signal were ignored in this study to prevent aliasing of data during the time when the filter was unstable. The maximum-peak-to-peak variation of this wave is calculated using Equation 4.2.

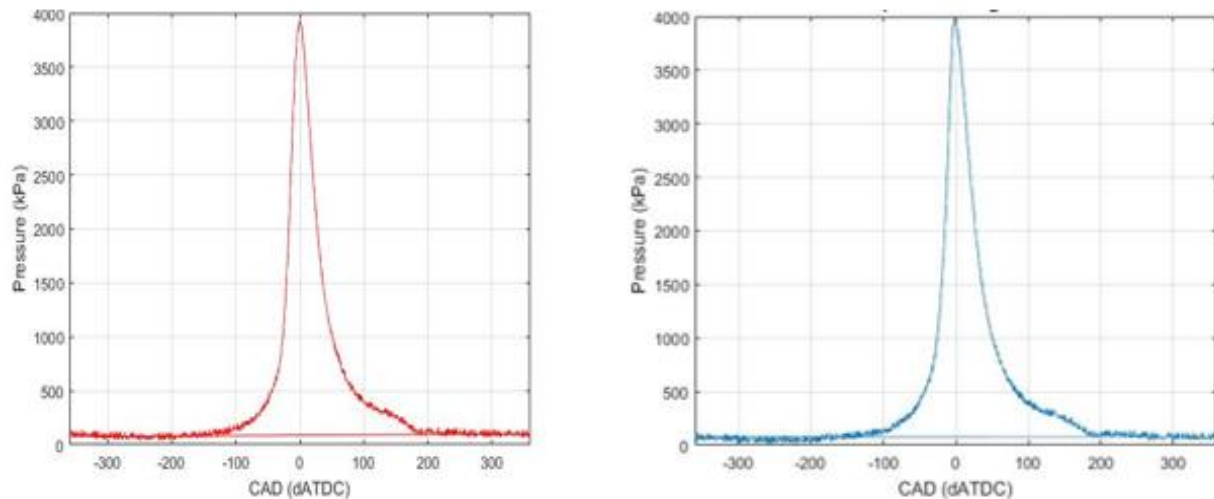Figure 4.1: Comparison of knocking (red) and non-knocking (blue) pressure curves for E0 91 fuel (1500 RPM /25 Nm)

As shown in Figure 4.1, there was not much of a difference that can be observed in the individual pressure curves for knocking versus non-knocking operation. This was expected since the magnitude of knock observed was not high enough to be significantly affect the cylinder pressure.
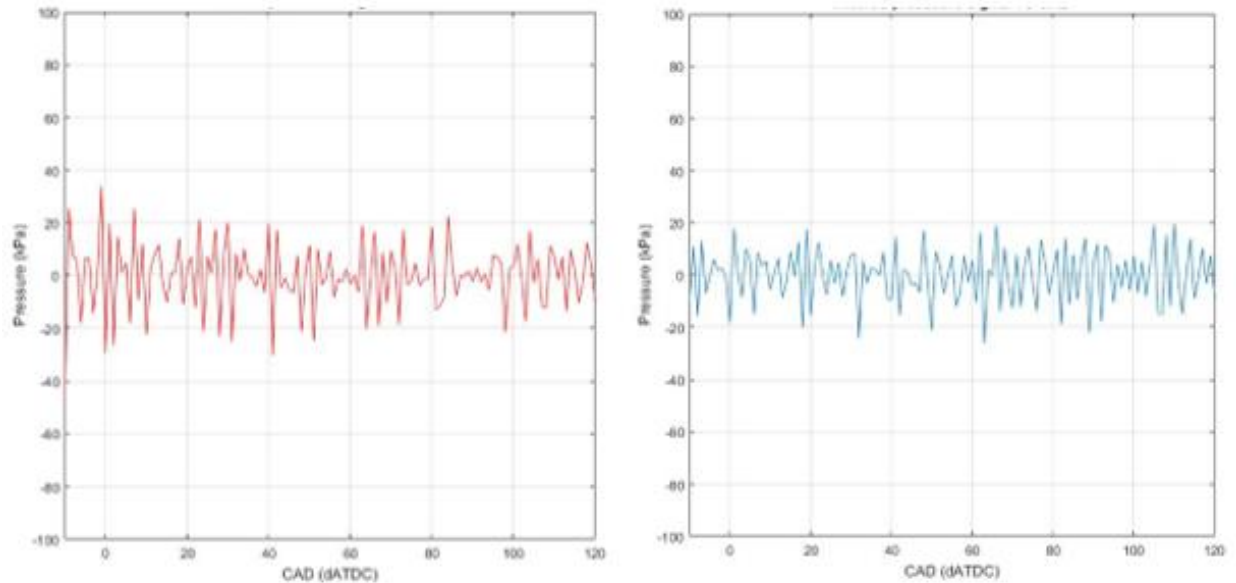
Figure 4.2: Comparison of knocking (red) and non-knocking (blue) filtered pressure signals for E0 91 fuel (1500 RPM /25 Nm)

As shown from Figure 4.2, the pressure values in the knocking cycle were slightly higher than that in the non-knocking cycle. Since the engine could not be loaded to a higher value due to experimental setup constraints, the magnitude of the peak-to-peak variation remained on the lower side. If the engine was loaded to a higher value, a higher magnitude of knock would be detected and analyzed following the same process.

The other method used for knock detection was an accelerometer mounted on the head of the second cylinder. The pressure transducers were mounted in the combustion chamber, next to the spark plug. For the accelerometer, the shock wave had to travel through the cylinder and cylinder head before it was detected. This was the reason for the delay in knock detected by the accelerometer, in terms of crank angle degrees, as compared to that by the pressure transducer for the same engine cycle.

The natural frequency for the engine was calculated using Equation 4.3.

$$\mathbf{F_n} = \frac{\mathbf{C} * \rho}{\pi * \mathbf{B}}$$
Equation 4.2

where
F_n: natural frequency of the engine

ρ: oscillatory mode of the engine

B: bore diameter = 0.08m (in this case)

C: speed of sound

The oscillatory mode factor can be found from Table 4.15 depending on the mode number in question.

Table 4.15: Predicted oscillatory modes for knock [9]

Mode	ρ	Frequency (kHz)
(1,0)	1.84	6.6
(2,0)	3.05	10.9
(3,0)	4.20	15.1
(4,0)	5.32	19.1
(5,0)	6.42	23.0
(0,1)	3.83	13.7
(1,1)	5.33	19.1
(2,1)	6.71	24.0

The speed of sound (C) is calculated using Equation 4.4

$$C = \sqrt{\gamma * R * T}$$
Equation 4.3

where   C: speed of sound (m/sec)

γ: ratio of specific heats = 1.38 (for this case)

R: gas constant for air = 286.9 J/kg K

T: adiabatic flame temperature (K)

The combustion process is assumed to be adiabatic for the calculation of flame temperature. Table 4.16 gives the adiabatic flame temperature and 1st mode natural frequencies of the engine for the three fuels used.

Table 4.16: Adiabatic flame temperature and natural frequencies

Fuel	Adiabatic flame temperature (K)	Natural frequency (kHz)
E0 91	2156	6.764
E10 87	2195	6.824
E15 91	2270	6.940

Figure 4.3 shows a comparison between the filtered accelerometer data for knocking and non-knocking cycles with E0 91 fuel.
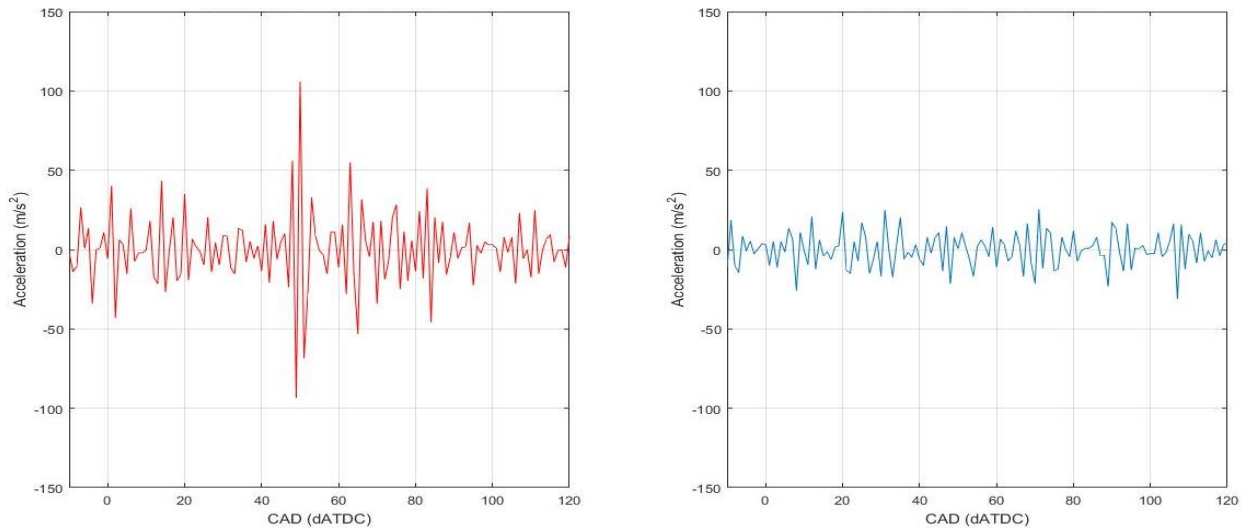

Figure 4.3: Comparison of knocking (red) and non-knocking (blue) filtered accelerometer signals for E0 91 fuel (1500 RPM /25 Nm)

As shown in Figure 4.3, there was a significant increase in accelerometer values at 50 dATDC. This spike was not observed for the non-knocking case. The non-knocking data remained fairly constant with a maximum value of 25 m/sec^2 and a minimum value of -31 m/sec^2. The knocking data had a maximum and minimum acceleration of 106 m/sec^2 and -93 m/sec^2, respectively. There was three times higher acceleration for the knocking case, compared to the non-knocking case. These results indicate and differentiate between a knocking and non-knocking case for the same speed, load, spark advance, and fuel.

For this study, the top dead center of the engine was located with respect to the first cylinder. The ACAP combustion analyzer used this TDC for knock calculation using the 1642 knock

module for cylinder 2. As cylinder 2 did not show any knocking tendency in the crank angle window, which was set according to the TDC with respect to cylinder 1, ACAP was unable to capture any knock results. The pressure and accelerometer data was post processed, using MATLAB, to calculate the peak-to-peak variations.

Table 4.17 shows the conditions where knock was detected for E0 91 fuel based on cylinder pressure data.

Table 4.17: Knocking vs non-knocking test points for E0 91 fuel based on cylinder pressure data

Test Condition	Fuel	0° Spark Advance	10° Spark Advance	20° Spark Advance
1500 RPM / 15 Nm	E0 91	No	No	No
1500 RPM / 25 Nm	E0 91	No	No	Yes
1800 RPM / 15 Nm	E0 91	No	No	No
1800 RPM / 25 Nm	E0 91	No	No	Yes
2100 RPM / 15 Nm	E0 91	No	No	Yes
2100 RPM / 25 Nm	E0 91	No	Yes	Yes

4.3 Effect of Spark Advance on Knocking Tendency

The following section discusses the influence of spark advance on knocking tendency of the engine. Since the stock engine was equivalent to 0° spark advance, this configuration was considered as the standard and all calculations for differences were performed considering 0° spark advance as the base line.

4.3.1 Effect of spark advance for E0 91

Figure 4.4 presents the effect of 10° and 20° spark advance for cylinder 2 based on the 95th percentile of peak-to-peak variation for E0 91 fuel. As mentioned in section 2.3.1, the peak-to-peak variation above 100 kPa is considered as a knocking condition. This limit is denoted by the 100 kPa horizontal line on the plot. Taking into account this criterion, it was concluded that there was no knock observed at 1500 RPM and 1800 RPM low load test points for any configuration while knock was identified for all test points at 2100 RPM.

As shown from Figure 4.4, with increase in spark timing, the influence on the knocking tendency of the engine also increased. Knock was expected to occur at the lowest speed and highest load point at maximum spark advance. This expectation is well met for the 20° spark advance configuration at 1500 RPM and 25 Nm test point. At this point, there was an increase of 40 % in the 95th percentile of peak-to-peak variation. This difference was a maximum for this set of data points. Another trend that can be observed from the figure was that the knocking tendency was higher at higher loads which also met the initial expectations.
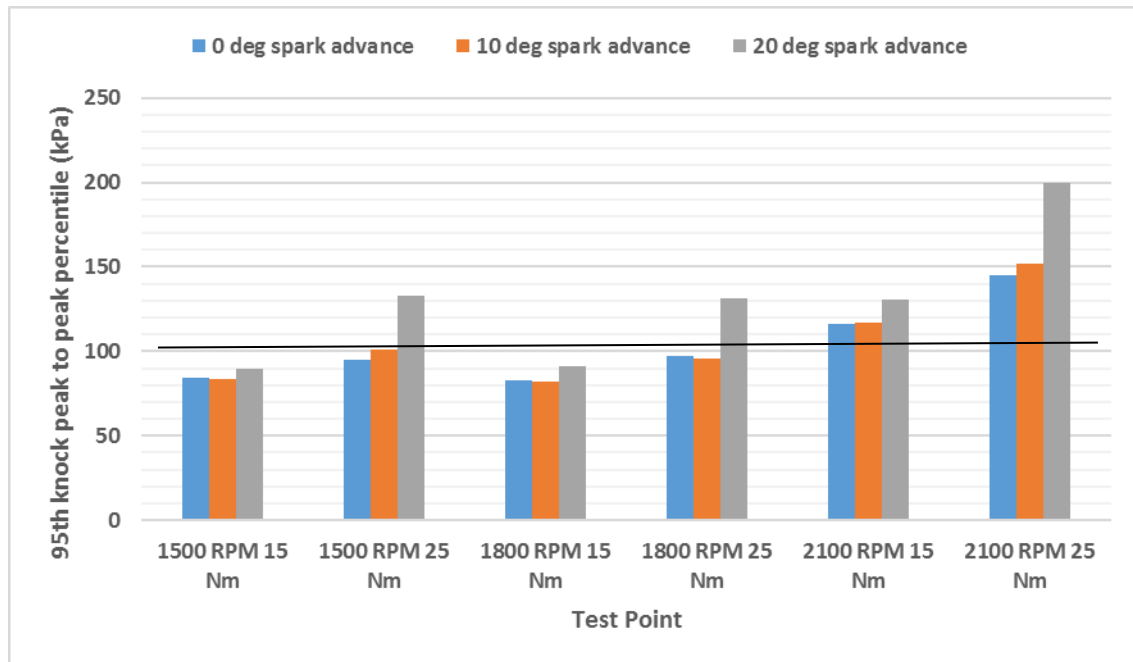

Figure 4.4: Effect of spark advance on 95th percentile of peak-to-peak variation for E0 91 fuel

As the engine speed increased, the knock tendency, at the same brake load, increased. To understand this trend, the BMEP and FMEP, derived from the Chen-Flynn friction model, were utilized to compute the GIMEP. Table 4.18 shows the values of BMEP, FMEP, and GIMEP for a 20º spark advance with E0 91 fuel at 1500 RPM / 25 Nm and 2100 RPM / 25 Nm.

Table 4.18: Mean effective pressure variation

	BMEP (bar)	Peak Pressure (bar)	FMEP (bar)	GIMEP (bar)
1500 RPM / 25 Nm	4.661	39.64	0.919	5.57
2100 RPM / 25 Nm	4.661	36.94	1.03	5.69

As shown, the GIMEP increased as the engine speed increased, due to friction. This was the primary reason for the increased knock tendency at the higher engine speeds. The remaining values for GIMEP are provided in Table 7.1.

Figure 4.5 shows the variation in acceleration from the data recorded using the accelerometer. In case of a knocking combustion, the vibrations of the cylinder block were expected to follow the same trend as the pressure peak-to-peak variation in Figure 4.4.
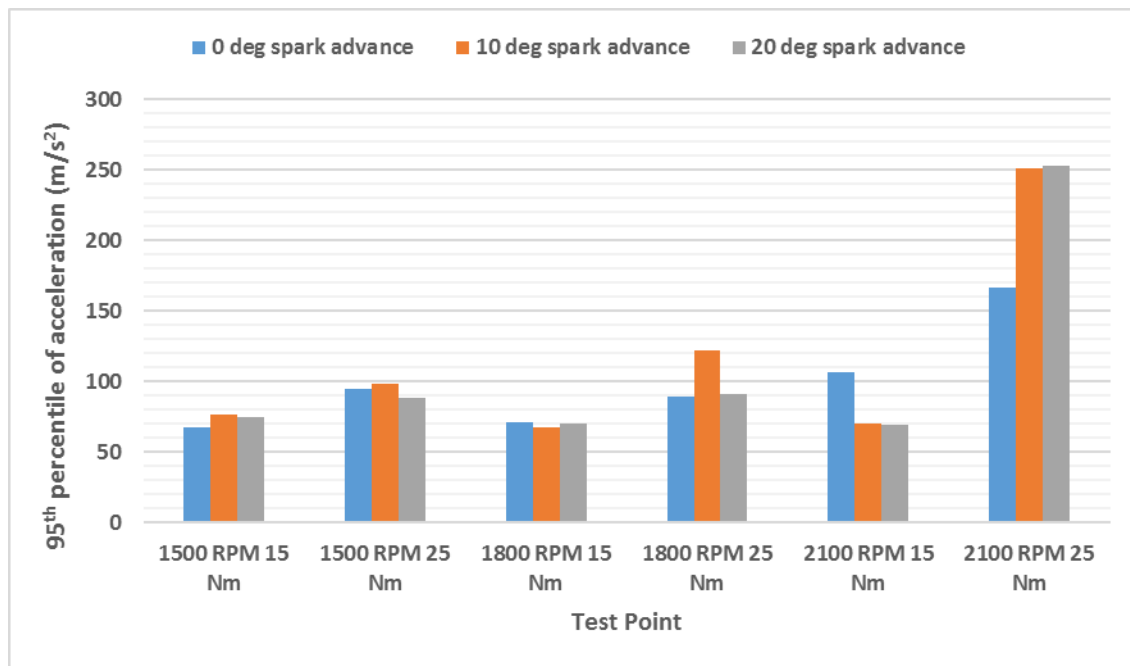

Figure 4.5: Effect of spark advance on peak-to-peak vibrations for E0 91 fuel

The vibrations of the cylinder block were observed to increase with increase in load. For the lower speed test points, the block vibrations remained comparable to each other. For 1800 RPM and 25 Nm test point, the vibrations showed a sharp increase at 10° spark advance, but the values for 0° and 20° remained comparable to one another. The vibrations for all test points at 2100 RPM and 25 Nm torque showed a larger magnitude as compared to other test points. The vibration increased as the spark was advanced. On comparison with the same test point in Figure 4.5, it was observed that the pressure peak-to-peak data indicated the presence of knock. This conclusion was further strengthened by the higher magnitude of vibrations.

Figure 4.6 shows the effect of spark advance on the exhaust gas temperature of the engine for E0 91 fuel. It can be observed from the graph that for any test point as the spark was advanced, the exhaust gas temperature decreased. With an increase in spark advance, the combustion event starts sooner. Since the exhaust valve opening time does not change, longer duration of time passes between completion of combustion process and exhaust valve opening. This leads to a drop on exhaust gas temperature.
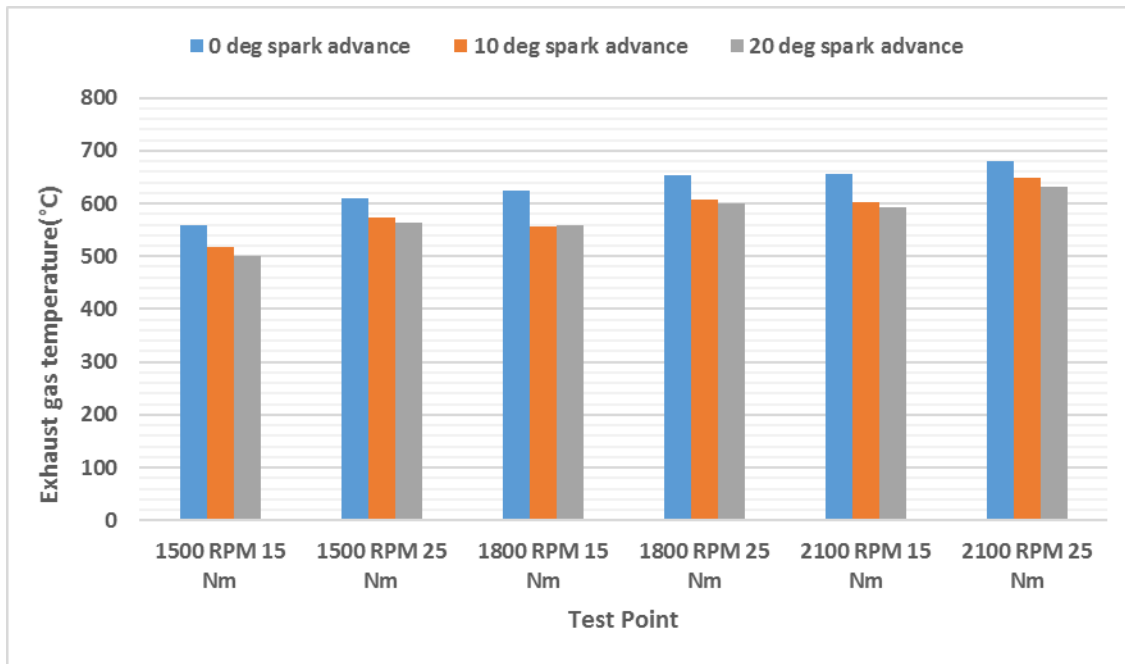

Figure 4.6: Effect of spark advance on exhaust gas temperature for E0 91 fuel

Figure 4.7 shows the variation in lambda values with an increase in spark advance. Since the engine had an open-loop control system for lambda, the values were not adjusted and maintained automatically. As the lambda value approaches stoichiometric, the combustion temperature increases. This resulted in a higher exhaust gas temperature. The comparison of Figure 4.6 and Figure 4.7 brought out this trend. In general, as the spark timing was advanced, the lambda values were lowered. As a result, the combustion temperature decreased leading to a decrease in exhaust gas temperature.
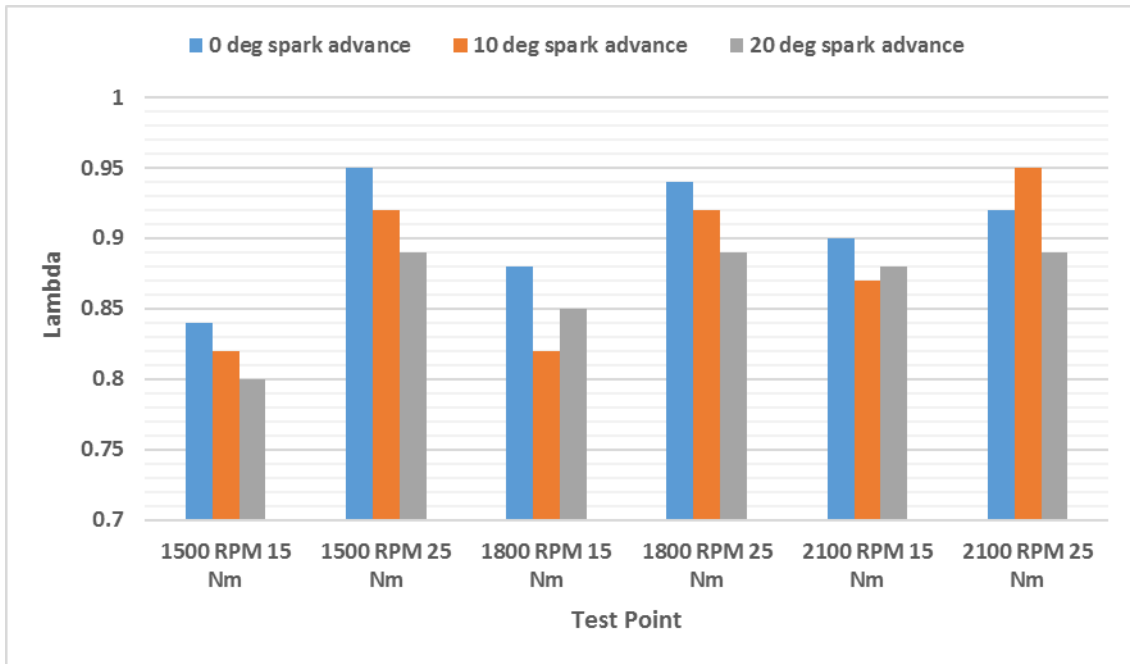
Figure 4.7: Effect of spark advance on lambda values for E0 91 fuel

Figure 4.8 shows the effect of spark advance on brake specific fuel consumption (BSFC) for E0 91 fuel.

The graph indicates that the BSFC values for all test points remained fairly constant in spite of the advance in spark timing. The exceptions were test points 1800 RPM / 25 Nm and 2100 RPM / 25 Nm. These test points showed a decrease in BSFC values for the 10° spark advance condition. The lower amount of fuel consumed to generate an equivalent amount of power was the reason for this exception.
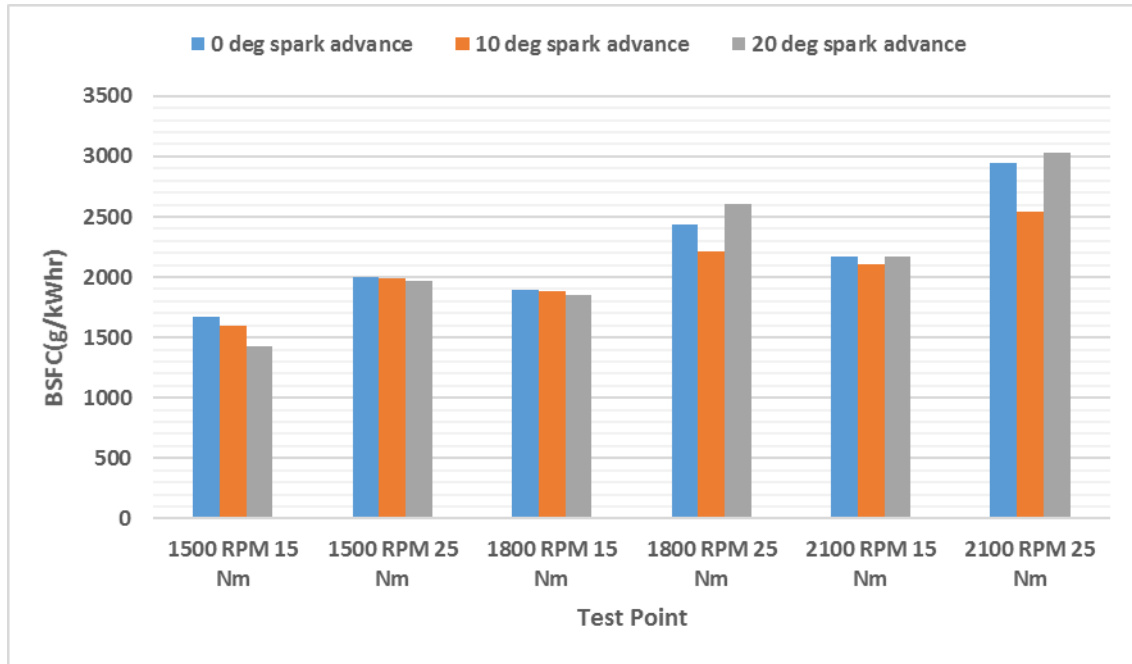

Figure 4.8: Effect of spark advance on brake specific fuel consumption for E0 91 fuel

4.3.2 Effect of spark advance for E15 91

Figure 4.9 shows a comparison between the 95th percentile of peak-to-peak variation at different test points and spark advance for E15 91 fuel.
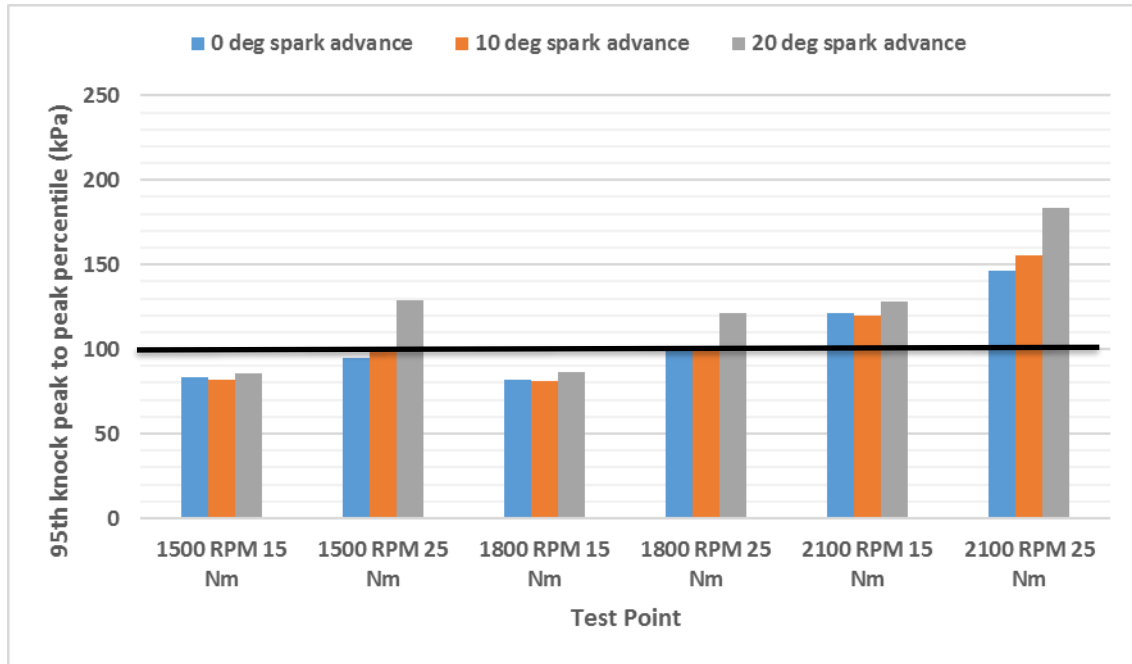

Figure 4.9: Effect of spark advance on 95th percentile of peak-to-peak variation for E15 91 fuel

From Figure 4.9 it can be inferred that, following the same trend as in previous case, the maximum effect of spark advance occurred at low speed and high load test point. The maximum increase in the 95th percentile peak-to-peak value of 31% was observed at 2100 RPM and 25 Nm. For the 10° spark advance setting, the 95th percentile was comparable for all test point except at the high speed and high load point of 2100 RPM and 25 Nm. At this point the increase was 12% which was considerably less compared to those at 20° spark advance configuration but is the maximum of 10° spark advance.

Figure 4.10 shows the variation in acceleration from the data recorded using the accelerometer for E15 91 fuel. The vibration levels increased at higher loads for all speeds. For all the test points except 2100 RPM and 25 Nm point, the values were comparable with a small difference. For the 2100 RPM / 25 Nm case, there was a sudden increase in vibration levels for all cases. Referring to Figure 4.9, it can be observed that this was a knocking case. The increases in vibration levels were attributed to the presence of knock. Similarly, for the 20° spark advance setting at 1500 RPM / 25 Nm, there was an increase in vibration levels. This was also attributed to knock based on the results from Figure 4.9. The 1800 RPM / 25 Nm test point contradicted the discussion. Although it was identified as a knocking case in Figure 4.9, the vibration level dropped at the 20° spark advance setting.
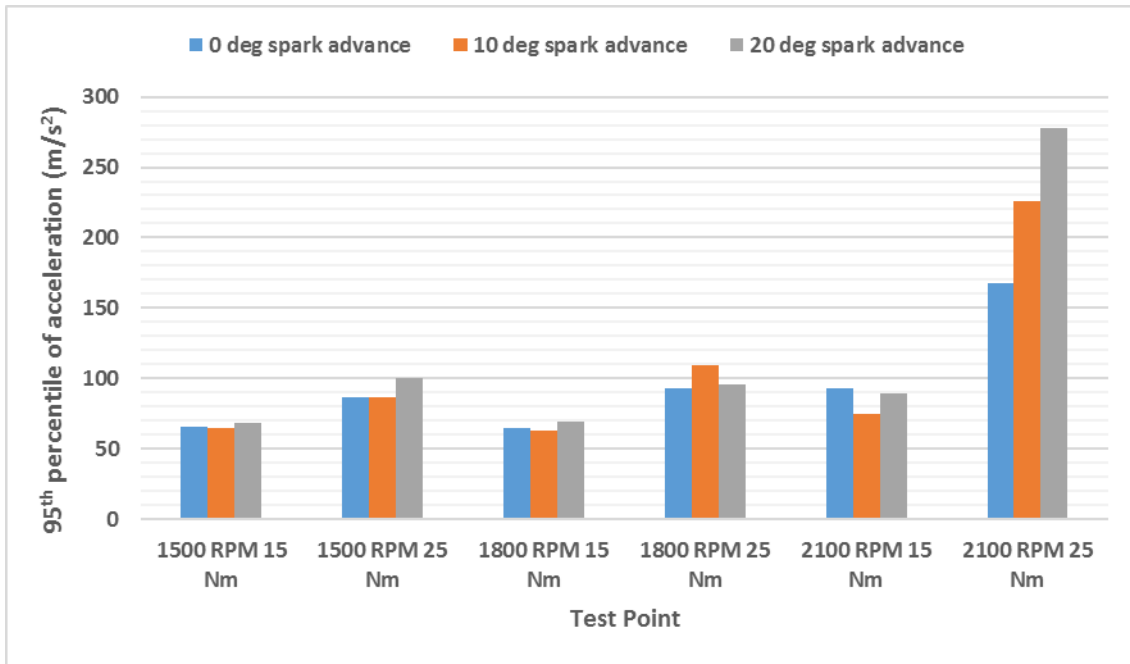
Figure 4.10: Effect of spark advance on peak-to-peak vibration for E15 91 fuel

Figure 4.11 shows the variation in exhaust gas temperature with spark advance for E15 91 fuel.
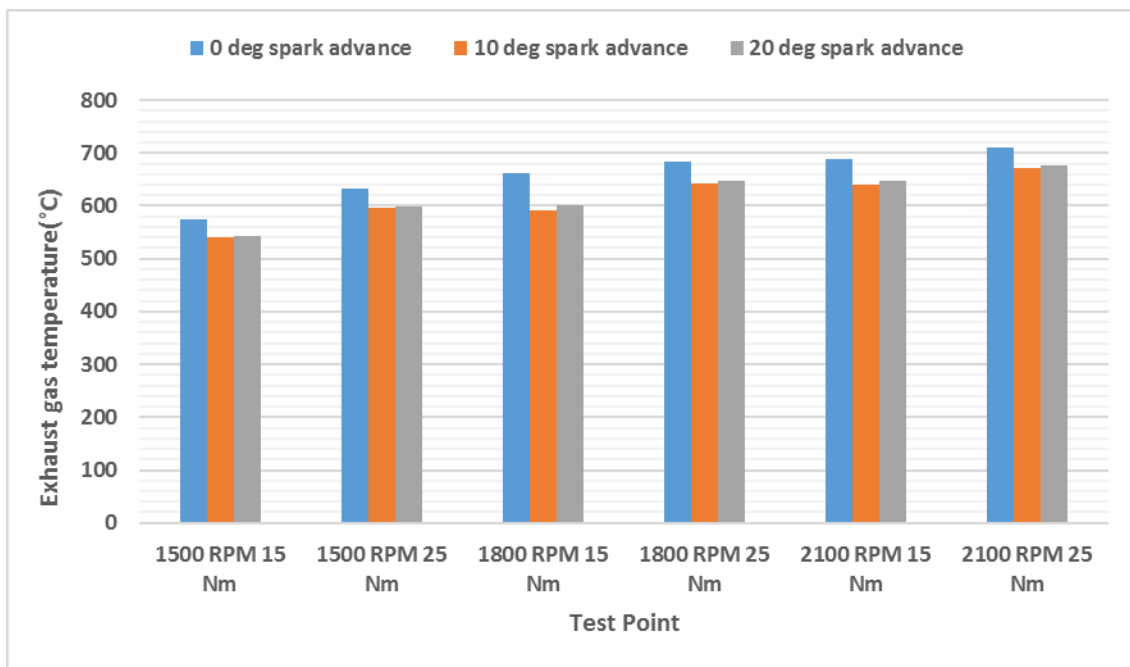

Figure 4.11: Effect of spark advance on exhaust gas temperature for E15 91 fuel

The Figure 4.11 shows a trend similar to that shown in Figure 4.6 for exhaust gas temperature with E0 91 fuel. The exhaust gas temperature was observed to reduce with an advance in spark

timing. The reason for this reduction is that there is a longer duration of time between the completion of combustion processes and exhaust valve opening.
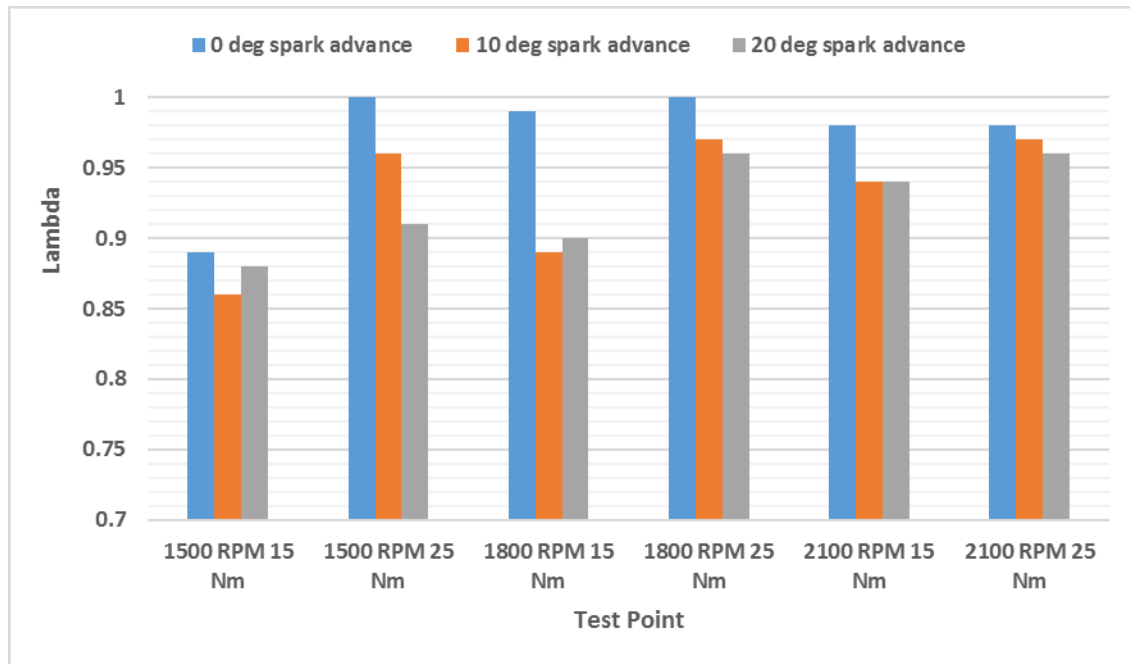

Figure 4.12: Effect of spark advance on lambda values for E15 91 fuel

The lambda values were observed to reduce with an advance in spark timing which led to a decrease in combustion temperature and consequently a reduction of exhaust gas temperature.

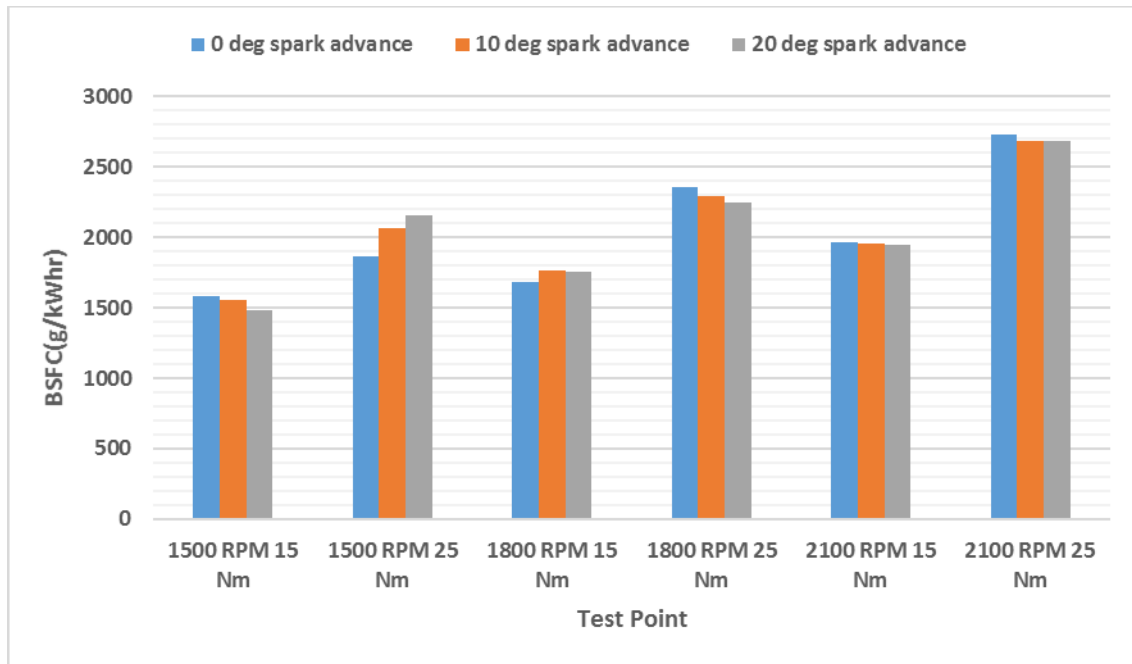Figure 4.13 shows the variation in BSFC with spark advance for E15 91 fuel.

Figure 4.13: Effect of spark advance on brake specific fuel consumption for E15 91 fuel

The graph for BSFC shows comparable values for BSFC for all test points with a maximum difference of 12%. This difference was attributed to the difference in throttle position resulting in difference in amount of fuel and the variability of the engine operation.

4.3.3 Effect of spark advance for E10 87

Continuing with the study, Figure 4.14 shows a comparison between the 95th percentile of peak-to-peak variation and the effect of spark advance for different test points for E10 87 fuel. The same trend was followed where the maximum increase in the 95th percentile peak-to-peak value was observed for the 20° spark advance and at a low speed and high load test point. In this case, the increase was 37%, which was a maximum among the three cases. The reduction in fuel octane number, which is discussed in the next section, was the leading cause of the increase in knock. In this case the maximum impact of 10° spark advance was 36% occurring at 2100 RPM and 25 Nm test point. It can also be concluded that for all speeds, a knocking condition was observed for 25 Nm loads, where peak-to-peak exceeded 100 kPa.
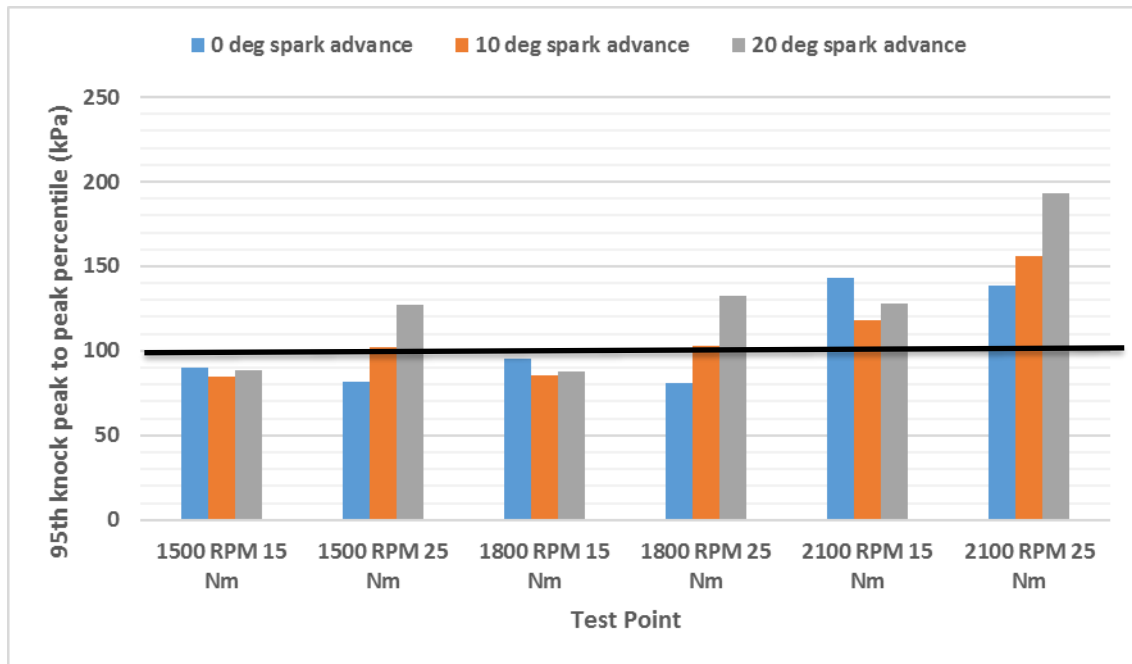

Figure 4.14: Effect of spark advance on 95th percentile of peak-to-peak variation for E10 87 fuel

Figure 4.15 shows the variations in cylinder block vibrations with a change in spark advance for E10 87 fuel. The 2100 RPM / 25 Nm test point showed the maximum amplitude of vibrations suggesting a knocking combustion. This result strengthened the result observed from Figure 4.14 where the knock was observed for the same point based on pressure data. Similarly, 1500 RPM and 25 Nm test point also showed an increase in vibration levels. This was attributed to the knock detected at this point based on pressure data from Figure 4.14. At all other test points, the vibration levels remained comparable in spite of the change in spark advance. These points are not detected as knocking points based on the results from Figure 4.14 except 1800 RPM / 25 Nm point which was an exception as in the case for E15 91 fuel.
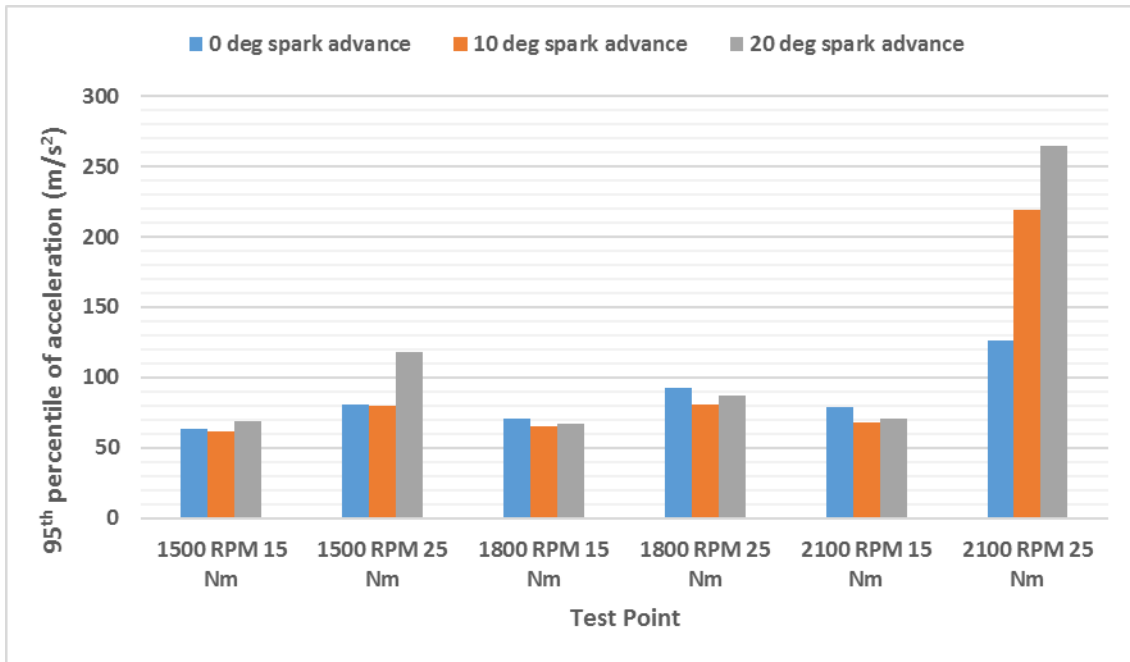
Figure 4.15: Effect of spark advance on peak-to-peak vibrations for E10 87 fuel

Figure 4.16 shows the effect of spark advance on exhaust gas temperature for E10 87 fuel. The temperatures were comparable to each other with a maximum difference of 10%. The reason for this reduction is that there is a longer duration of time between the completion of combustion processes and exhaust valve opening.
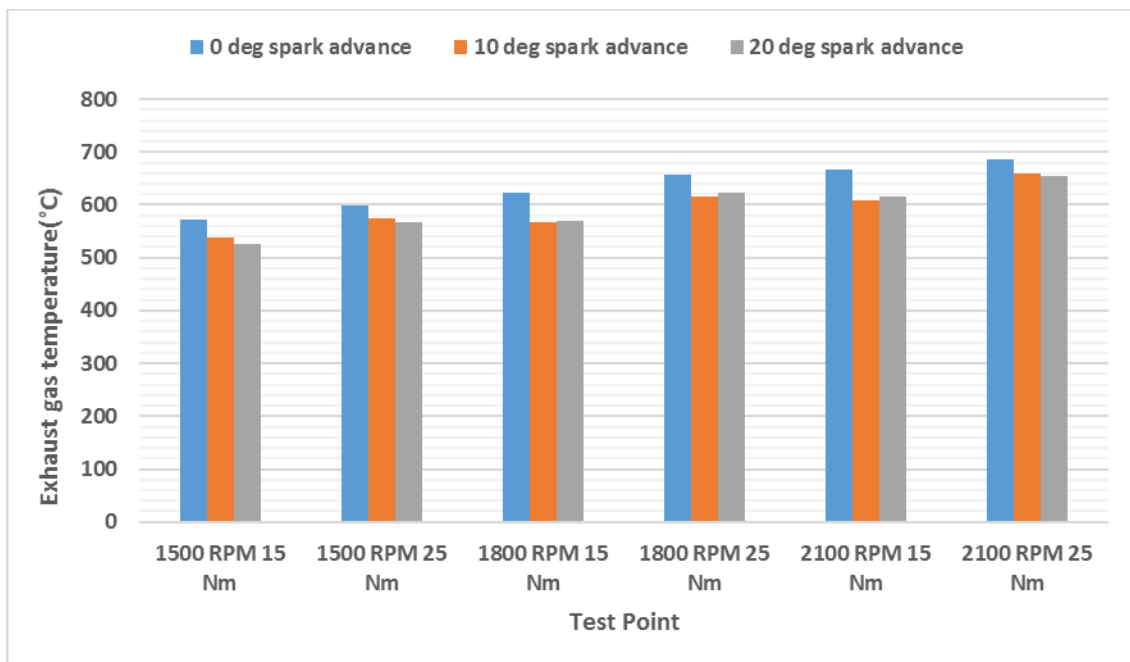

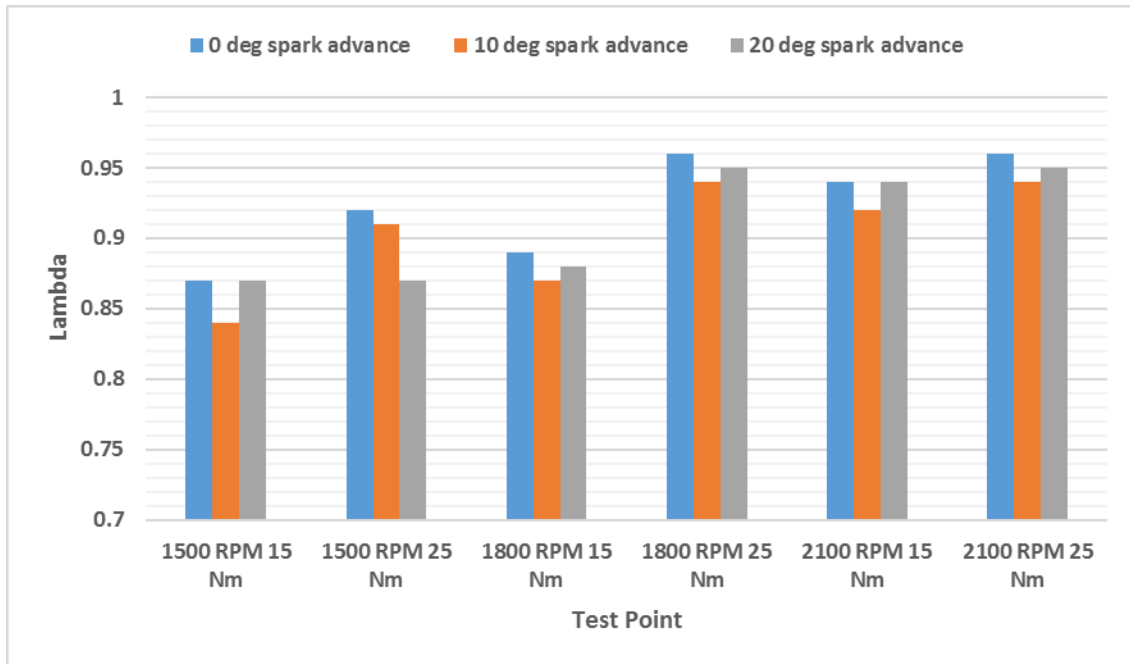Figure 4.16: Effect of spark advance on exhaust gas temperature for E10 87 fuel

Figure 4.17: Effect of spark advance on lambda values for E10 87 fuel

The lambda values were observed to reduce with an advance in spark timing and this led to a decrease in combustion temperature and consequently the reduction of exhaust gas temperature.
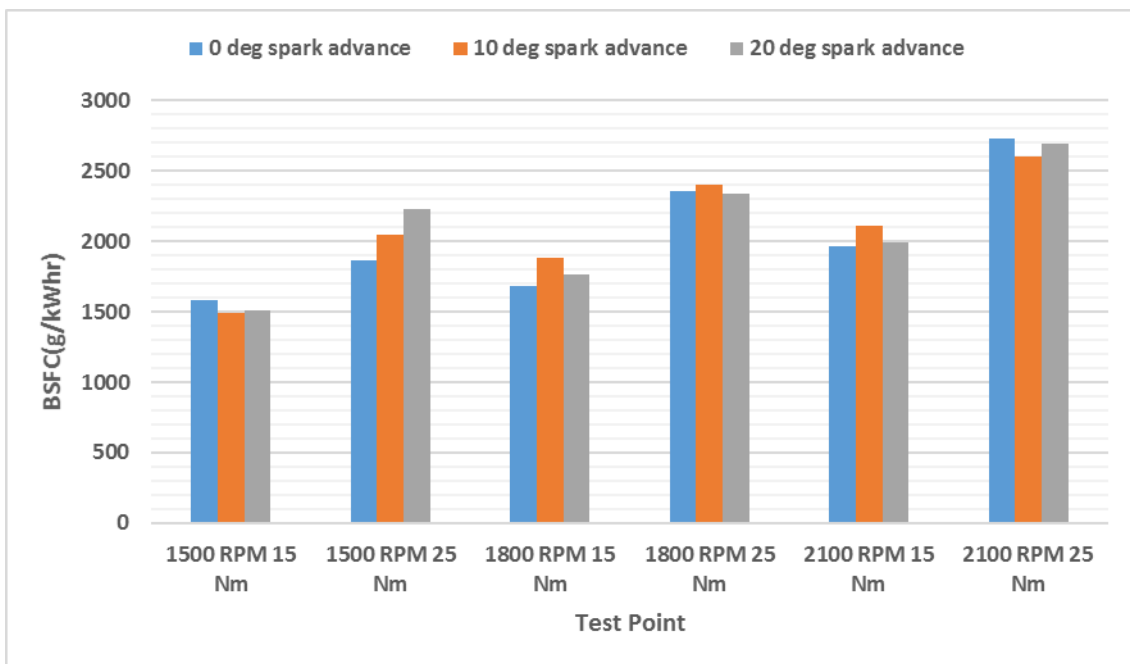

Figure 4.18: Effect of spark advance on BSFC for E10 87 fuel

Figure 4.18 shows the variation in BSFC values caused by spark advance for E10 87 fuel. The BSFC values were comparable to one another with a maximum difference of 10%. This was due to the slight difference in throttle opening required to meet the brake torque set point. This changed the fuel flow and was reflected in the higher BSFC value.

4.4 Effect of Change in Fuel Ethanol Content on Knocking Tendency

In this section, the effect of changing the ethanol content of the fuel, without changing the octane rating, on knocking tendency of the engine was compared. E0 91 was considered the baseline case and the results for E15 91 were analyzed in this regard. Similar to the previous comparison, the peak-to-peak knocking limit was indicated by the horizontal line at 100 kPa.
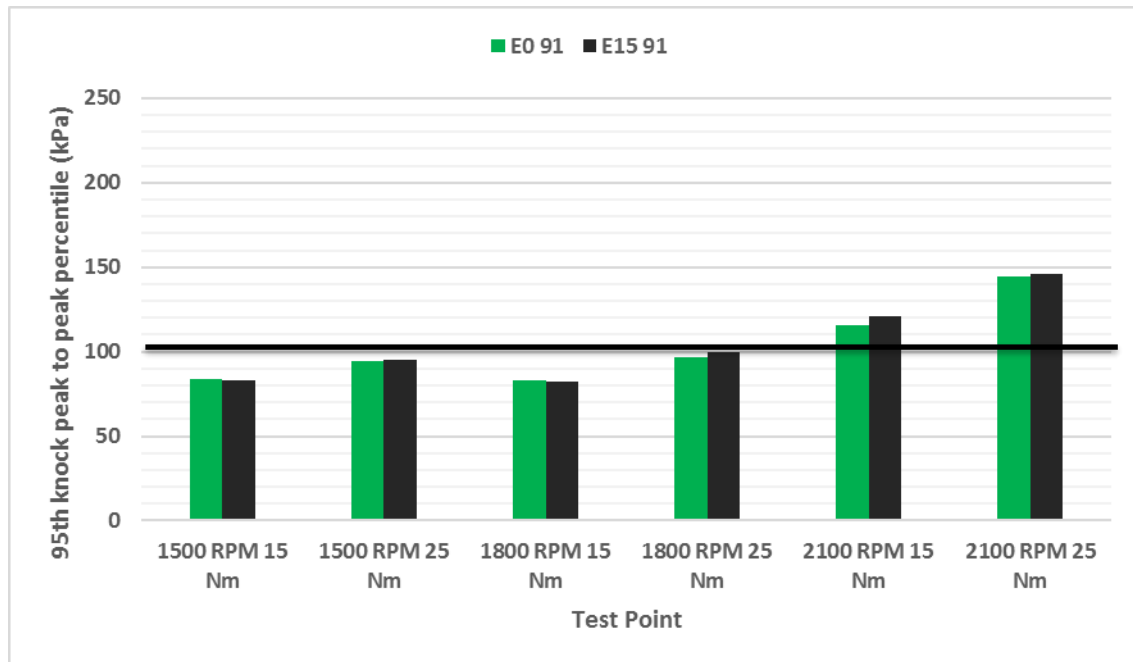
4.4.1 E0 91 vs E15 91 for 0° spark advance

Figure 4.19: Effect of ethanol content on 95th percentile of peak-to-peak variation for 0° spark advance

Figure 4.19 compares the change in the 95th percentile of peak-to-peak variations for E0 91 and E15 91 fuels at 0° spark advance. The 95th percentiles for the two fuels considered remained more or less equivalent at all test points. The maximum difference occurred at the 1800 RPM and 25 Nm test point where the 95th percentile for E15 91 fuel increased by approximately 33%. Also, there was no knock identified for any test points at 1500 RPM and 1800 RPM irrespective of the fuels or loads. Marginal knock identification was observed at the 2100 RPM and 25 Nm load point.

Figure 4.20 shows the effect of ethanol content on peak-to-peak variation of cylinder block vibrations. The knocking case identified in Figure 4.19 is confirmed by the rise in vibration

levels for the 2100 RPM / 25 Nm test point. Also, the marginal knock identified in Figure 4.19 at 1800 RPM and 25 Nm was reflected in the form of an increase in vibration levels.
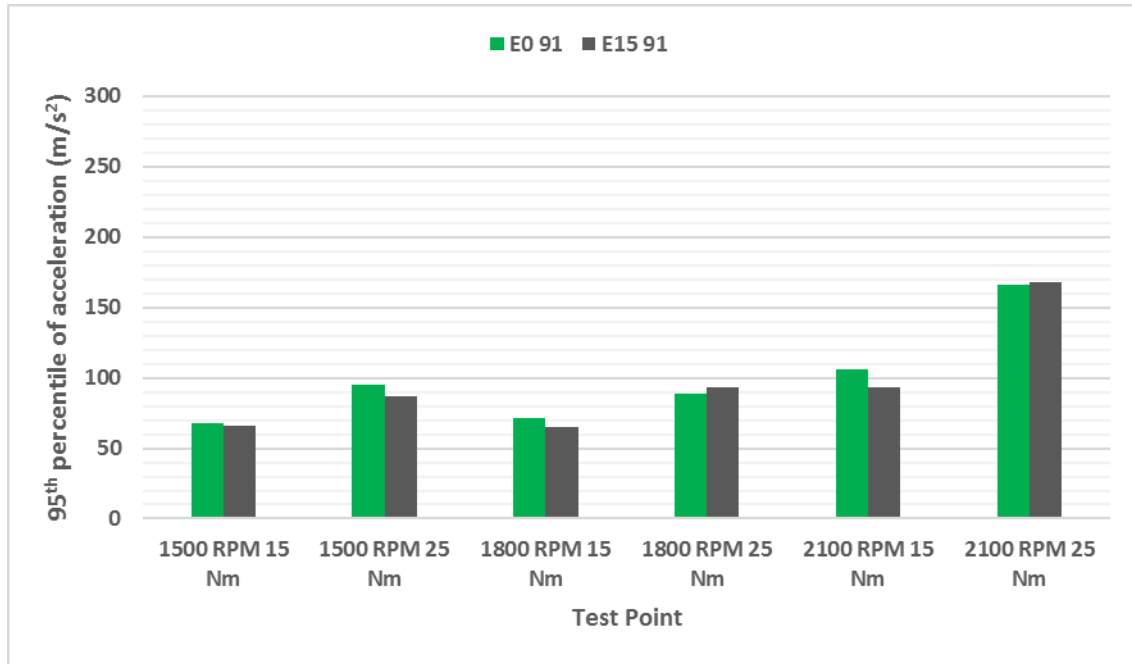

Figure 4.20: Effect of ethanol content on peak-to-peak vibrations for 0° spark advance

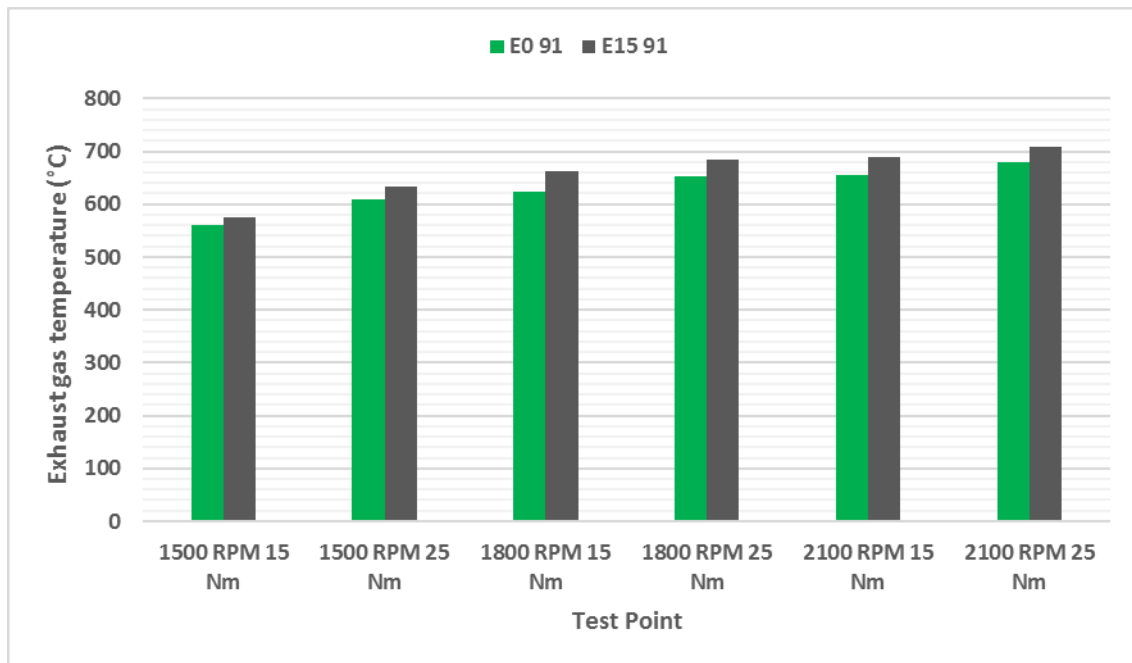Figure 4.21 shows the effect of ethanol content on exhaust gas temperature.

Figure 4.21: Effect of ethanol content on exhaust gas temperature for 0° spark advance

The exhaust gas temperature increases at all points for E15 91 fuel, compared to E0 91. As shown in Figure 4.22, as the ethanol content of the fuel was increased, the lambda values increased closer to the fuel stoichiometric value. Since the combustion temperature increases as lambda moves toward stoichiometric values, the exhaust gas temperature also increases with an increase in ethanol content.
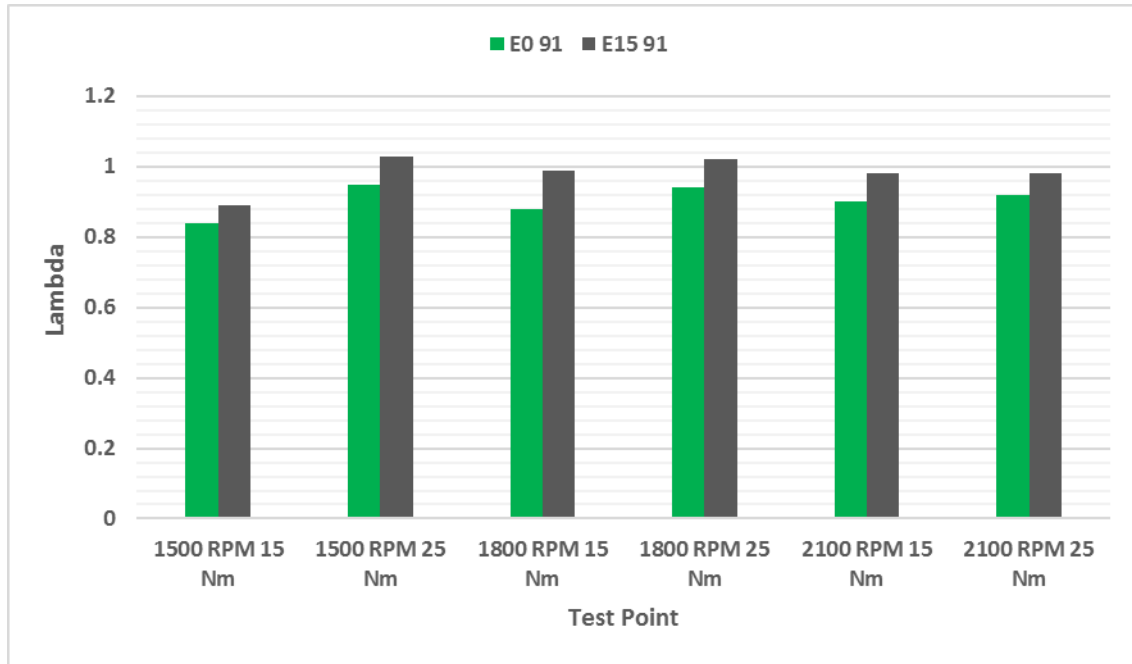

Figure 4.22: Effect of ethanol content on lambda values for 0° spark advance

The Figure 4.23 shows that the BSFC values decreased with an increase in ethanol content. Due to a more complete combustion process, lesser amount of fuel was required for generating the same power. This was reflected in lower BSFC values.
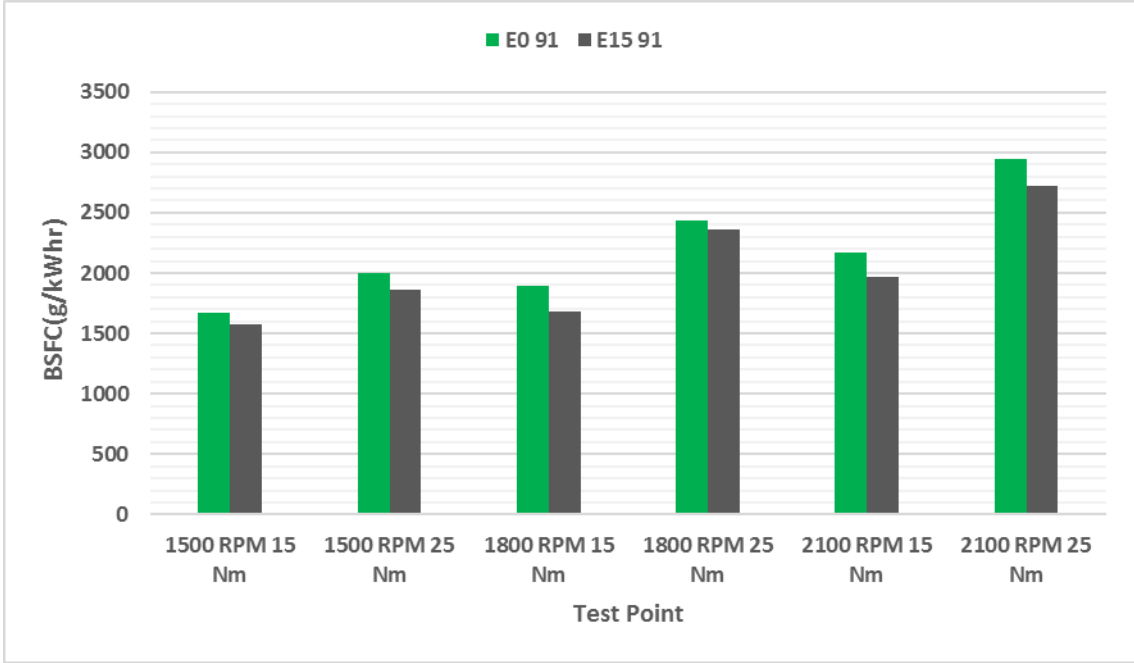
Figure 4.23: Effect of ethanol content on BSFC for 0° spark advance

4.4.2   E0 vs. E15 for 10° spark advance

Figure 4.24 shows a comparison between E0 91 and E15 91 for 10° spark advance for cylinder 2. The values of the 95th percentile peak-to-peak values are similar at all test points. The maximum change occurs at 1800 RPM and 25 Nm load point where the 95th percentile for E15 91 increased by 6%. In spite of this change, since the 95th percentile peak-to-peak value did not exceed the knock threshold of 100 kPa, it can be said that the tendency of knock increased at this test point but had not resulted in actual engine knock. The only knocking condition that was recorded was for 2100 RPM for both fuel blends.
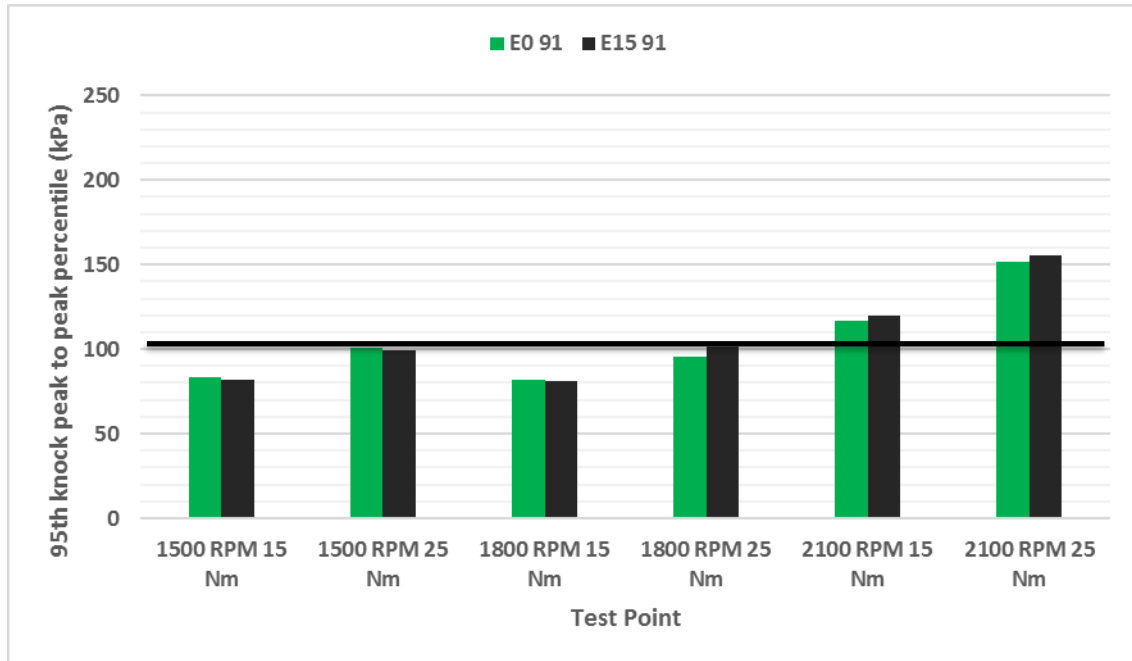

Figure 4.24: Effect of ethanol content on 95th percentile of peak-to-peak variation for 10° spark advance

Figure 4.25 shows the effect of ethanol content on cylinder block vibrations for 10° spark advance. The trends shown in Figure 4.24 are well matched in Figure 4.25. In cases where knock was detected based on pressure values in Figure 4.24, there was an increase in cylinder block vibration levels. The only exception to this was the 1800 RPM / 25 Nm case where, though marginal knock was detected for E15 91, the vibration levels were higher for E0 91.
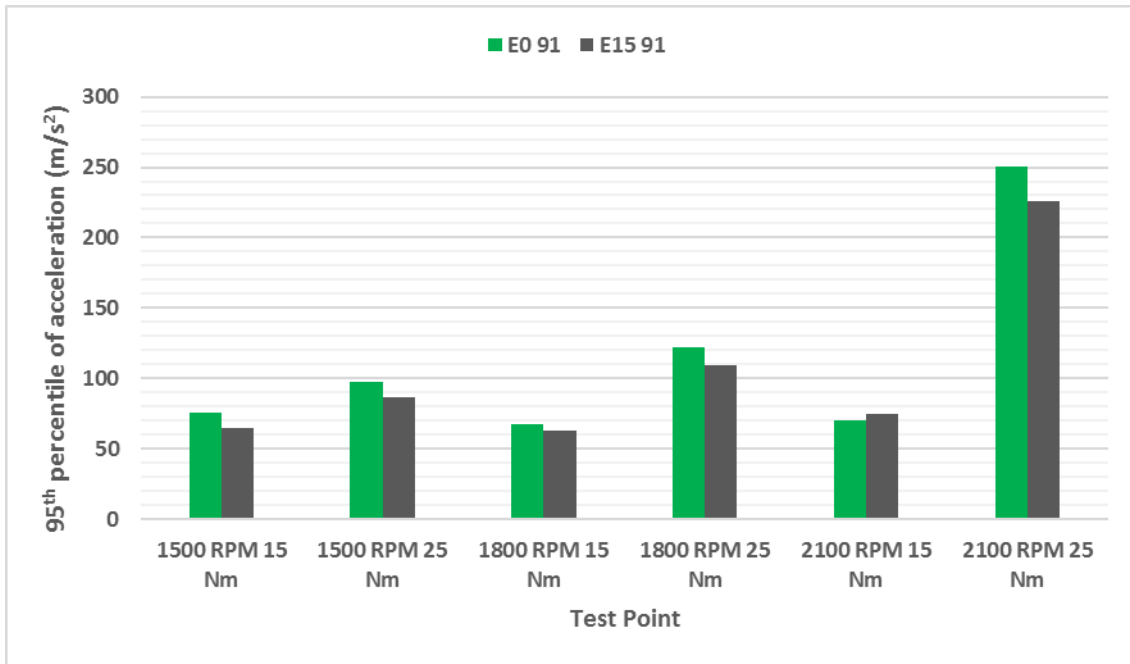
Figure 4.25: Effect of change in fuel ethanol content on peak-to-peak vibrations for 10° spark advance

Figure 4.26 shows the increase in exhaust gas temperature with higher ethanol content. Figure 4.27 also shows an increase in lambda values as the ethanol content increased. This led to an increase in combustion temperature and consequently the exhaust gas temperature increase.
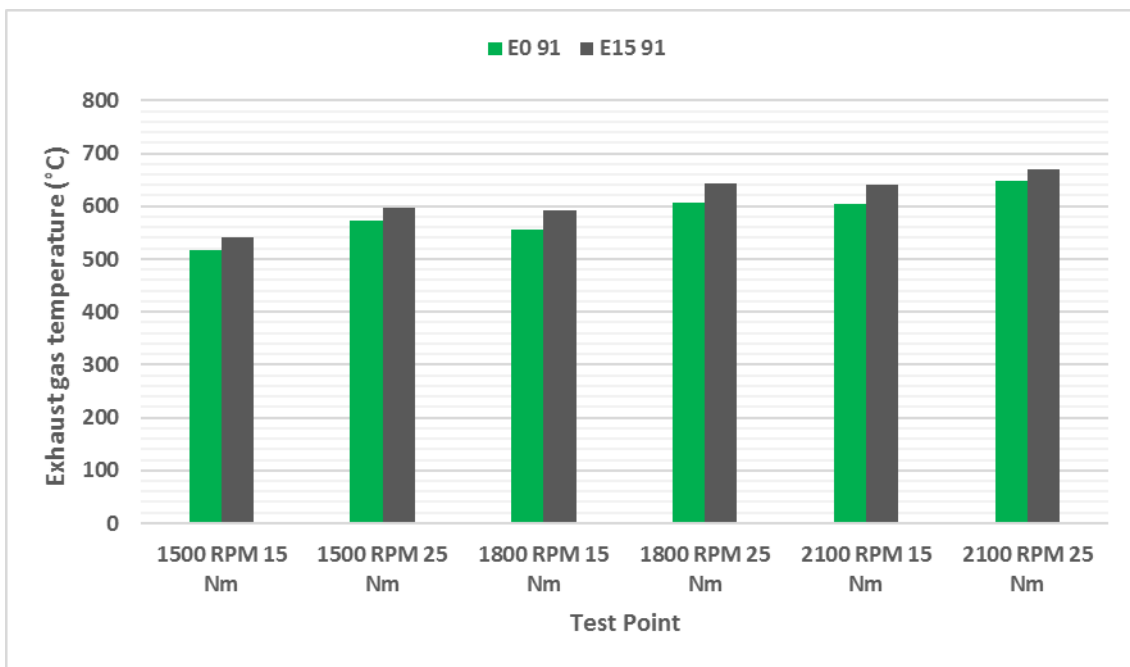

Figure 4.26: Effect of ethanol content on exhaust gas temperature for 10° spark advance
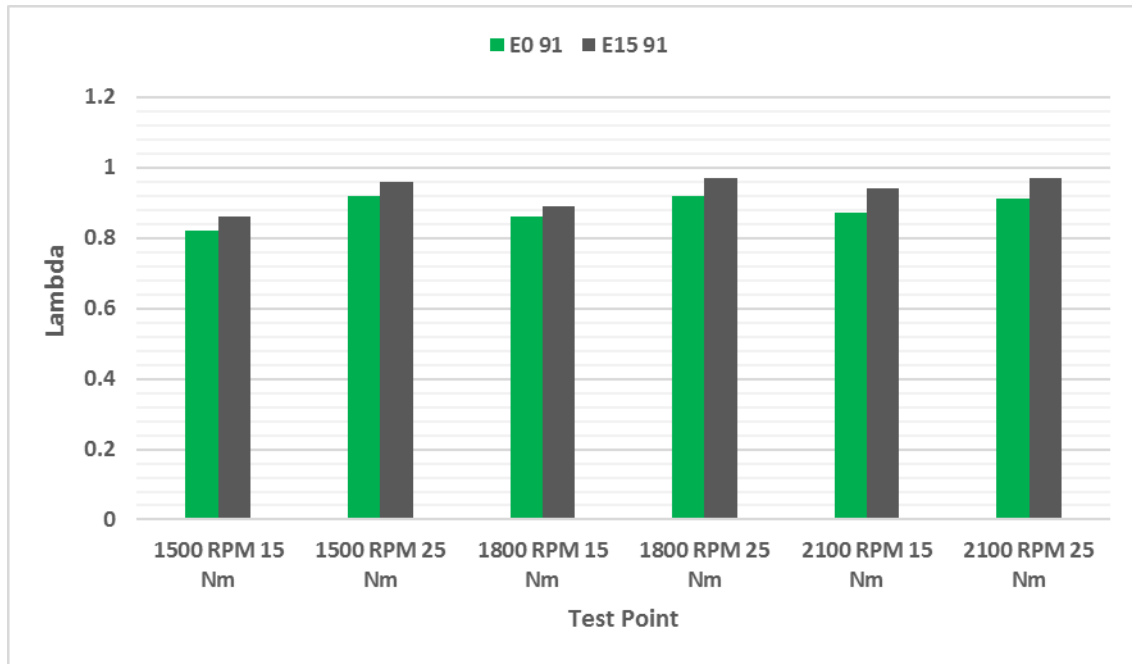
Figure 4.27: Effect of ethanol content on lambda values for 10° spark advance

Figure 4.28 shows a mixed response of BSFC to change in ethanol content. While the expected trend of lower BSFC was followed for the higher loads, the trend was opposite for lower loads.
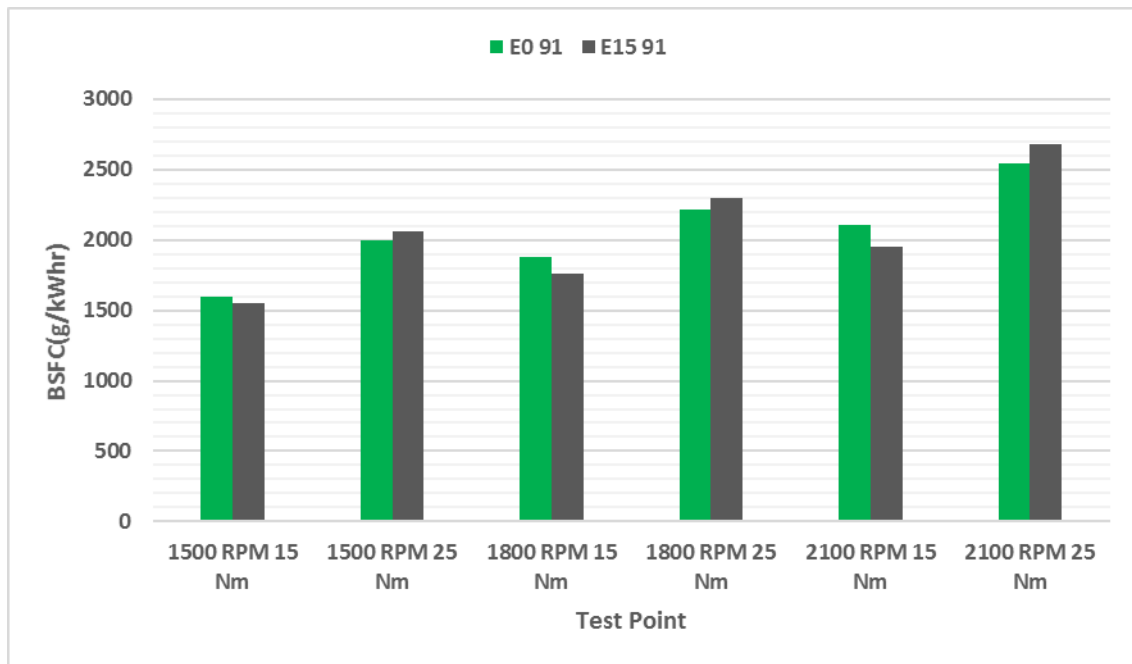

Figure 4.28: Effect of ethanol content on BSFC for 10° spark advance

4.4.3 E0 vs. E15 for 20° spark advance

Figure 4.29 shows the 95th percentile peak-to-peak variation for E0 91 and E15 91 at 20° spark advance. E15 consistently reduced the knocking tendency of the engine. The latent heat of vaporization of ethanol is higher than gasoline, resulting in ethanol absorbing a larger amount of energy for evaporation. This led to a reduction in the end gas temperature for E15 91 compared to E0 91. As the knocking tendency of the engine is directly related to the end gas temperature, the knocking intensity also decreased.
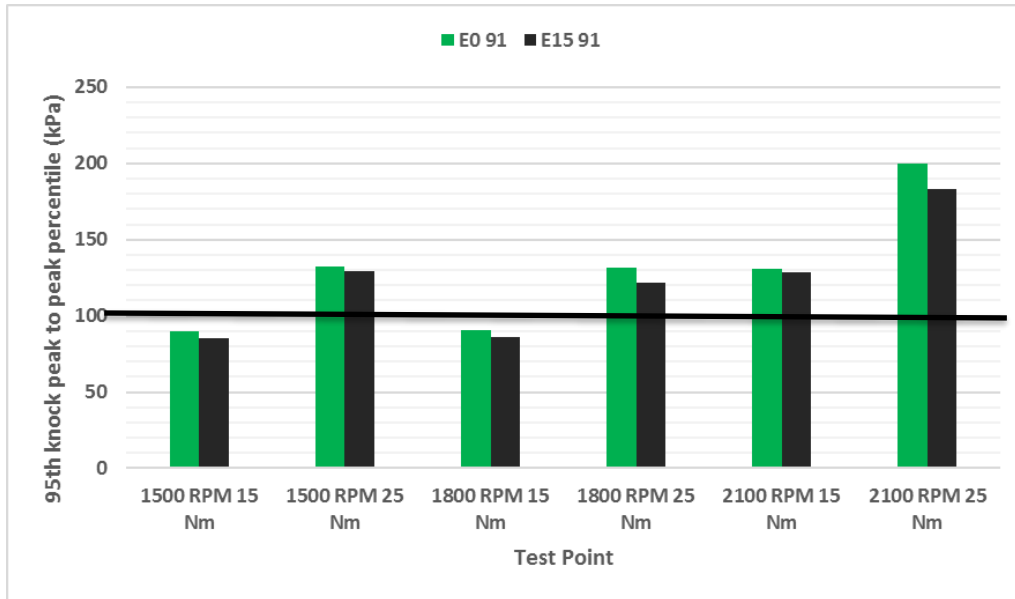

Figure 4.29: Effect of ethanol content on 95th percentile of peak-to-peak variation for 20° spark advance

Figure 4.30 shows an increase in vibrations for the 2100 RPM / 25 Nm case. This was identified as a knocking case in Figure 4.29 as well. This supports the increase in cylinder block vibration levels for this case. However, the vibrations for E0 91 fuel are lower than E15 91 even though the knocking tendency was higher for E0 91. This was a deviation from the expected trend. Also, for all the cases identified as knocking in Figure 4.29 an increase in cylinder block vibration levels were observed.

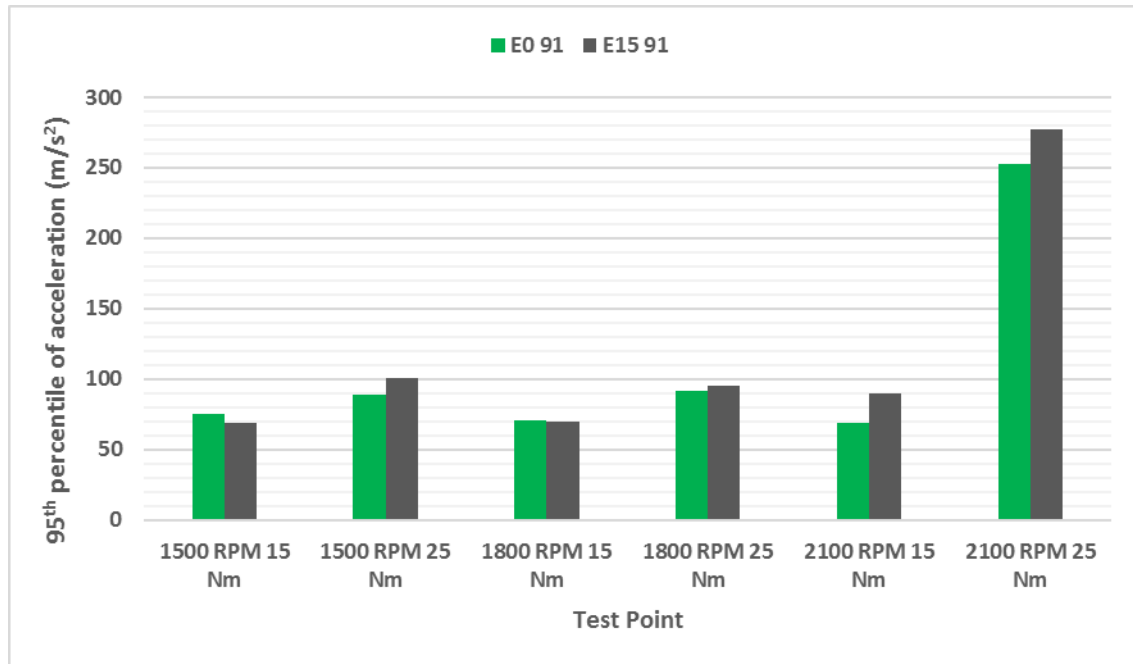Figure 4.30: Effect of ethanol content on 95th percentile of peak-to-peak vibrations for 20° spark advance

Figure 4.31 shows the same trend for exhaust gas temperature as discussed in sections 4.4.1 and 4.4.2. Figure 4.32 indicates a trend where the lambda values increased as the ethanol content of the fuel increased. This led to a higher combustion temperature thereby increasing the exhaust gas temperature.
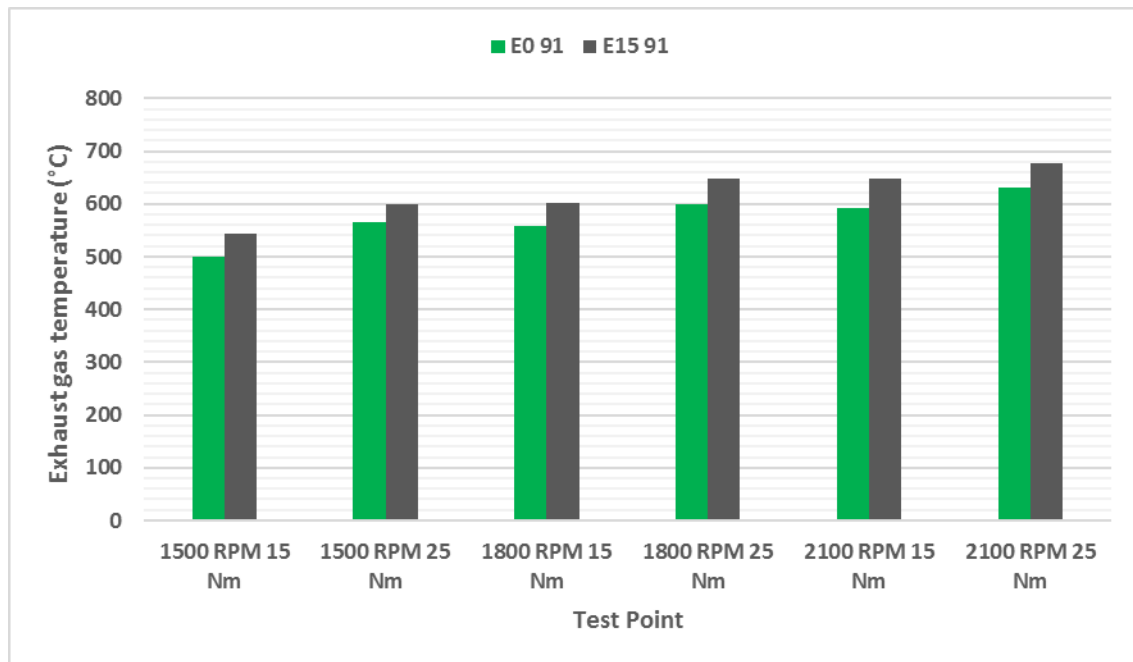
Figure 4.31: Effect of ethanol content on exhaust gas temperature for 20° spark advance

Figure 4.32: Effect of ethanol content on lambda values for 20° spark advance

Figure 4.33 shows a decrease in BSFC values with an increase in ethanol content. This was the same trend as discussed in sections 4.4.1 and 4.4.2. However, the 1500 RPM cases present an exception. The BSFC values were higher for E15 91 for these cases. This was due to a higher amount of throttle opening in order to attain the test point load condition.
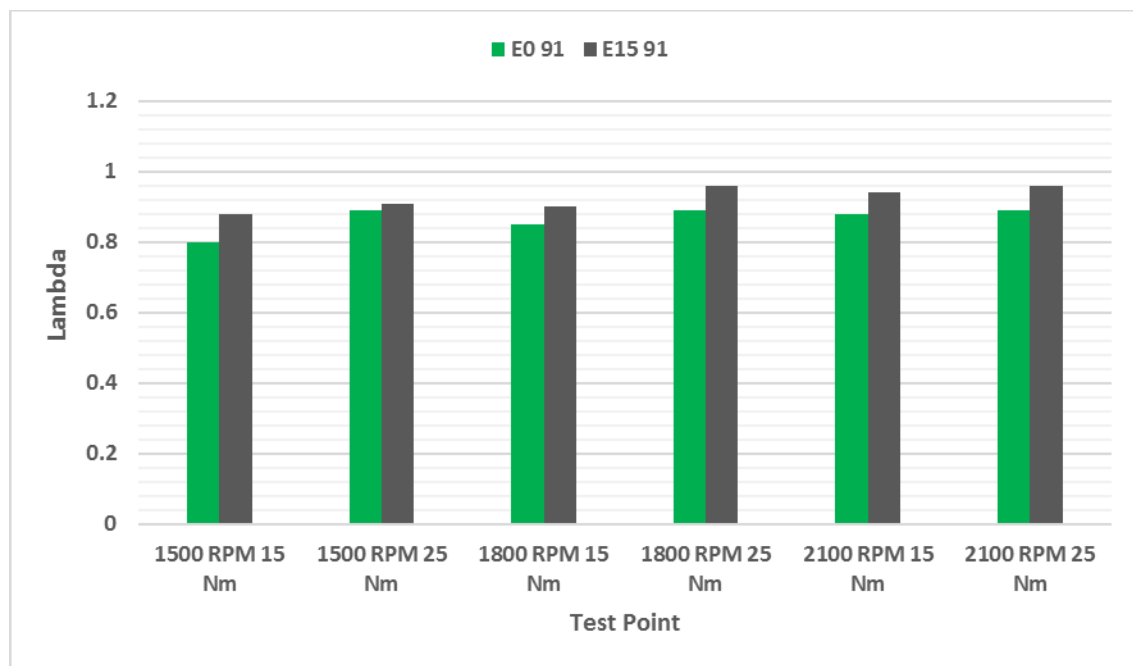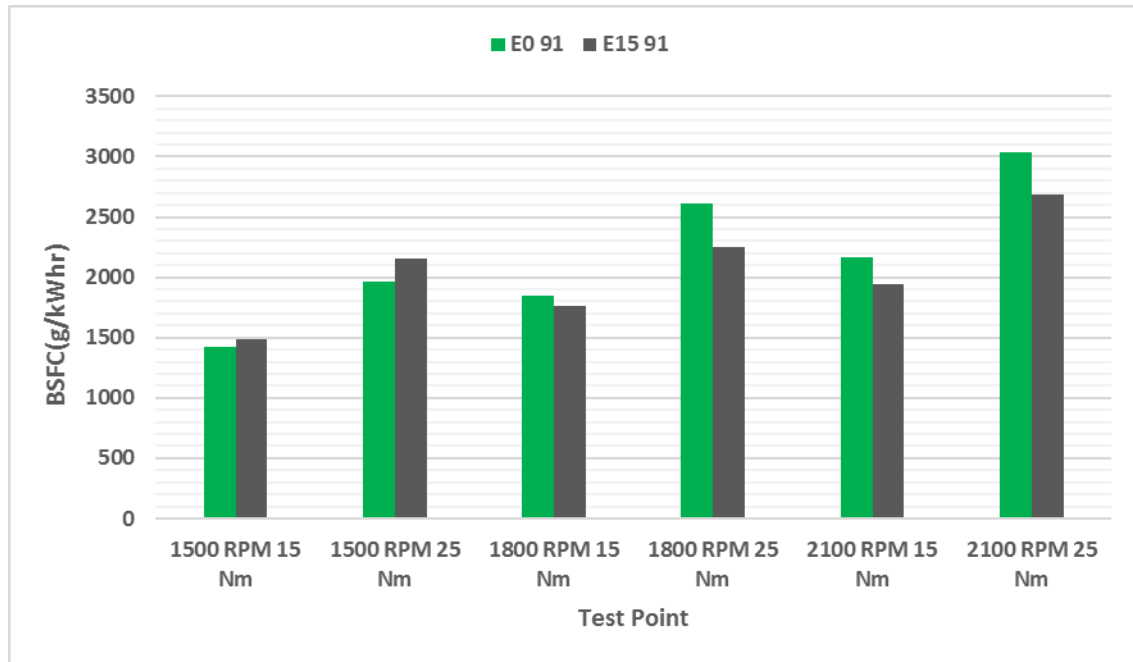
Figure 4.33: Effect of ethanol content on BSFC for 20° spark advance

4.5 Effect of Change in Fuel Octane Number on Knocking Tendency

In this section, the effect of changing the fuel octane on knock is discussed. E15 91 and E10 87 were used for comparison. Though there was a difference between the ethanol content of the fuel and the octane rating, the difference in octane number is expected to have a stronger influence on the knocking tendency.

4.5.1 E15 91 vs. E10 87 for 0° spark advance

Figure 4.34 presents the change in the 95th percentile of peak-to-peak variation for 0° spark advance. It was concluded that at lower loads (15 Nm), the effect of reduction in octane number dominates the increase in ethanol content and the knock intensity increased. This trend was reversed for the case of higher loads (25 Nm) where the 95th percentile for E10 87 showed a decrease in value irrespective of the engine speed. The maximum increase was 20% at 2100 RPM and 15 Nm load and the maximum reduction was 16 % at 1800 RPM and 25 Nm load.
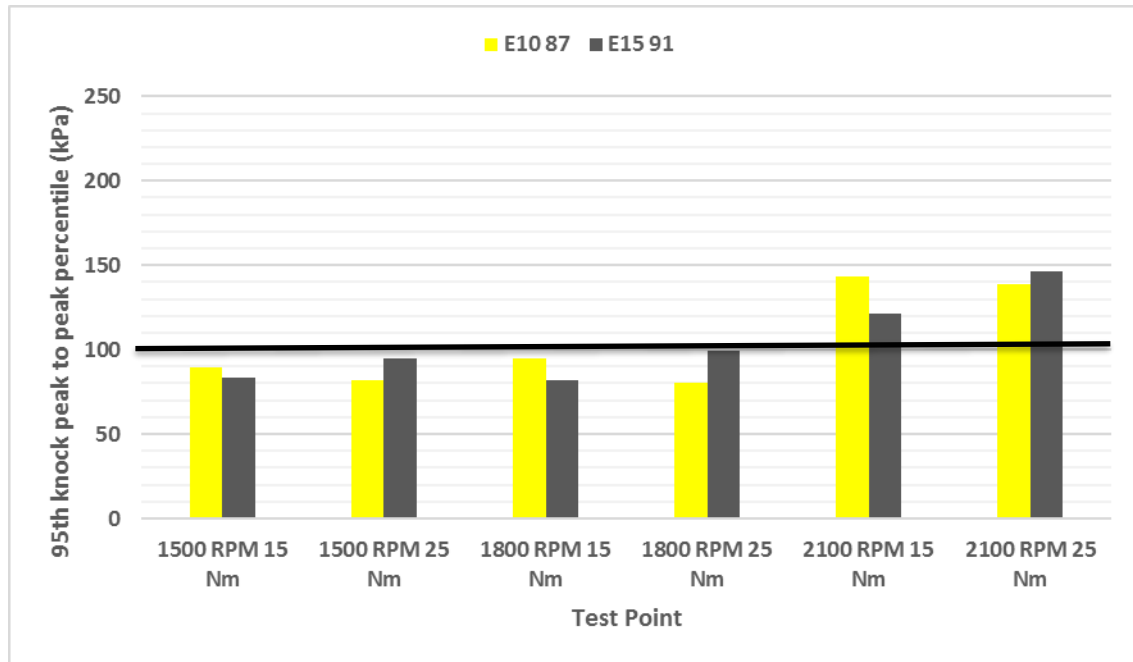
Figure 4.34: Effect of octane number on 95th percentile of peak-to-peak variation for 0° spark advance

Figure 4.35 shows higher levels of cylinder block vibrations for E15 91 fuel for higher load (25Nm) and lower for low load (15 Nm). This trend matches the trend presented in Figure 4.34. The highest values for vibrations were observed at the 2100 RPM and 25 Nm test point which also had the heaviest knock based on pressure data calculations. The exception was at 1800 RPM and 25 Nm test point where vibration levels for E15 91 were higher even though the knocking tendency was lower. This was related to the design of the engine since 1800 RPM data points present exception on multiple occasions.
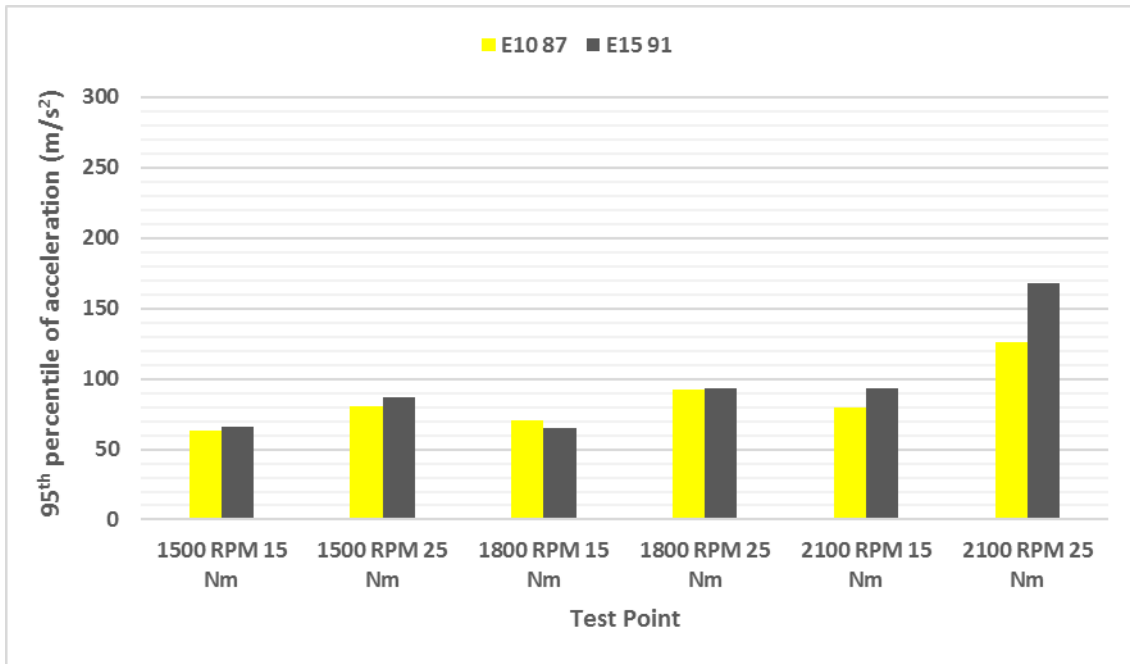
Figure 4.35: Effect of octane number on peak-to-peak vibration for 0° spark advance

Figure 4.36 shows a higher exhaust gas temperature for E15 91 in all cases. This is in line with the previous observations and can be attributed to an increase in lambda values with an increase in ethanol content of the fuel. The lambda values are shown in Figure 4.37

Figure 4.36: Effect of octane number on exhaust gas temperature for 0° spark advance

Figure 4.37: Effect of octane number on lambda values for 0° spark advance

Figure 4.38 shows a lower BSFC with an increase in ethanol content. This is in line with the expectations and the previous results from this section. The lower BSFC was due to a more complete combustion process thus requiring less fuel to generate the same power.

Figure 4.38: Effect of octane number on BSFC for 0° spark advance

4.5.2 E15 91 vs. E10 87 for 10° spark advance

Figure 4.39 shows the 10° spark advance data for E15 91 and E10 87 fuels. The trend remains similar to the one presented for 0° spark advance. However, the magnitude of variation is lower. The maximum rise in the 95th percentile value of approximately 8% occurred at the 1800 RPM and 25 Nm test point.
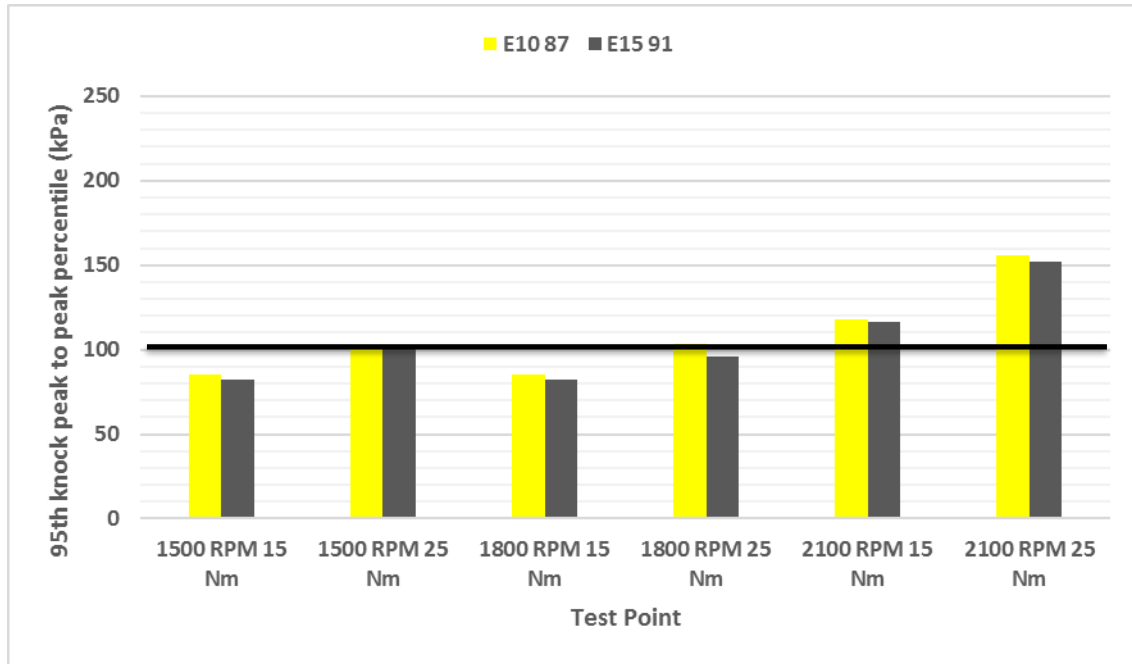
Figure 4.39: Effect of octane number on 95th percentile of peak-to-peak variation for 10° spark advance

Figure 4.40 shows a knocking case at the 2100 RPM and 25 Nm test point. This was also a point identified as knocking using pressure calculations. For other test points, cylinder block vibrations were higher for E15 91 fuel although its knocking tendency was lower in all the cases based on conclusions from Figure 4.39. This was not in line with the expected trend.

Figure 4.40: Effect of octane number on peak-to-peak vibrations for 10° spark advance

Figure 4.41 shows higher exhaust gas temperatures with an increase in ethanol content. This was in line with the previous observations and was attributed to an increase in lambda values with an increase in ethanol content of the fuel. The lambda values are shown in Figure 4.42
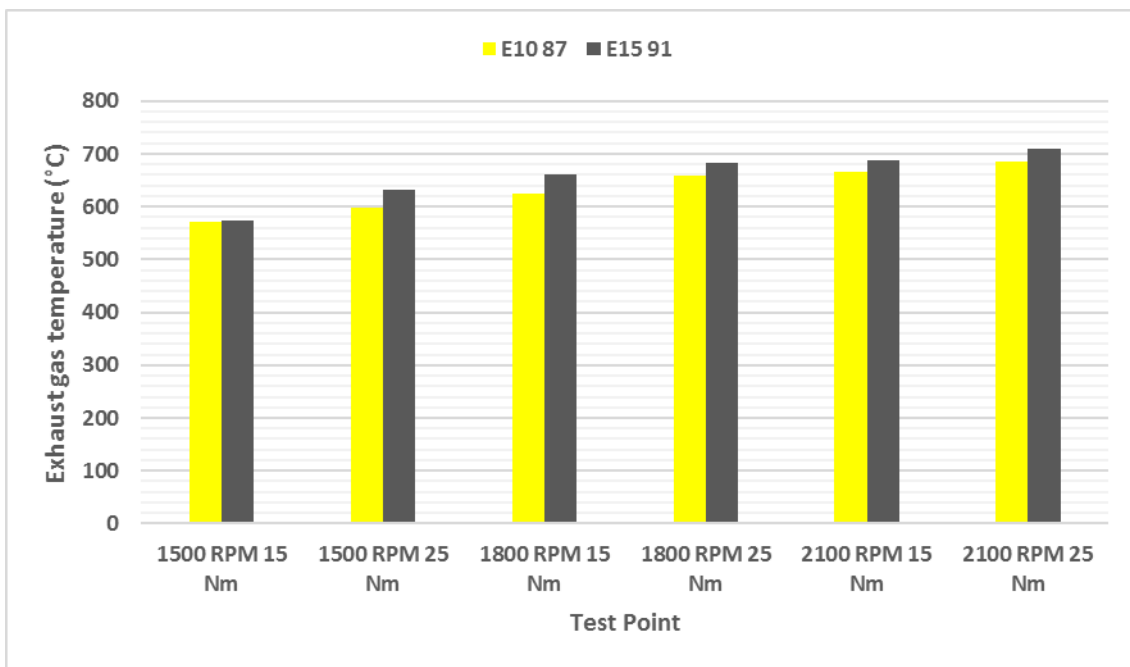

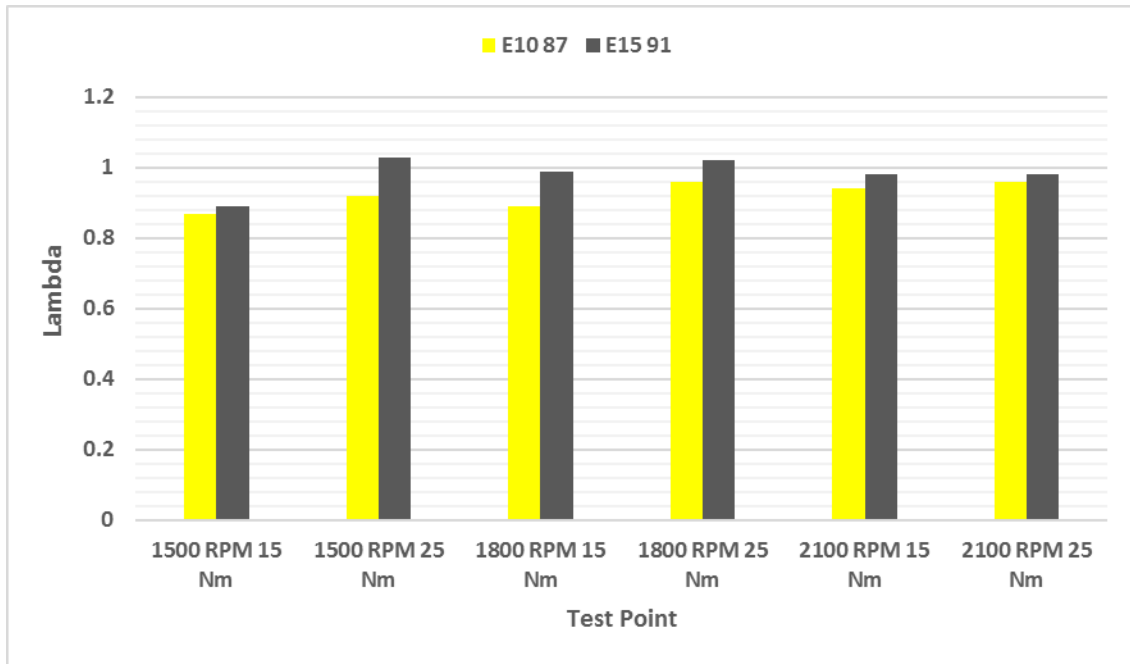Figure 4.41: Effect of octane number on exhaust gas temperature for 10° spark advance

Figure 4.42: Effect of octane number on lambda values for 10° spark advance

Figure 4.43 shows lower BSFC values for fuel with higher ethanol content. This was in line with the expected trend and the results from the previous sections of this study.
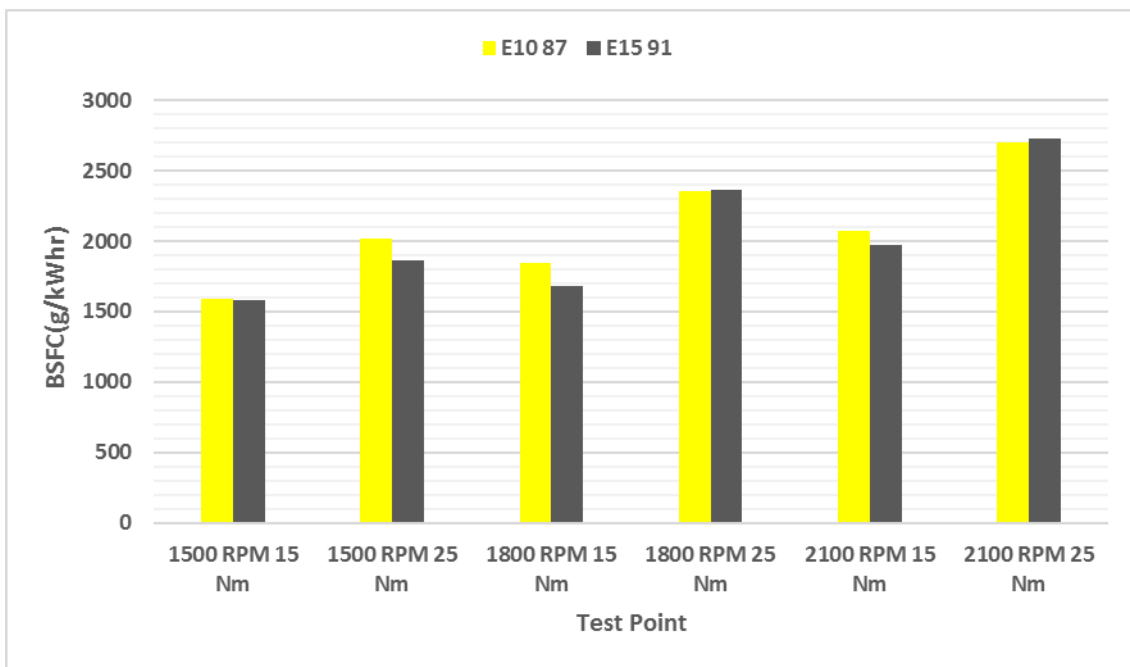

Figure 4.43: Effect of octane number on BSFC for 10° spark advance

4.5.3 E15 91 vs. E10 87 for 20° spark advance

Figure 4.44 shows the comparison for 20° spark advance with E15 91 and E10 87 fuels. The 95th percentile value for E10 87 fuel was higher than that of E15 91. This trend was the same as observed for 0° and 10° spark advance in the earlier sections 4.5.1 and 4.5.2. Considering the simultaneous effect of higher ethanol content and higher-octane number this result was in line with the expectation.
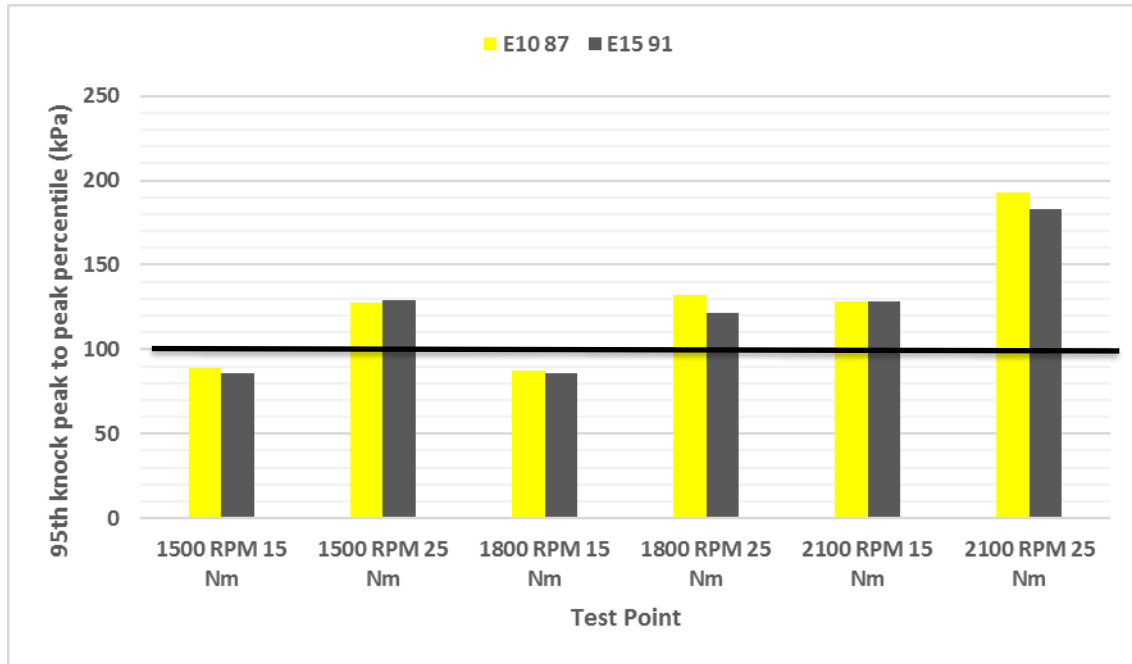
Figure 4.44: Effect of change in fuel octane number on 95th percentile of peak-to-peak variation for 20° spark advance

All cases in Figure 4.44, except 1500 RPM and 1800 RPM low load (15Nm) were identified as knocking conditions based on pressure data analysis.

Figure 4.45 show a rise in cylinder block vibration levels for the 2100 RPM and 25 Nm test point. Since this point was identified as a knocking case based on cylinder pressure data, this result was in line with the expectation. For other cases, the vibration levels for E10 87 were much lower than E15 91 even though the knocking tendencies based on pressure were nearly equal. This contradicts the expectation.
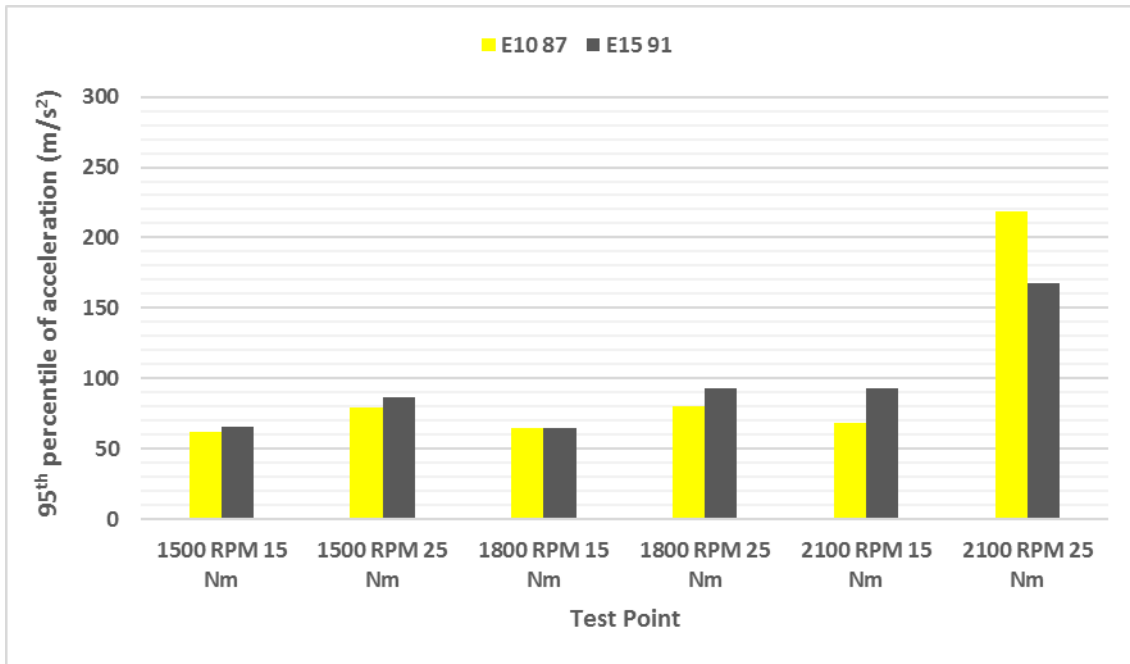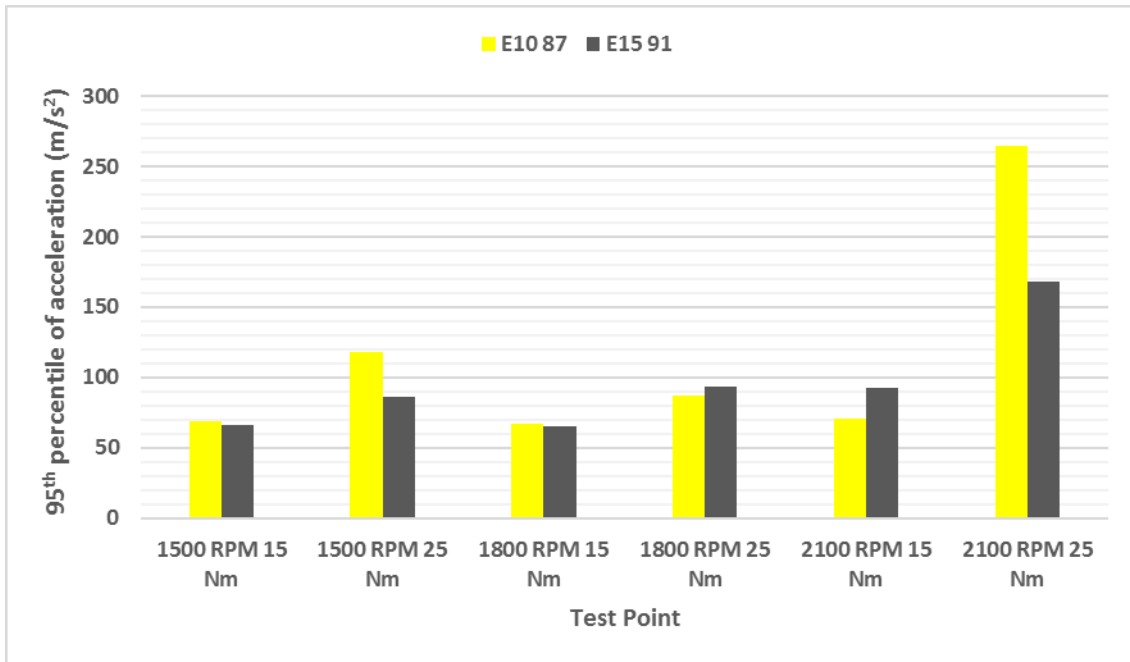
Figure 4.45: Effect of octane number on peak-to-peak vibrations for 20° spark advance

Figure 4.46 shows higher exhaust gas temperatures with an increase in ethanol content. This is in line with the previous observations and was attributed to an increase in lambda values with an increase in ethanol content of the fuel. The lambda values are shown in Figure 4.47
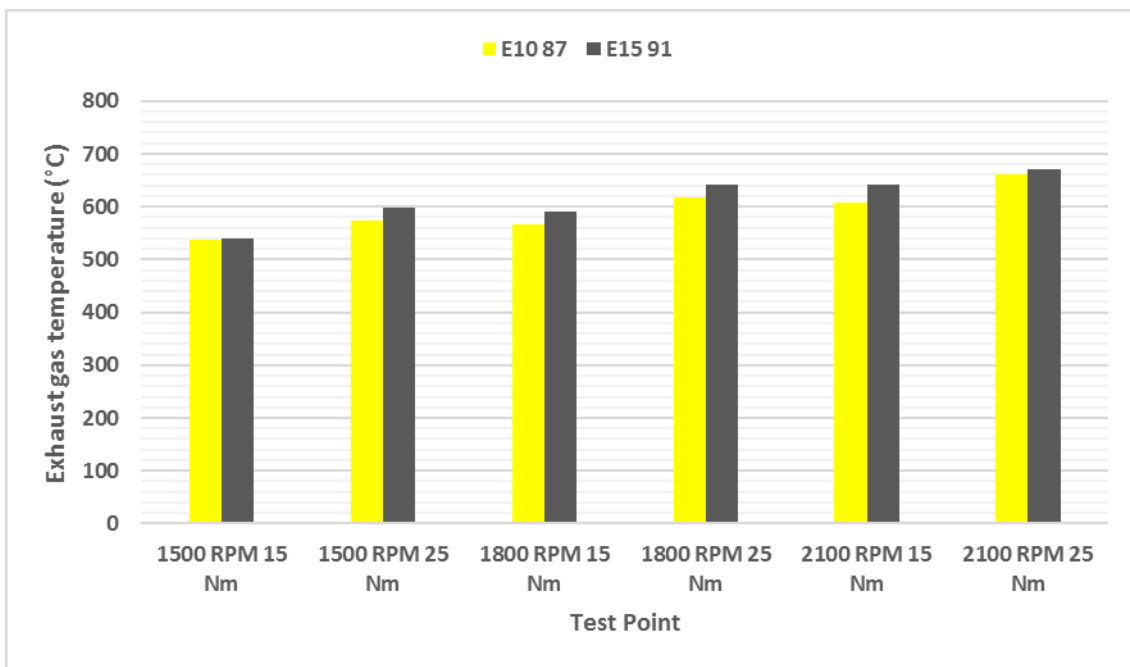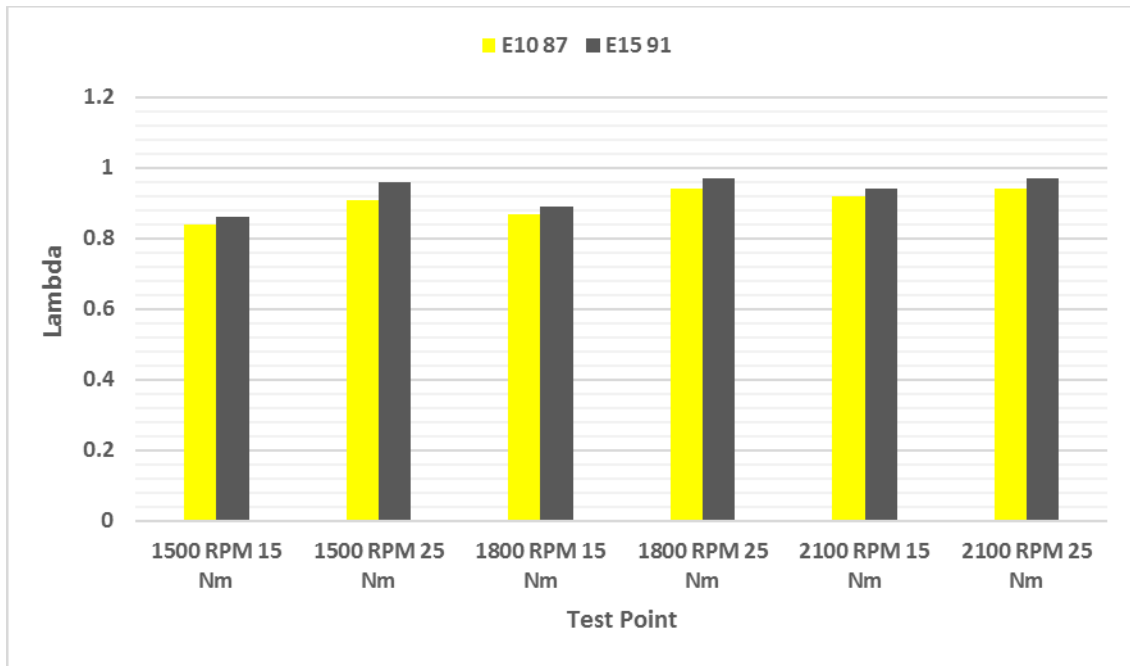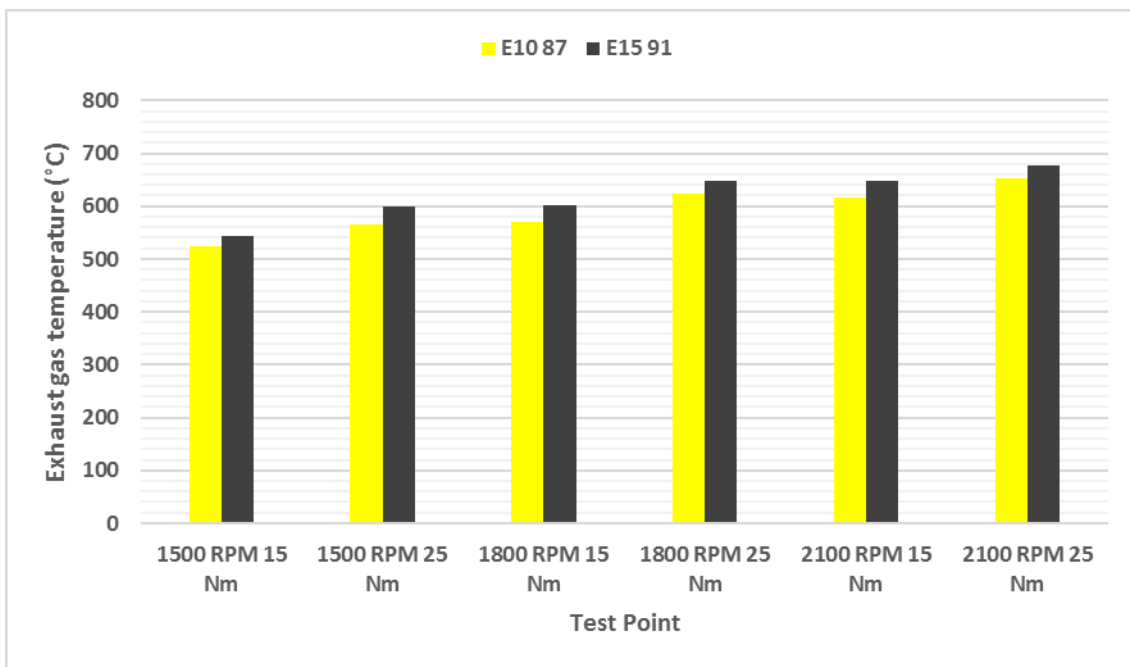

Figure 4.46: Effect of octane number on exhaust gas temperature for 20° spark advance
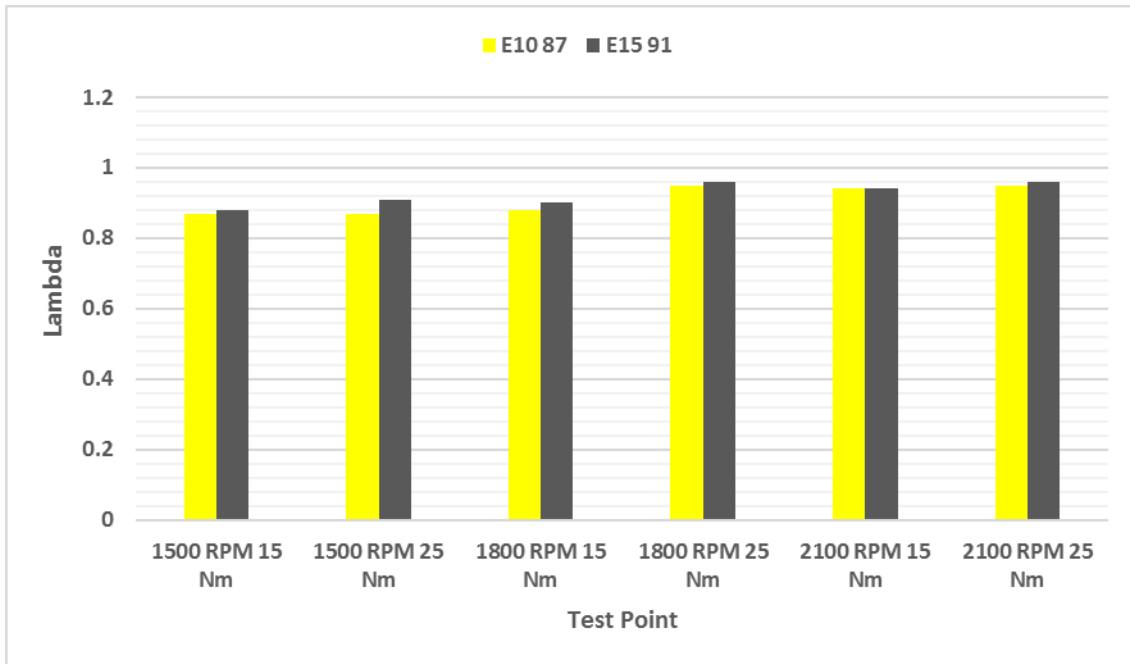
Figure 4.47: Effect of octane number on lambda values for 20° spark advance

Figure 4.48 shows lower BSFC values for fuel with higher ethanol content. This was in line with the expected trend and the results from the previous sections of this study.
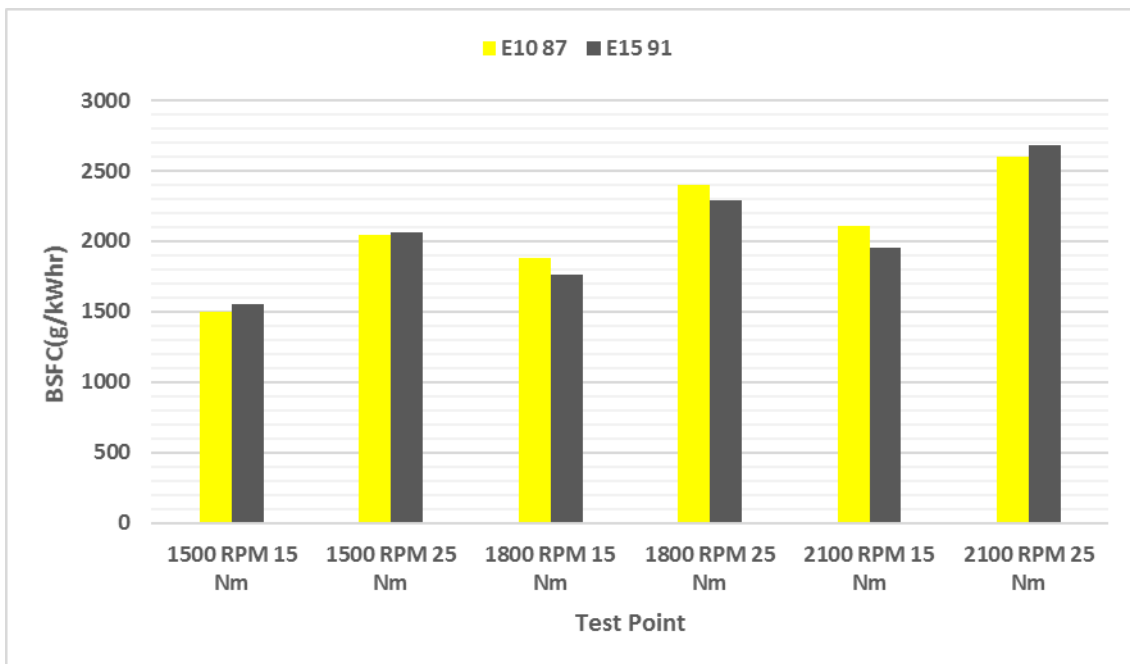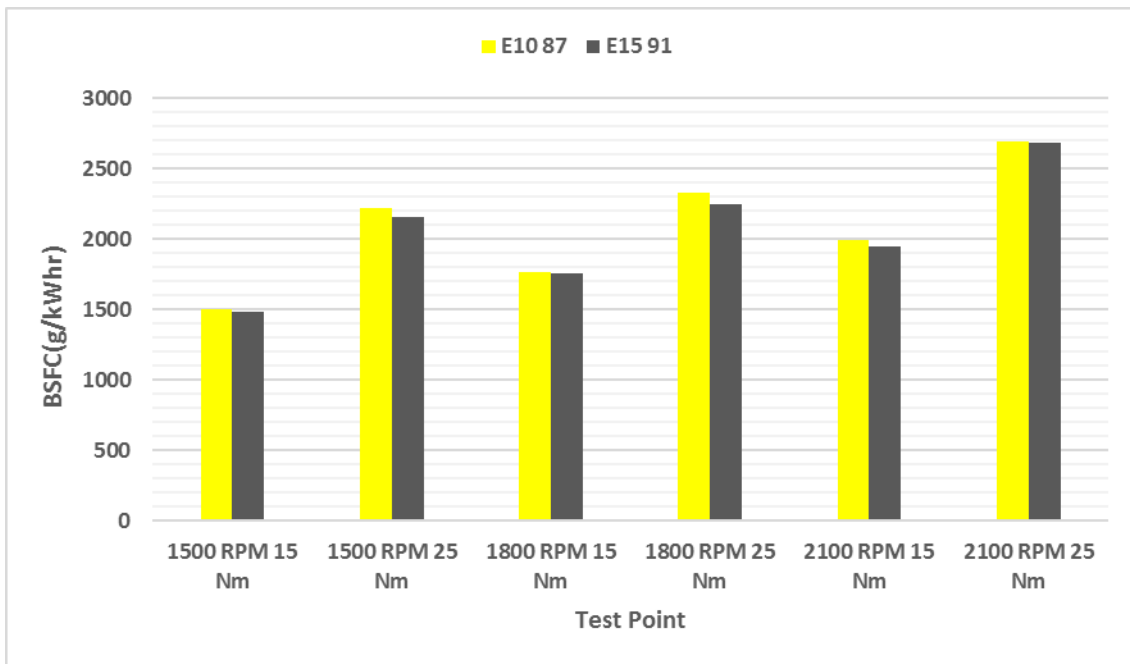

Figure 4.48: Effect of octane number on BSFC for 20° spark advance

5   Conclusions

- Pressure based knock intensity was observed to increase with an increase in spark advance regardless of the fuel or speed load conditions.
- An increase in ethanol content suppressed the knocking tendency of the engine.
- The combined effect of increase in ethanol content and octane rating of the fuel was found to suppress the knocking tendency of the engine.
- The accelerometer based knock intensity was not as consistent as the pressure based knock intensity.
- The increase in ethanol content leads to higher exhaust gas temperature. Since the engine had an open loop control for lambda, the fuels with a higher ethanol content had lambda values closer to stoichiometric thus resulting in higher flame temperature.
- The BSFC was lower for fuels with higher ethanol content mainly due to the reduction in amount of unburnt fuel.
- The use of in-cylinder pressure measurement for knock identification was found to be more accurate than accelerometer-based measurements.

6 References

1. Heywood, John B. Internal combustion engine fundamentals. Vol. 930. New York: Mcgraw-hill, 1988.

2. Lee, Seokhwan, Choongsik Bae, Robert Prucka, Gerald Fernandes, Zoran Filipi, and Dennis N. Assanis. Quantification of thermal shock in a piezoelectric pressure transducer. No. 2005-01-2092. SAE Technical Paper, 2005.

3. Bueno, André V., José A. Velásquez, and Luiz F. Milanez. "Internal Combustion Engine Indicating Measurements." In Applied Measurement Systems. InTech, 2012.

4. Wang, Zhi, Hui Liu, and Rolf D. Reitz. "Knocking combustion in spark-ignition engines." Progress in Energy and Combustion Science 61 (2017): 78-112.

5. Zhen, Xudong, Yang Wang, Shuaiqing Xu, Yongsheng Zhu, Chengjun Tao, Tao Xu, and Mingzhi Song. "The engine knock analysis–an overview." Applied Energy 92 (2012): 628-636.

6. Randolph, Andrew L. Cylinder-pressure-transducer mounting techniques to maximize data accuracy. No. 900171. SAE Technical Paper, 1990.

7. Bi, Fengrong, Teng Ma, Jian Zhang, Lin Li, and Chunfang Shi. "Knock Detection in Spark Ignition Engines Base on Complementary Ensemble Empirical Mode Decomposition-Hilbert Transform." Shock and Vibration 2016 (2016).

8. Shahlari, Arsham J., and Jaal B. Ghandhi. A comparison of engine knock metrics. No. 2012-32-0007. SAE Technical Paper, 2012.

9. Naber, Jeffrey, Jason R. Blough, Dave Frankowski, Monroe Goble, and John E. Szpytman. Analysis of combustion knock metrics in spark-ignition engines. No. 2006-01-0400. SAE Technical Paper, 2006.

10. Bertola, Andrea, Reinhold Dolt, and Jens Höwing. The Use of Spark Plug Pressure Transducers for Engine Indication Measurements-Possibilities and Limits. No. 2015-26-0041. SAE Technical Paper, 2015.

11. Chun, Kwang Min, and Kyung Woon Kim. Measurement and analysis of knock in a SI engine using the cylinder pressure and block vibration signals. No. 940146. SAE Technical Paper, 1994.

7 Appendix

7.1 Test Matrix

The adjoining table shows the test matrix followed for this study. A total of 54 test points were considered which were distributed over three speeds, a high and a low load point for every speed, three fuels and three sparks advances for cylinder two. The combustion data is recorded for 300 cycles at every test point while the engine and dyno data is recorded for three minutes. Since the engine does not have an ECU, the spark timing cannot be changed dynamically. The spark timing remains constant for the entire duration of the test.

Table 7.1: Test Matrix

Test Number	Speed (RPM)	Load (Nm)	GIMEP (bar)	Spark advance (deg)	Fuel
1	1500	15	3.57	0	E0 91
2	1500	25	5.50	0	E0 91
3	1800	15	3.64	0	E0 91
4	1800	25	5.55	0	E0 91
5	2100	15	3.70	0	E0 91
6	2100	25	5.62	0	E0 91
7	1500	15	3.58	10	E0 91
8	1500	25	5.53	10	E0 91
9	1800	15	3.65	10	E0 91
10	1800	25	5.57	10	E0 91
11	2100	15	3.72	10	E0 91
12	2100	25	5.64	10	E0 91
13	1500	15	3.61	20	E0 91

14	1500	25	5.57	20	E0 91
15	1800	15	3.68	20	E0 91
16	1800	25	5.63	20	E0 91
17	2100	15	3.74	20	E0 91
18	2100	25	5.69	20	E0 91
19	1500	15	3.57	0	E15 91
20	1500	25	5.49	0	E15 91
21	1800	15	3.64	0	E15 91
22	1800	25	5.56	0	E15 91
23	2100	15	3.70	0	E15 91
24	2100	25	5.62	0	E15 91
25	1500	15	3.59	10	E15 91
26	1500	25	5.54	10	E15 91
27	1800	15	3.65	10	E15 91
28	1800	25	5.59	10	E15 91
29	2100	15	3.72	10	E15 91
30	2100	25	5.65	10	E15 91
31	1500	15	3.61	20	E15 91
32	1500	25	5.57	20	E15 91
33	1800	15	3.67	20	E15 91
34	1800	25	5.61	20	E15 91
35	2100	15	3.74	20	E15 91
36	2100	25	5.68	20	E15 91
37	1500	15	3.57	0	E10 87

| 38	1500	25	5.50	0	E10 87
39	1800	15	3.64	0	E10 87
40	1800	25	5.55	0	E10 87
41	2100	15	3.71	0	E10 87
42	2100	25	5.62	0	E10 87
43	1500	15	3.59	10	E10 87
44	1500	25	5.55	10	E10 87
45	1800	15	3.66	10	E10 87
46	1800	25	5.60	10	E10 87
47	2100	15	3.73	10	E10 87
48	2100	25	5.66	10	E10 87
49	1500	15	3.61	20	E10 87
50	1500	25	5.57	20	E10 87
51	1800	15	3.68	20	E10 87
52	1800	25	5.62	20	E10 87
53	2100	15	3.75	20	E10 87
54	2100	25	5.68	20	E10 87

7.2 Engine Stability Parameters
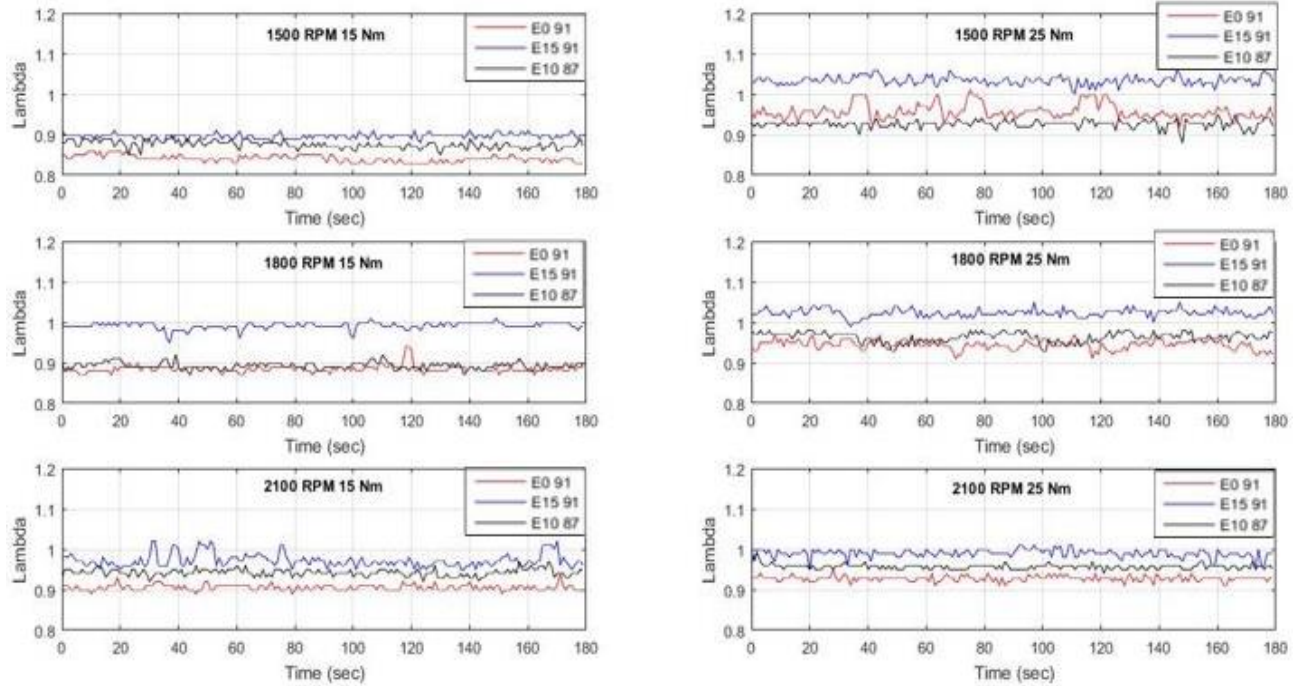
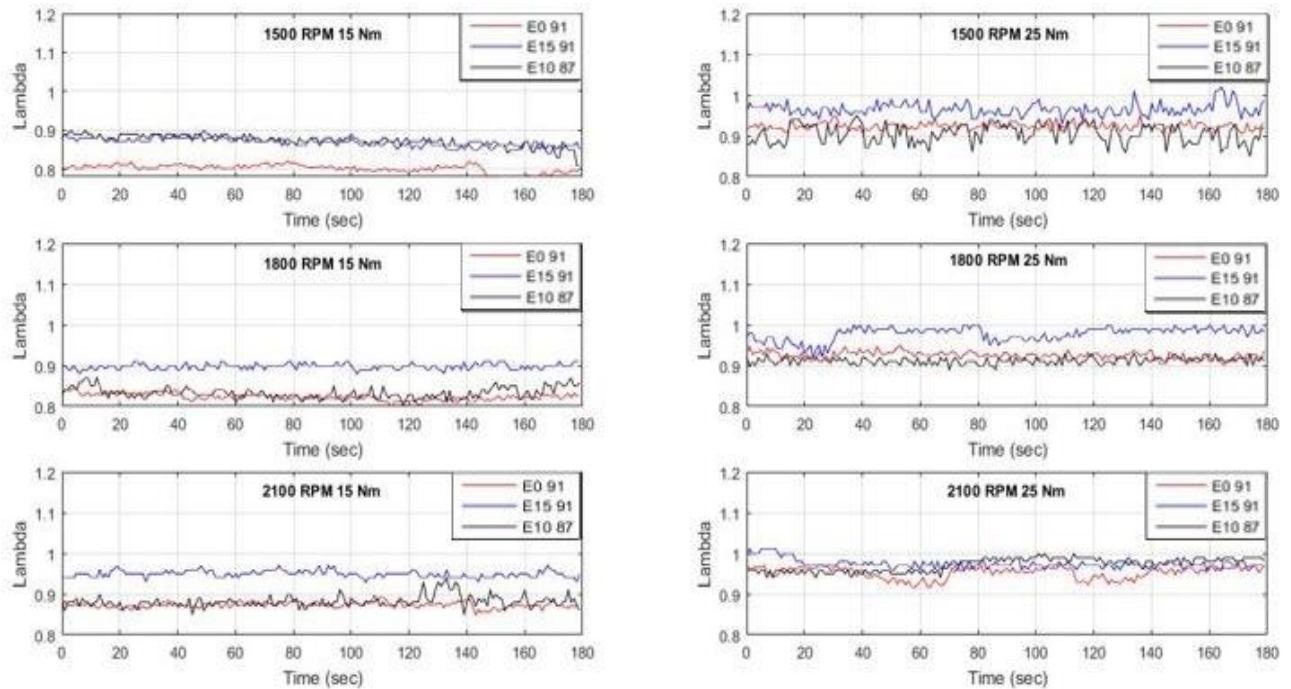Figure 7.1: Variation of lambda with time at 0 deg spark advance for E0 91, E15 91 and E10 87 fuels

Figure 7.2: Variation of lambda with time at 10 deg spark advance for E0 91, E15 91 and E10 87 fuels
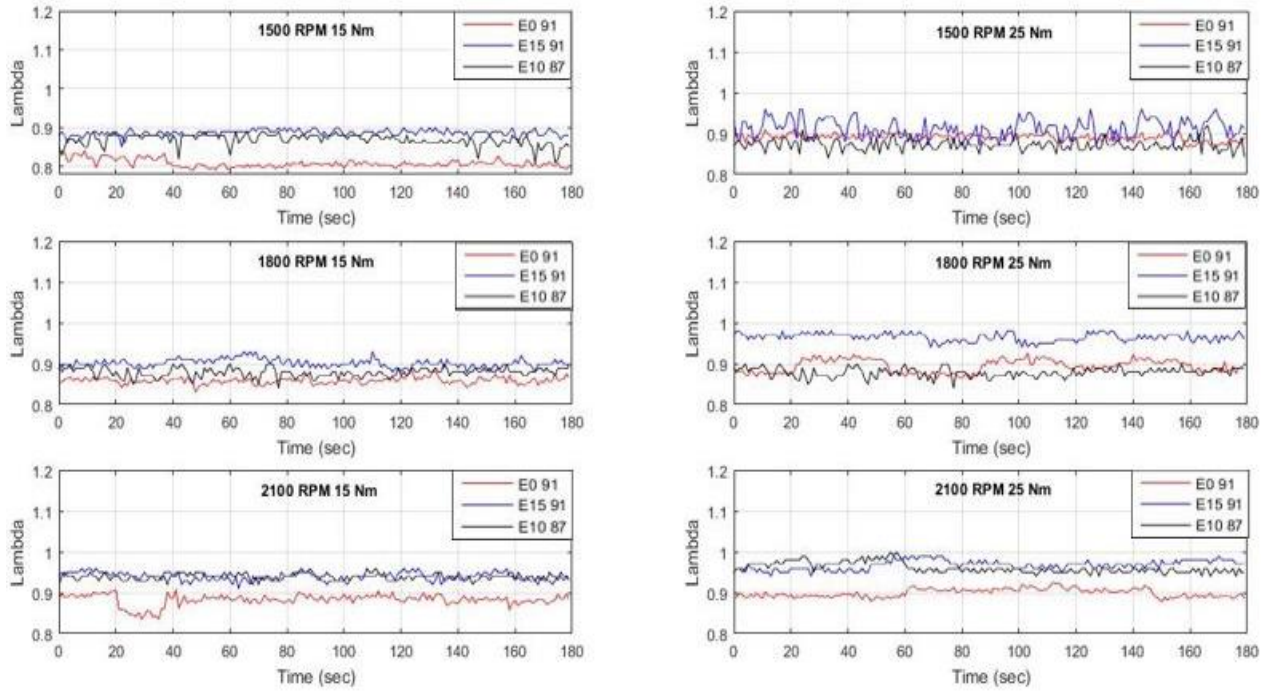
Figure 7.3: Variation of lambda with time at 20 deg spark advance for E0 91, E15 91 and E10 87 fuels

Figure 7.4: Variation of exhaust gas temperature for cylinder 2 with time at 0 deg spark advance for E0 91, E15 91 and E10 87 fuels

Figure 7.5: Variation of exhaust gas temperature for cylinder 2 with time at 10 deg spark advance for E0 91, E15 91 and E10 87 fuels
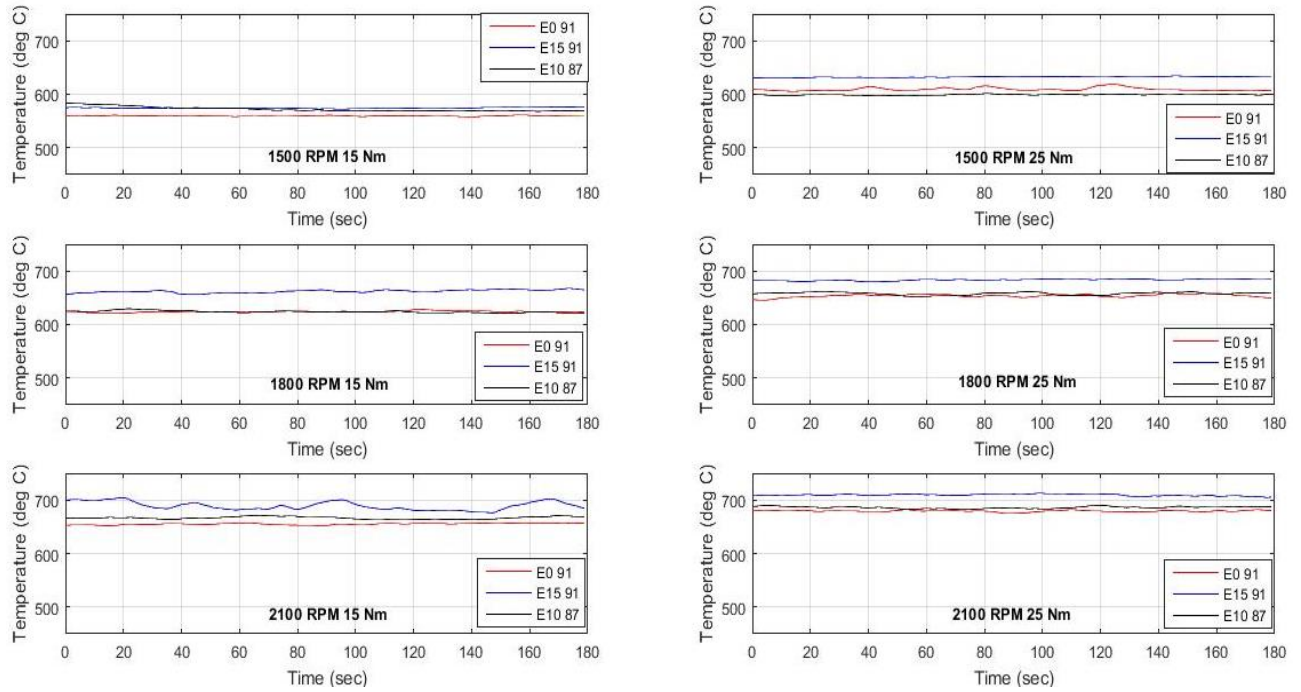

Figure 7.6: Variation of exhaust gas temperature for cylinder 2 with time at 20 deg spark advance for E0 91, E15 91 and E10 87 fuels
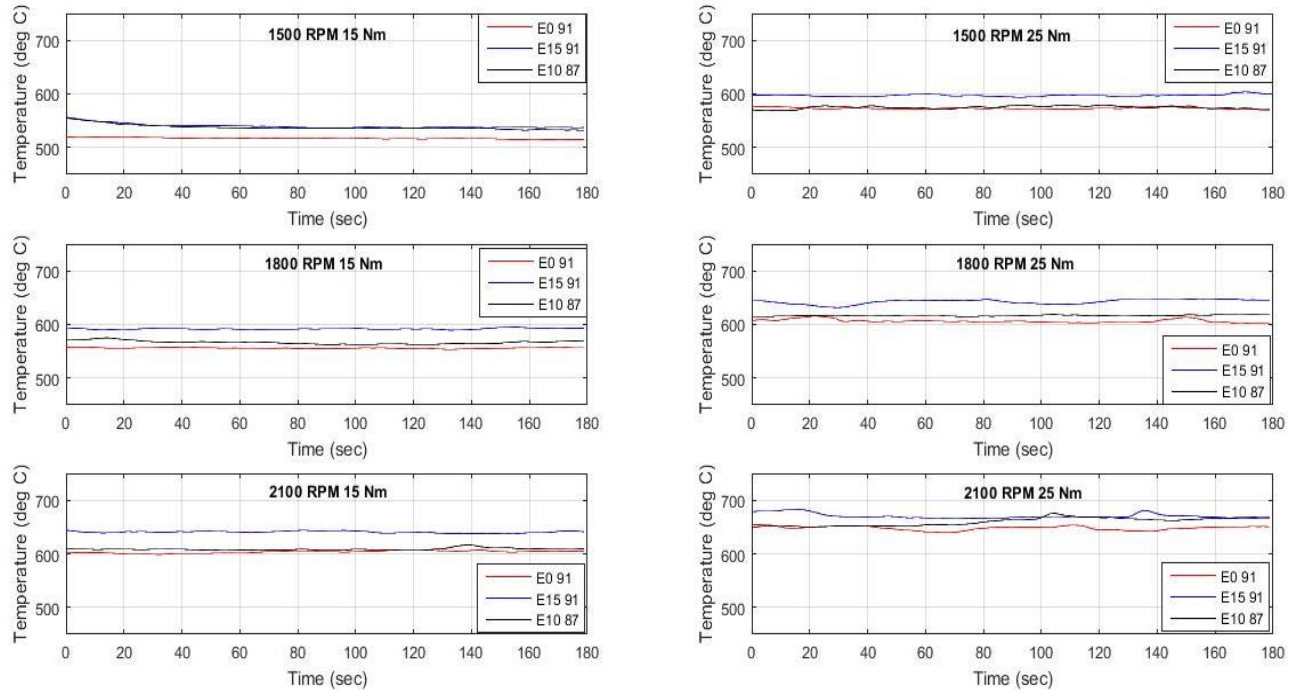
Figure 7.7: Variation of coolant out temperature with time at 0 deg spark advance for E0 91, E15 91 and E10 87

Figure 7.8: Variation of coolant out temperature with time at 10 deg spark advance for E0 91, E15 91 and E10 87 fuels
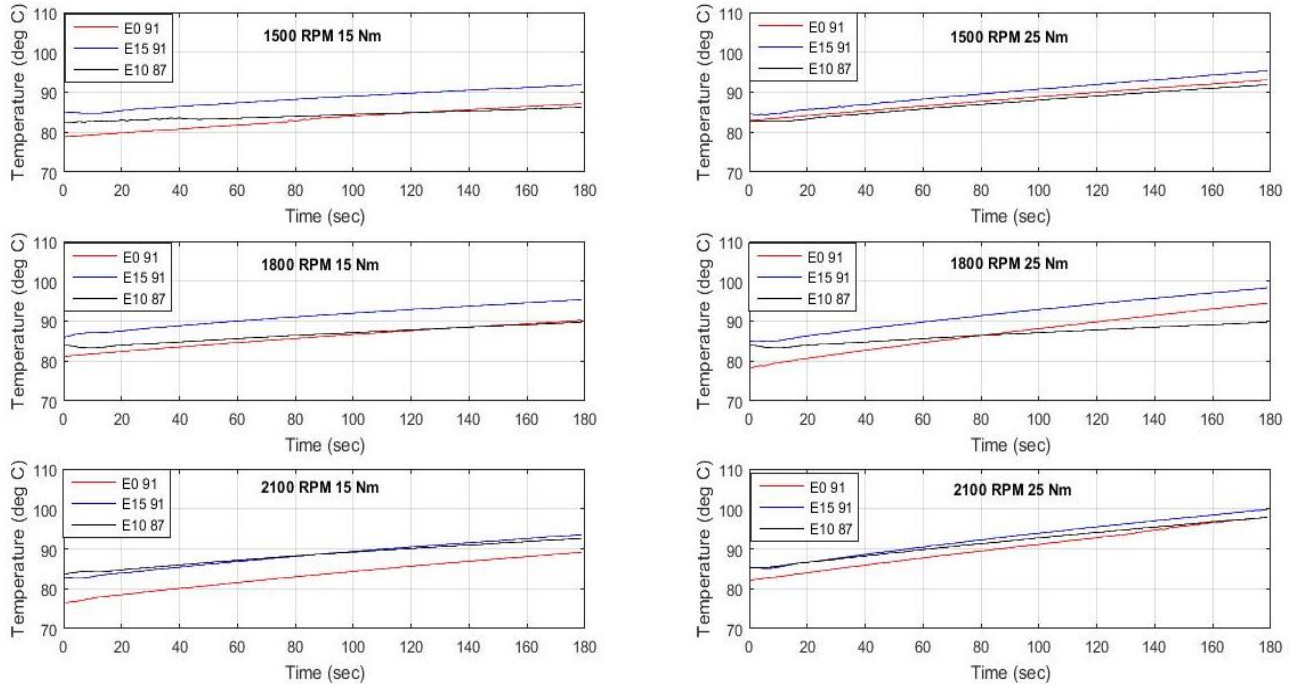
Figure 7.9: Variation of coolant out temperature with time at 20 deg spark advance for E0 91, E15 91 and E10 87 fuels
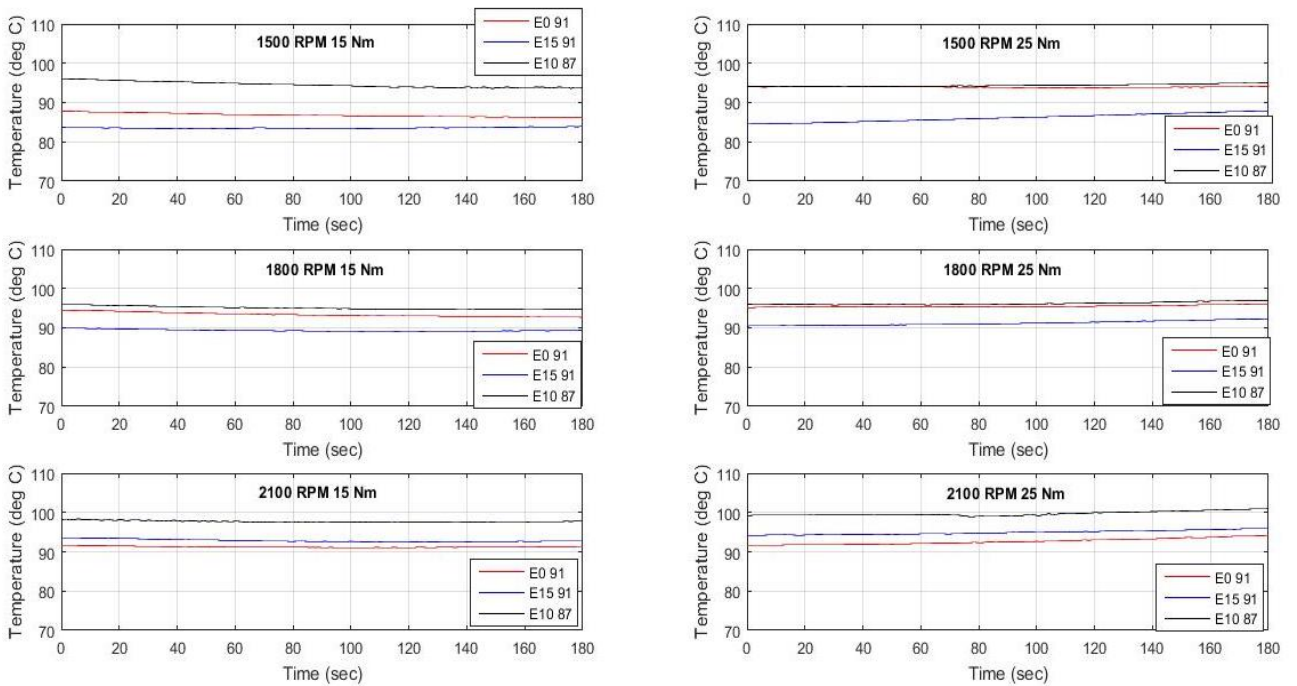
Figure 7.10: Variation of oil temperature with time at 0 deg spark advance for E0 91, E15 91 and E10 87 fuels
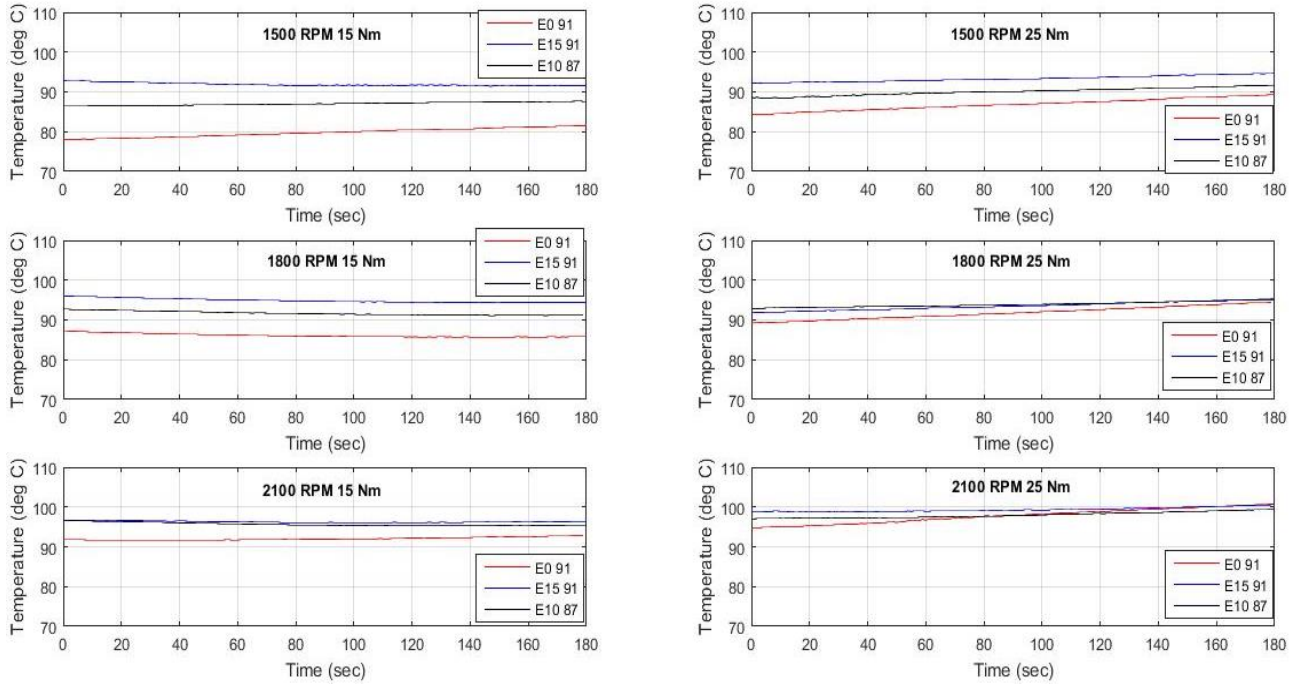
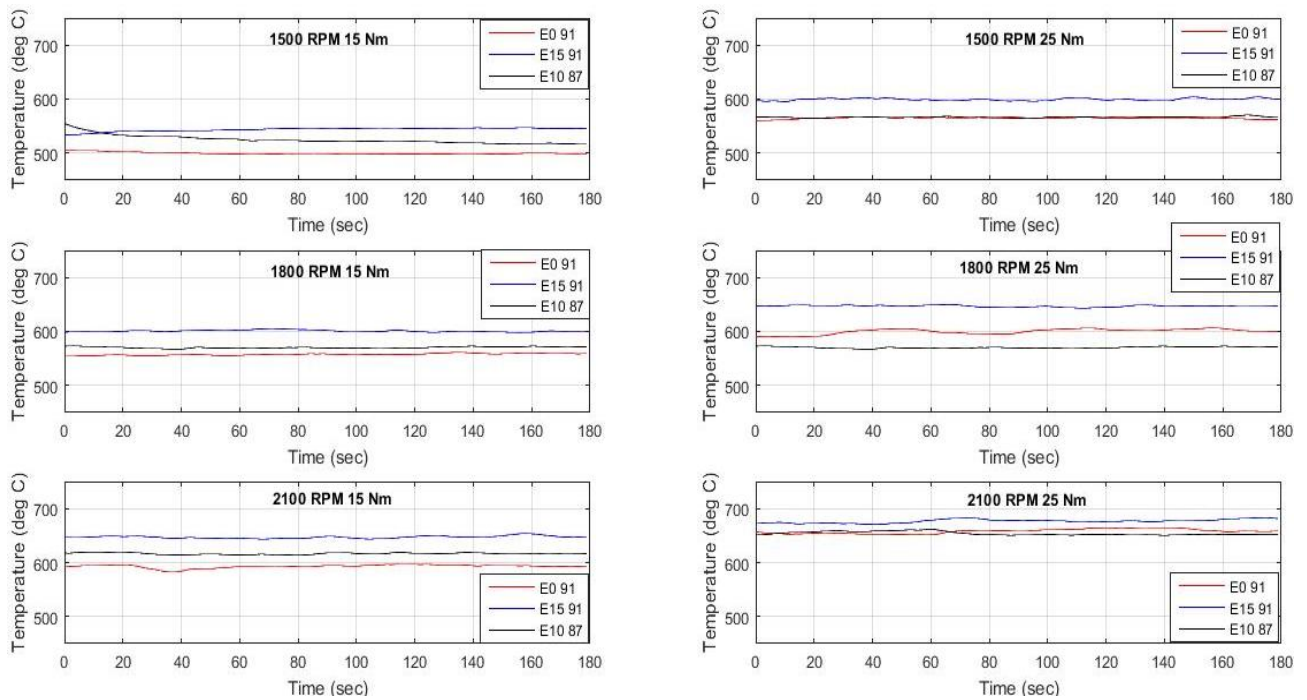Figure 7.11: Variation of oil temperature with time at 10 deg spark advance for E0 91, E15 91 and E10 87 fuels
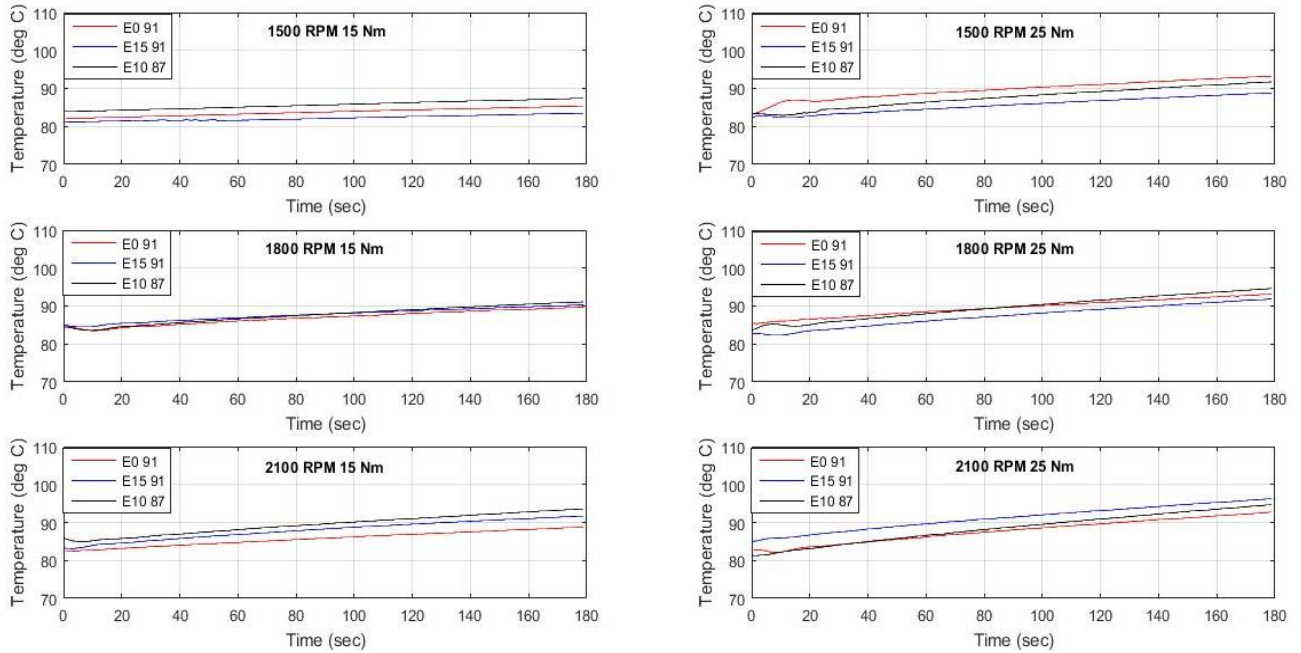

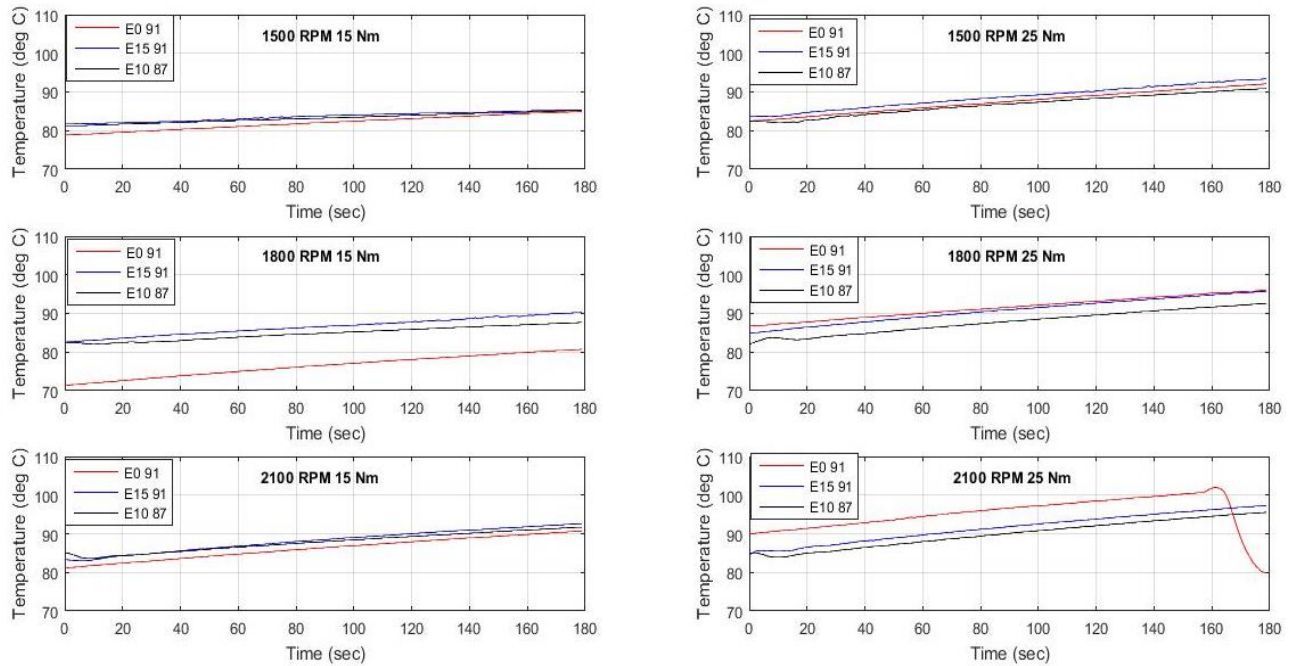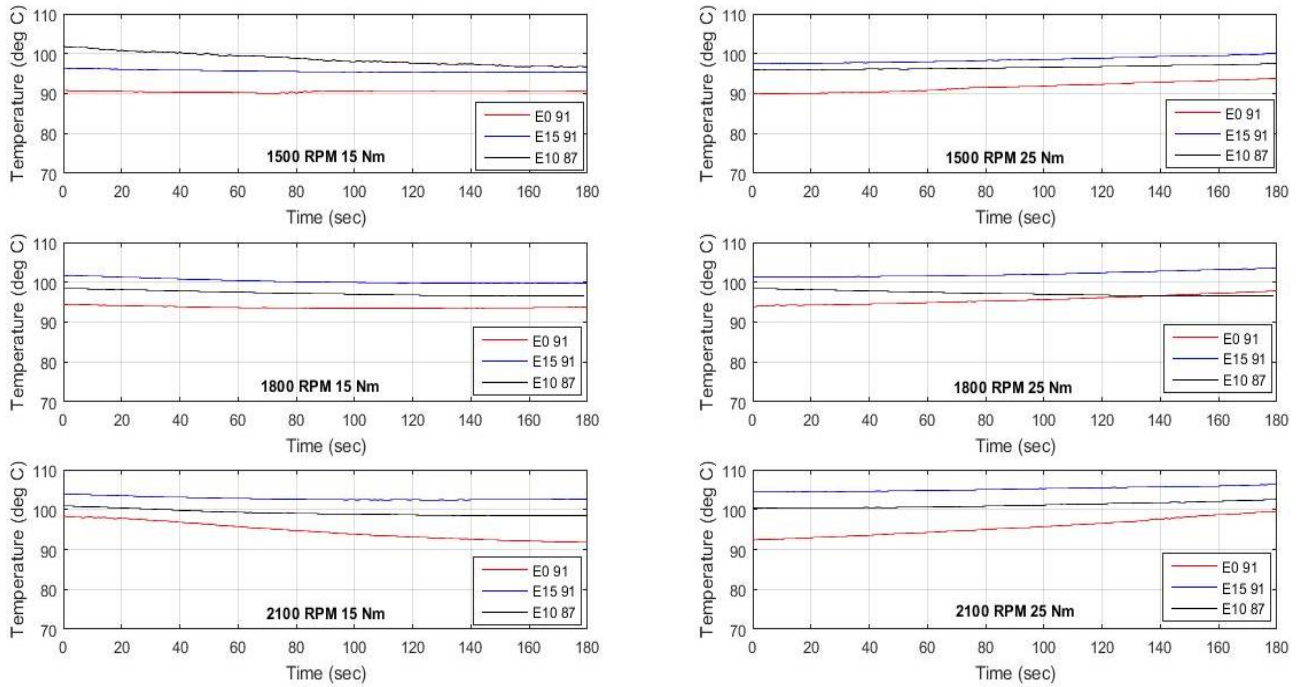Figure 7.12: Variation of oil temperature with time at 20 deg spark advance for E0 91, E15 91 and E10 87 fuels
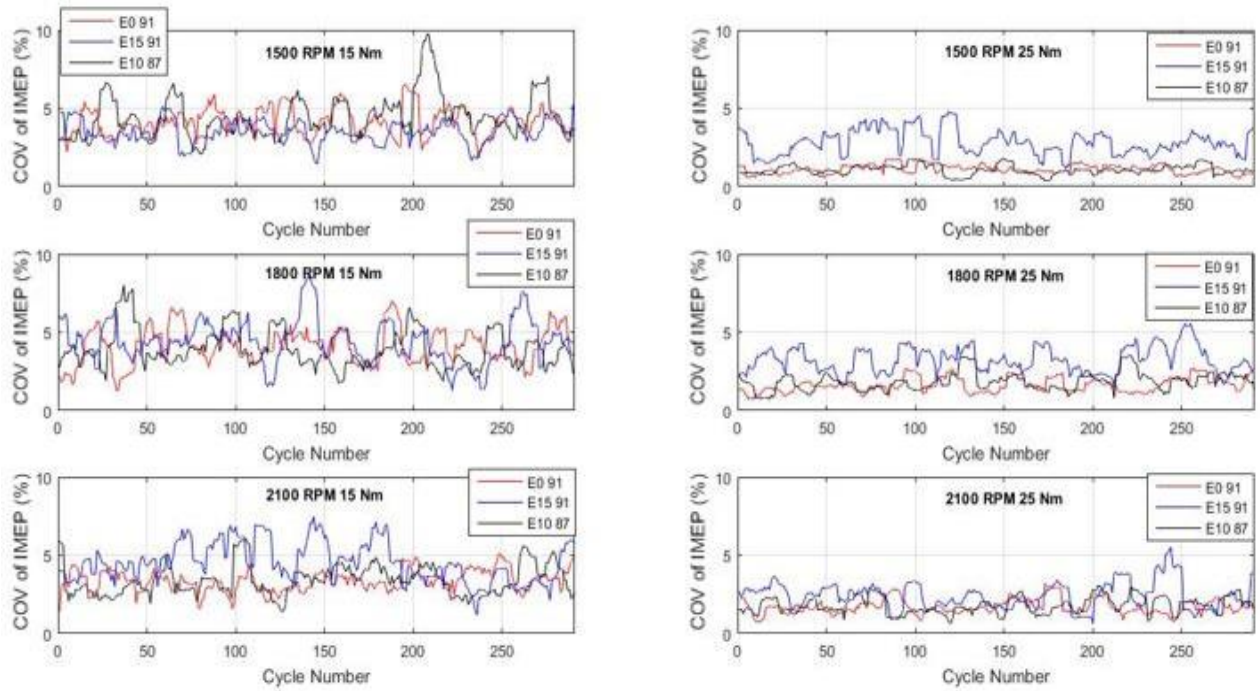
Figure 7.13: Variation of COV of IMEP with recorded number of cycles at 0 deg spark advance for E0 91, E15 91 and E10 87 fuels
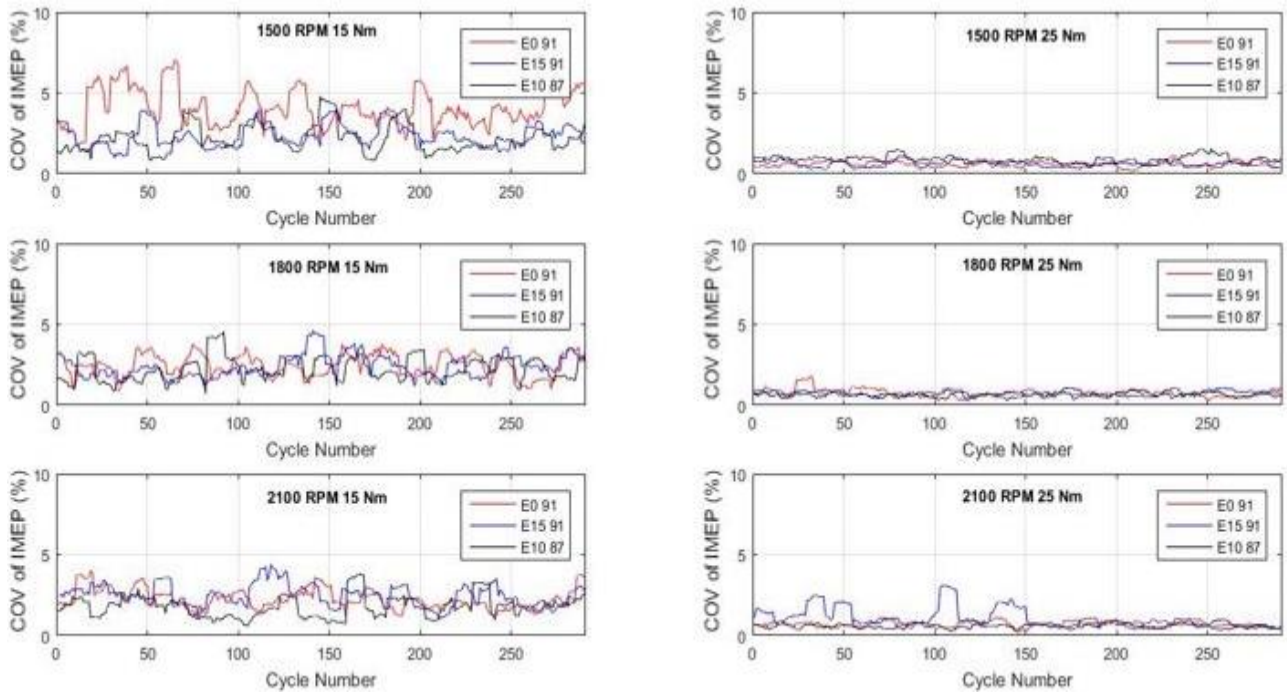
Figure 7.14: Variation of COV of IMEP with recorded number of cycles at 0 deg spark advance for E0 91, E15 91 and E10 87 fuels
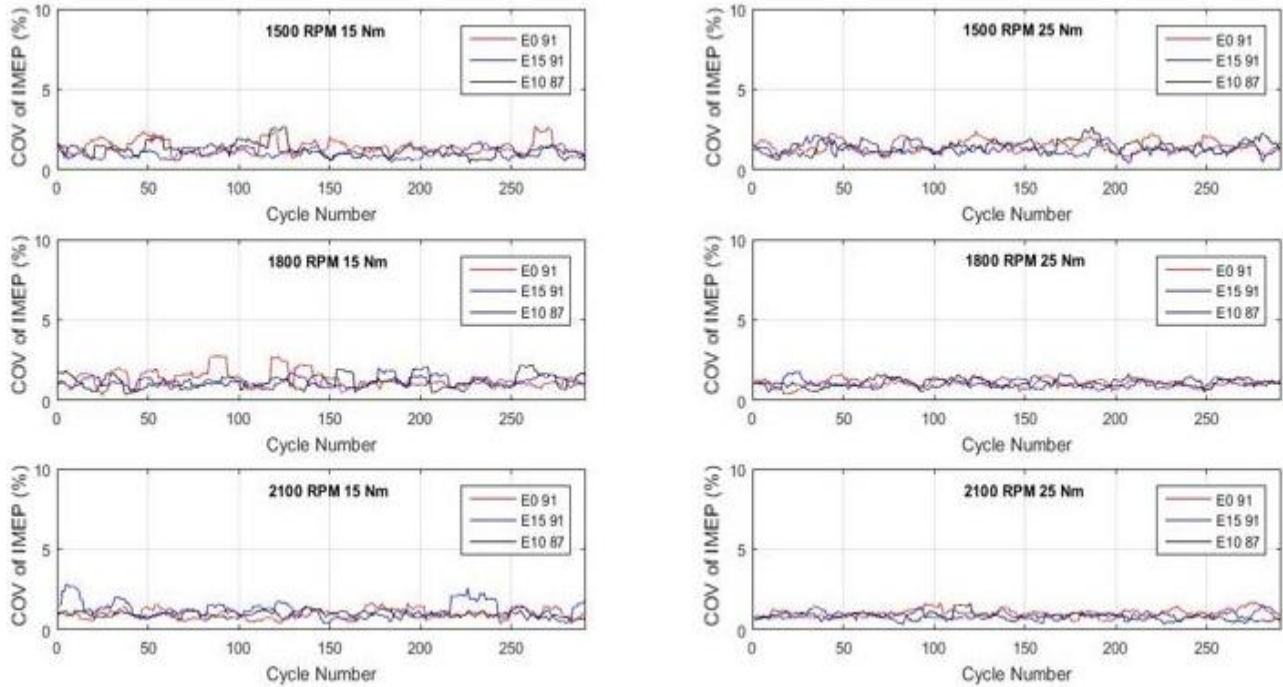
Figure 7.15: Variation of COV of IMEP with recorded number of cycles at 0 deg spark advance for E0 91, E15 91 and E10 87 fuels
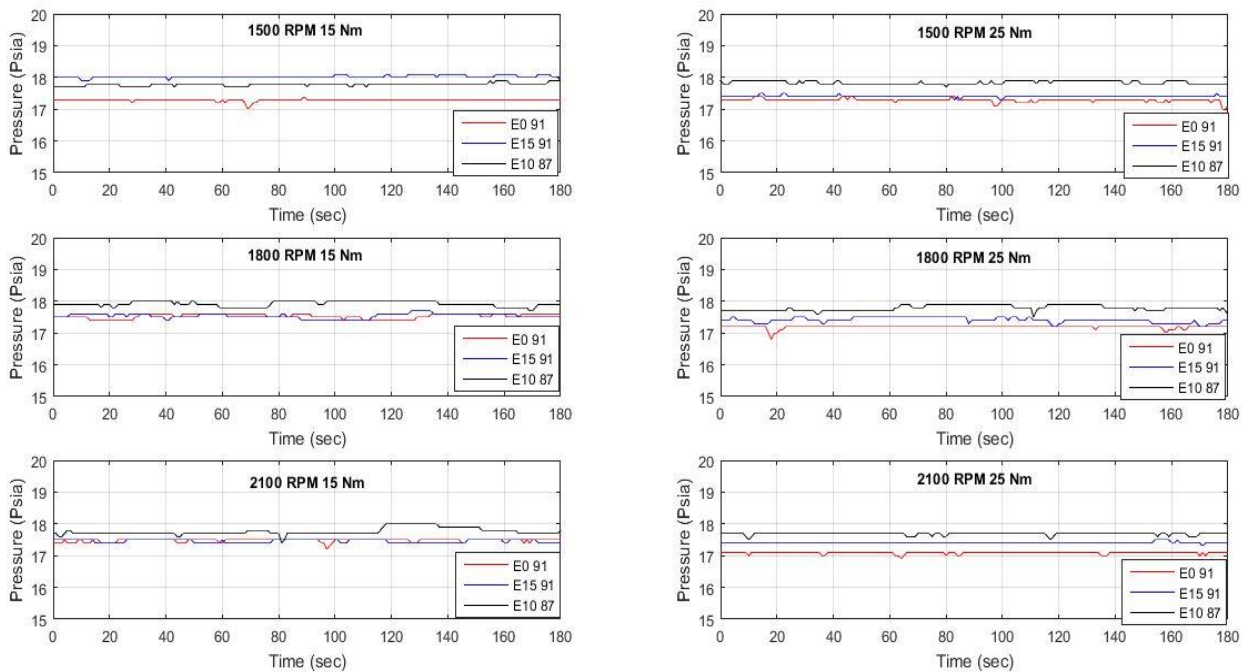
Figure 7.16: Variation of fuel pressure at carburetor inlet with time at 0 deg spark advance for E0 91, E15 91 and E10 87 fuels
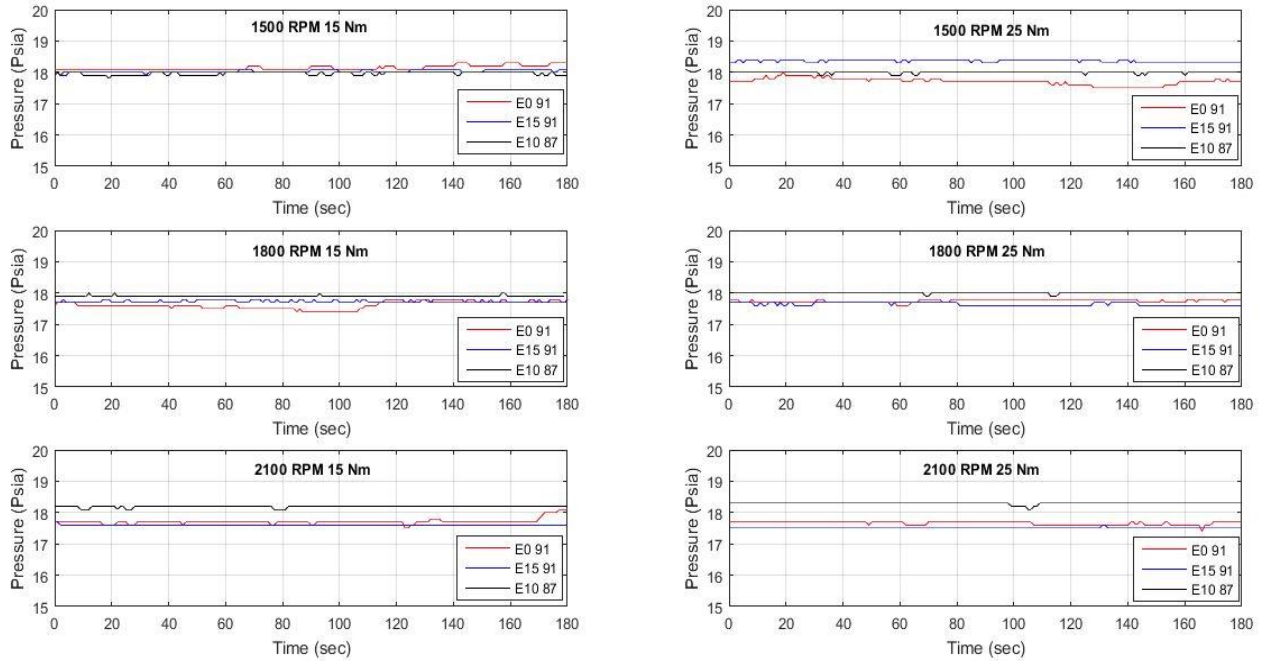
Figure 7.17: Variation of fuel pressure at carburetor inlet with time at 10 deg spark advance for E0 91, E15 91 and E10 87 fuels
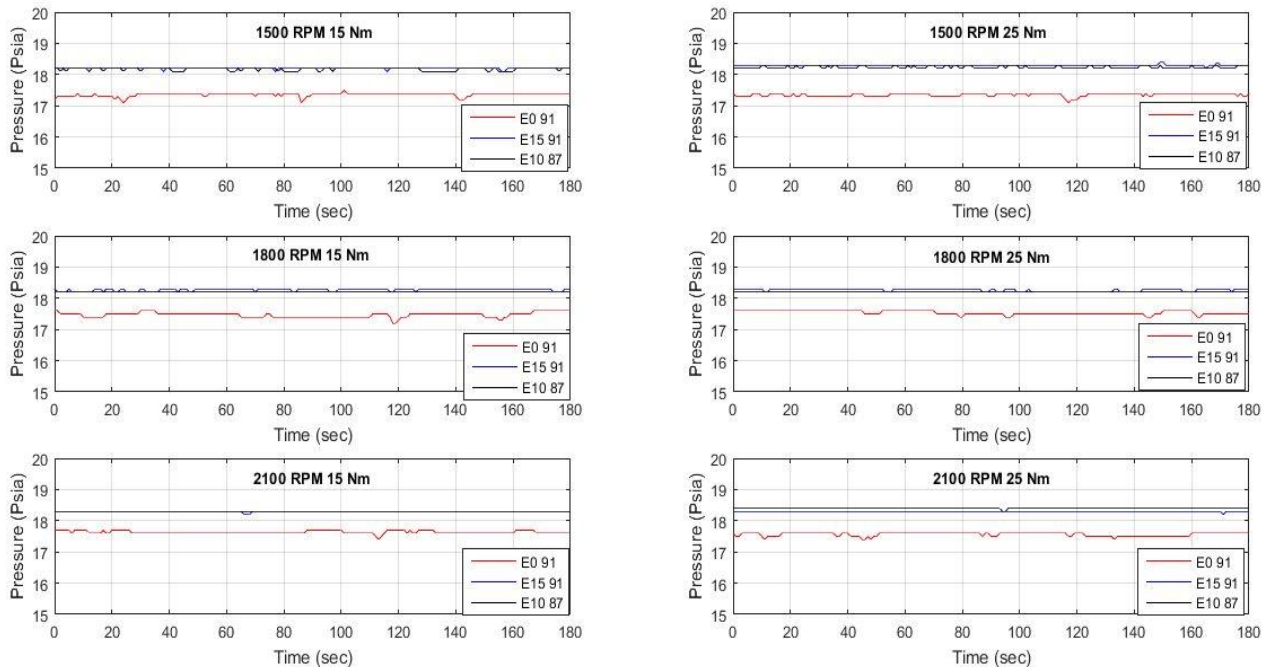
Figure 7.18: Variation of fuel pressure at carburetor inlet with time at 20 deg spark advance for E0 91, E15 91 and E10 87 fuels
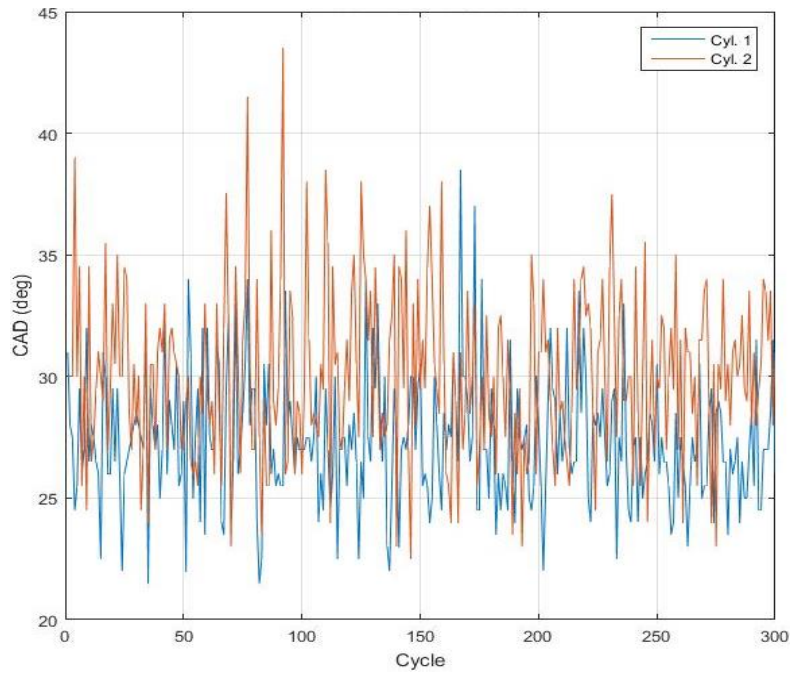
Figure 7.19: Burn duration (10 – 90) for cylinder 1 and 2 at 0 deg spark advance
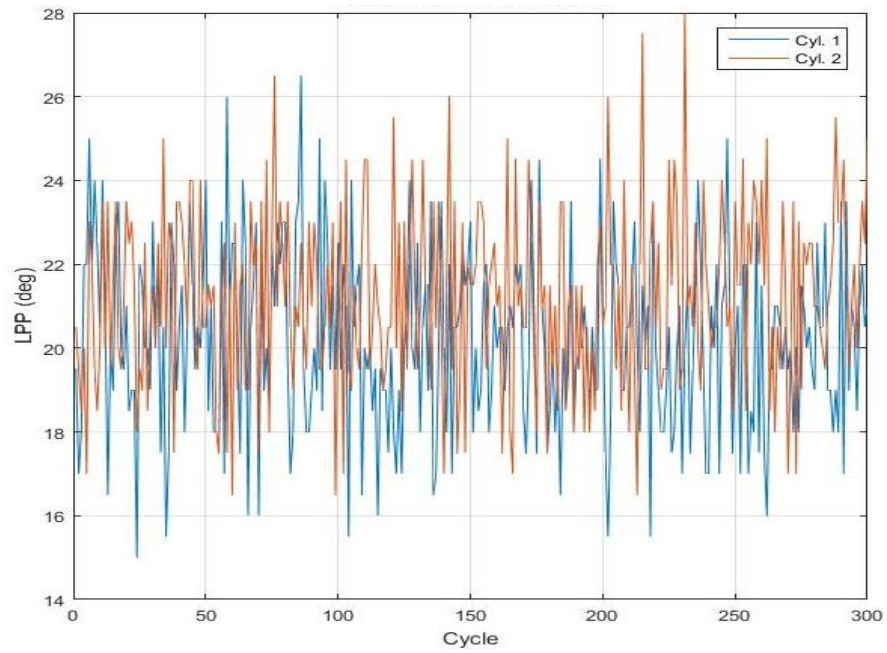
Figure 7.20: Location of peak pressure for cylinder 1 and 2 at 0 deg spark advance

Figure 7.21: Burn duration (10 – 90) for cylinder 1 and cylinder 2 at 20 deg spark advance
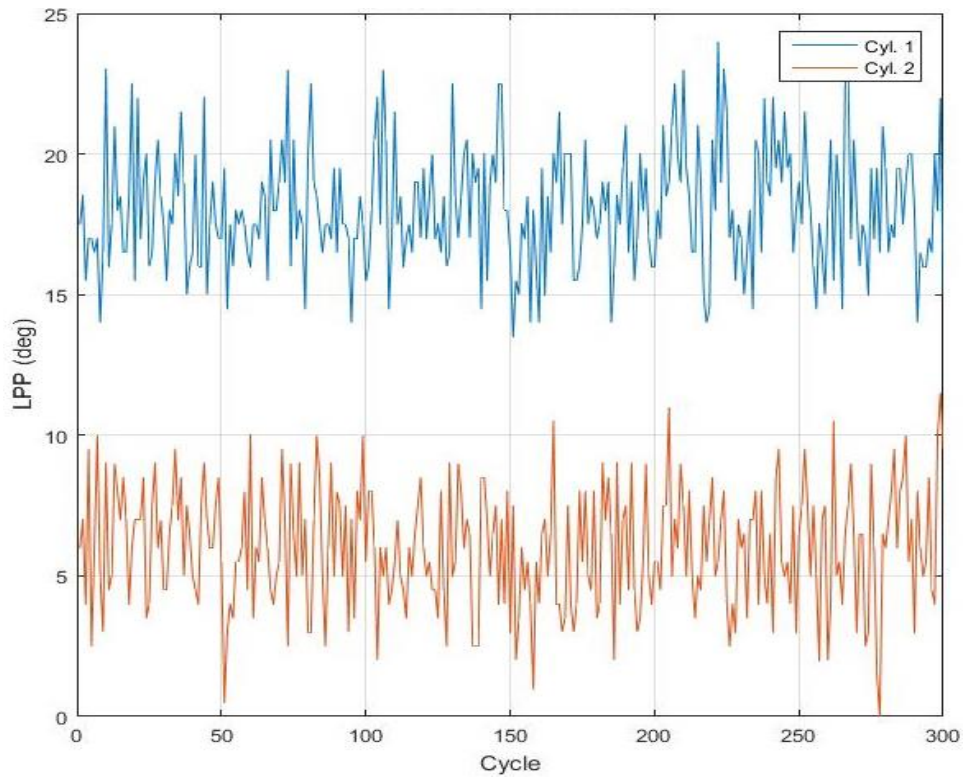
Figure 7.22: Location of peak pressure for cylinder 1 and cylinder 2 at 20 deg spark advance

7.3 Matlab code for data processing

```matlab
clear all;
clc;
%% IMPORT DATA
% BURN DURATIONS
b0010_1=importdata('B001001.p01','-ascii'); % 0-10 Burn Duration - Cyl 1
b0010_2=importdata('B001002.p01','-ascii'); % 0-10 Burn Duration - Cyl 2
b1025_1=importdata('B102501.p01','-ascii'); % 10-25 Burn Duration - Cyl 1
b1025_2=importdata('B102502.p01','-ascii'); % 10-25 Burn Duration - Cyl 2
b1090_1=importdata('B109001.p01','-ascii'); % 10-90 Burn Duration - Cyl 1
b1090_2=importdata('B109002.p01','-ascii'); % 10-90 Burn Duration - Cyl 2
b2550_1=importdata('B255001.p01','-ascii'); % 25-50 Burn Duration - Cyl 1
b2550_2=importdata('B255002.p01','-ascii'); % 25-50 Burn Duration - Cyl 2
b5075_1=importdata('B507501.p01','-ascii'); % 50-75 Burn Duration - Cyl 1
b5075_2=importdata('B507502.p01','-ascii'); % 50-75 Burn Duration - Cyl 2


% CRANK ANGLE
CA10_1=importdata('CA1001.p01','-ascii'); % 10% Mass Burn Angle - Cyl 1
CA10_2=importdata('CA1002.p01','-ascii'); % 10% Mass Burn Angle - Cyl 2
CA25_1=importdata('CA2501.p01','-ascii'); % 25% Mass Burn Angle - Cyl 1
CA25_2=importdata('CA2502.p01','-ascii'); % 25% Mass Burn Angle - Cyl 2
CA50_1=importdata('CA5001.p01','-ascii'); % 50% Mass Burn Angle - Cyl 1
CA50_2=importdata('CA5002.p01','-ascii'); % 50% Mass Burn Angle - Cyl 2
CA75_1=importdata('CA7501.p01','-ascii'); % 75% Mass Burn Angle - Cyl 1
CA75_2=importdata('CA7502.p01','-ascii'); % 75% Mass Burn Angle - Cyl 2
CA90_1=importdata('CA9001.p01','-ascii'); % 90% Mass Burn Angle - Cyl 1
CA90_2=importdata('CA9002.p01','-ascii'); % 90% Mass Burn Angle - Cyl 2


%IMEP
IMEP_1=importdata('IMEP01.p01','-ascii'); % IMEP - Cyl 1
IMEP_2=importdata('IMEP02.p01','-ascii'); % IMEP - Cyl 2
%NIMEP
nIMEP_1=importdata('IMEPN01.p01','-ascii'); % IMEP - Cyl 1
nIMEP_2=importdata('IMEPN02.p01','-ascii'); % IMEP - Cyl 2


%LOCATION OF PEAK PRESSURE
LPP_1=importdata('LP01.p01','-ascii'); % LPP - Cyl 1
LPP_2=importdata('LP02.p01','-ascii'); % LPP - Cyl 2


%IMEP
NMEP_1=importdata('NMEP01.p01','-ascii'); % NMEP - Cyl 1
NMEP_2=importdata('NMEP02.p01','-ascii'); % NMEP - Cyl 2


%PEAK PRESSURE
PP_1=importdata('P01.p01','-ascii'); % Peak Pressure - Cyl 1
PP_2=importdata('P02.p01','-ascii'); % Peak Pressure - Cyl 2


%PMEP
PMEP_1=importdata('PMEP01.p01','-ascii'); % PMEP - Cyl 1
PMEP_2=importdata('PMEP02.p01','-ascii'); % PMEP - Cyl 2


%KNOCK
KNIN_2_kpa=importdata('KNIN02.p01','-ascii'); % KNOCK INTENSITY - Cyl 2
KNIN_2=KNIN_2_kpa/100;  % Bar
```
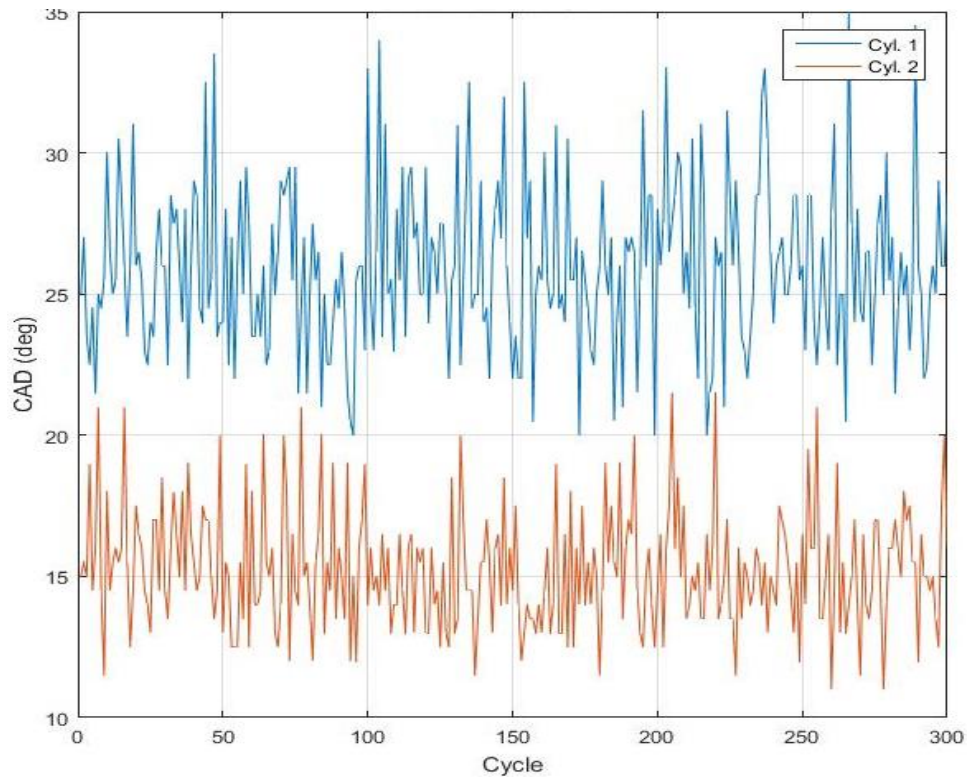
```matlab
KNPK_2_kpa=importdata('KNPK02.p01','-ascii'); % KNOCK PEAK - Cyl 2
KNPK_2=KNPK_2_kpa/100;  % Bar
%PRESSURE DATA
P1=importdata('TQ01.p01','-ascii'); % In-cylinder Pressure - Cyl 1
P2=importdata('TQ02.p01','-ascii'); % In-cylinder Pressure - Cyl 2
encd=importdata('TQRWENCD.p01','-ascii');   % Crank angle from encoder
% COV of IMEP
cov1=importdata('COV01.p01','-ascii'); % COV of IMEP - Cyl 1
cov2=importdata('COV02.p01','-ascii'); % COV of IMEP - Cyl 1
% ACCELEROMETER
acc=importdata('TQACCE.p01','-ascii'); % Accelerometer data

%% CALCULATIONS
n_cycle=floor(length(encd)/1440); % Number of cycles recorded
n_P1=P1(1:n_cycle*1440);      % In-cylinder pressure for all cycles in cyl 1
n_P2=P2(1:n_cycle*1440);      % In-cylinder pressure for all cycles in cyl 2
n_encd=encd(1:n_cycle*1440);   % Encoder signal for all cycles
n_P1_re=reshape(n_P1,1440,n_cycle);   % Table for cyl 1 pressure data divided
by cycles
n_P2_re=reshape(n_P2,1440,n_cycle);   % Table for cyl 2 pressure data divided
by cycles
n_encd_re=reshape(n_encd,1440,n_cycle);   % Table for encoder data divided by
cycles
n_P1_re_avg=mean(n_P1_re,2);        % Average pressure data for cyl 1
n_P2_re_avg=mean(n_P2_re,2);        % Average pressure data for cyl 2
n_encd_re_avg=mean(n_encd_re,2);       % Average encoder data for cyl
n_acc=acc(1:n_cycle*1440);
n_acc_re=reshape(n_acc,1440,n_cycle);
n_acc_re_avg=mean(n_acc_re,2);
avg_CA50= mean(CA50_2);
avg_d1090=mean(b1090_2);
avg_COV=mean(cov2);
avg_imep=mean(IMEP_2)
%% KNOCK INTENSITY
tdc=880; % Position of TDC
rpm=2100;
fs=rpm*360*2/60000;
order=3;
flow=4;
fhigh=8.9;
k_window=tdc+40;% Knock window
t=40/(rpm*6);    % Time to cover knock window
ki_cyl=0;
for i=1:n_cycle;
for j=tdc:tdc+80;
ki_1(j,i)=(n_P1_re(j,i)-n_P1_re(j-1,i));
ki_1_abs(j,i)=abs(ki_1(j,i));
ki_2(j,i)=(n_P2_re(j,i)-n_P2_re(j-1,i));
ki_2_abs(j,i)=abs(ki_2(j,i));
j=j+1;
end;
i=i+1;
end;
for t=1:n_cycle;
    for u=tdc:tdc+50;
        n_P2_re_pk(u,t)=n_P2_re(u,t);
        u=u+1;
```

```matlab
        end
        t=t+1;
    end;
    n_P2_re_pk( ~any(n_P2_re_pk,2), : ) = [];
    [b,a]=butter(order,[flow,fhigh]/(fs/2),'bandpass');
    filtsig_re=filter(b,a,n_P2_re_pk);   %filtered signal
    filtsig=filtsig_re;
    filtsig_re(1:10,:)=[];
    p2p=max(filtsig_re)-min(filtsig_re);
    max=max(p2p);
    min=min(p2p);
    p2p_95_percentile=prctile(p2p,95);
    %% Open PowerPoint as a COM Automation server
    h = actxserver('PowerPoint.Application');
    % Show the PowerPoint window
    h.Visible = 1;
    % View the methods that can be invoked
    h.Presentation.invoke
    % Add a presentation via "Add" method
    Presentation = h.Presentation.Add;
    % View the methods that can be invoked
    Presentation.Slides.invoke
    blankSlide = Presentation.SlideMaster.CustomLayouts.Item(1);
    Slide1 = Presentation.Slides.AddSlide(1,blankSlide);
    Slide2 = Presentation.Slides.AddSlide(1,blankSlide);
    Slide3 = Presentation.Slides.AddSlide(1,blankSlide);
    Slide4 = Presentation.Slides.AddSlide(1,blankSlide);
    Slide5 = Presentation.Slides.AddSlide(1,blankSlide);
    Slide6 = Presentation.Slides.AddSlide(1,blankSlide);
    Slide7 = Presentation.Slides.AddSlide(1,blankSlide);
    Slide8 = Presentation.Slides.AddSlide(1,blankSlide);
    Slide9 = Presentation.Slides.AddSlide(1,blankSlide);
    Slide10 = Presentation.Slides.AddSlide(1,blankSlide);
    Slide11 = Presentation.Slides.AddSlide(1,blankSlide);
    Slide12 = Presentation.Slides.AddSlide(1,blankSlide);
    Slide13 = Presentation.Slides.AddSlide(1,blankSlide);
    Slide14 = Presentation.Slides.AddSlide(1,blankSlide);
    Slide15 = Presentation.Slides.AddSlide(1,blankSlide);
    Slide16 = Presentation.Slides.AddSlide(1,blankSlide);
    Slide17 = Presentation.Slides.AddSlide(1,blankSlide);
    Slide18 = Presentation.Slides.AddSlide(1,blankSlide);
    Slide19 = Presentation.Slides.AddSlide(1,blankSlide);
    Slide20 = Presentation.Slides.AddSlide(1,blankSlide);
    Slide21 = Presentation.Slides.AddSlide(1,blankSlide);

    %% PLOTS
    x=1:1:300;
    %% BURN DURATIONS
    figure(1);
    plot(x,b0010_1);
    hold on;
    plot(x,b0010_2);
    hold off;
    title('Burn Duration (0-10)');
    xlabel('Cycle');
    ylabel('CAD (deg)');
    grid on;
```

```
legend ('Cyl. 1','Cyl. 2');
print('-dpng','-r150','F:\Final Data Kohler
LH690\ACAP\12152016\images\img1.png')

figure(2);
plot(x,b1025_1);
hold on;
plot(x,b1025_2);
hold off;
title('Burn Duration (10-25)');
xlabel('Cycle');
ylabel('CAD (deg)');
grid on;
legend ('Cyl. 1','Cyl. 2');
print('-dpng','-r150','F:\Final Data Kohler
LH690\ACAP\12152016\images\img2.png')

figure(3);
plot(x,b1090_1);
hold on;
plot(x,b1090_2);
hold off;
title('Burn Duration (10-90)');
xlabel('Cycle');
ylabel('CAD (deg)');
grid on;
legend ('Cyl. 1','Cyl. 2');
print('-dpng','-r150','F:\Final Data Kohler
LH690\ACAP\12152016\images\img3.png')

figure(4);
plot(x,b2550_1);
hold on;
plot(x,b2550_2);
hold off;
title('Burn Duration (25-50)');
xlabel('Cycle');
ylabel('CAD (deg)');
grid on;
legend ('Cyl. 1','Cyl. 2');
print('-dpng','-r150','F:\Final Data Kohler
LH690\ACAP\12152016\images\img4.png')

figure(5);
plot(x,b5075_1);
hold on;
plot(x,b5075_2);
hold off;
title('Burn Duration (50-75)');
xlabel('Cycle');
ylabel('CAD (deg)');
grid on;
legend ('Cyl. 1','Cyl. 2');
print('-dpng','-r150','F:\Final Data Kohler
LH690\ACAP\12152016\images\img5.png')
```

```matlab
figure(6);
plot(x,CA10_1);
hold on;
plot(x,CA10_2);
hold off;
title('10% Mass Burn Angle');
xlabel('Cycle');
ylabel('CAD (deg)');
grid on;
legend ('Cyl. 1','Cyl. 2');
print('-dpng','-r150','F:\Final Data Kohler
LH690\ACAP\12152016\images\img6.png')

figure(7);
plot(x,CA25_1);
hold on;
plot(x,CA25_2);
hold off;
title('25% Mass Burn Angle');
xlabel('Cycle');
ylabel('CAD (deg)');
grid on;
legend ('Cyl. 1','Cyl. 2');
print('-dpng','-r150','F:\Final Data Kohler
LH690\ACAP\12152016\images\img7.png')

figure(8);
plot(x,CA50_1);
hold on;
plot(x,CA50_2);
hold off;
title('50% Mass Burn Angle');
xlabel('Cycle');
ylabel('CAD (deg)');
grid on;
legend ('Cyl. 1','Cyl. 2');
print('-dpng','-r150','F:\Final Data Kohler
LH690\ACAP\12152016\images\img8.png')

figure(9);
plot(x,CA75_1);
hold on;
plot(x,CA75_2);
hold off;
title('75% Mass Burn Angle');
xlabel('Cycle');
ylabel('CAD (deg)');
grid on;
legend ('Cyl. 1','Cyl. 2');
print('-dpng','-r150','F:\Final Data Kohler
LH690\ACAP\12152016\images\img9.png')

figure(10);
plot(x,CA90_1);
hold on;
plot(x,CA90_2);
```

```matlab
hold off;
title('90% Mass Burn Angle');
xlabel('Cycle');
ylabel('CAD (deg)');
grid on;
legend ('Cyl. 1','Cyl. 2');
print('-dpng','-r150','F:\Final Data Kohler
LH690\ACAP\12152016\images\img10.png')

figure(11);
plot(x,IMEP_1);
hold on;
plot(x,IMEP_2);
hold off;
title('IMEP');
xlabel('Cycle');
ylabel('IMEP (kPa)');
grid on;
legend ('Cyl. 1','Cyl. 2');
print('-dpng','-r150','F:\Final Data Kohler
LH690\ACAP\12152016\images\img11.png')

figure(12);
plot(x,LPP_1);
hold on;
plot(x,LPP_2);
hold off;
title('Location of Peak Pressure');
xlabel('Cycle');
ylabel('LPP (deg)');
grid on;
legend ('Cyl. 1','Cyl. 2');
print('-dpng','-r150','F:\Final Data Kohler
LH690\ACAP\12152016\images\img12.png')

figure(13);
plot(x,NMEP_1);
hold on;
plot(x,NMEP_2);
hold off;
title('NMEP');
xlabel('Cycle');
ylabel('NMEP (kPa)');
grid on;
legend ('Cyl. 1','Cyl. 2');
print('-dpng','-r150','F:\Final Data Kohler
LH690\ACAP\12152016\images\img13.png')

figure(14);
plot(x,PP_1);
hold on;
plot(x,PP_2);
hold off;
title('Peak Pressure');
xlabel('Cycle');
ylabel('Peak Pressure (kPa)');
```

```matlab
grid on;
legend ('Cyl. 1','Cyl. 2');
print('-dpng','-r150','F:\Final Data Kohler
LH690\ACAP\12152016\images\img14.png')

figure(15);
plot(x,PMEP_1);
hold on;
plot(x,PMEP_2);
hold off;
title('PMEP');
xlabel('Cycle');
ylabel('PMEP (kPa)');
grid on;
legend ('Cyl. 1','Cyl. 2');
print('-dpng','-r150','F:\Final Data Kohler
LH690\ACAP\12152016\images\img15.png')

figure(16);
plot(x,KNIN_2);
title('KNOCK INTENSITY');
xlabel('Cycle');
ylabel('KNOCK INTENSITY (bar)');
grid on;
print('-dpng','-r150','F:\Final Data Kohler
LH690\ACAP\12152016\images\img16.png')

figure(17);
plot(x,KNPK_2);
title('KNOCK PEAK');
xlabel('Cycle');
ylabel('KNOCK PEAK (bar)');
grid on;
print('-dpng','-r150','F:\Final Data Kohler
LH690\ACAP\12152016\images\img17.png')

figure(18)
plot(n_encd_re_avg,n_P1_re_avg,'r');
hold on;
plot(n_encd_re_avg,n_P2_re_avg);
title('PRESSURE VS CRANK ANGLE');
xlabel('CAD (deg)');
ylabel('PRESSURE(kPa)');
axis([0 720 0 3000]);
legend('Cylinder 1','Cylinder 2','location','northwest');
grid on;
print('-dpng','-r150','F:\Final Data Kohler
LH690\ACAP\12152016\images\img18.png')

figure(19)
plot(n_encd_re,n_P1_re);
title('PRESSURE VS CRANK ANGLE (CYL 1)');
xlabel('CAD (deg)');
ylabel('PRESSURE(kPa)');
axis([0 720 0 6000]);
grid on;
```

```matlab
print('-dpng','-r150','F:\Final Data Kohler
LH690\ACAP\12152016\images\img19.png')

figure(20)
plot(n_encd_re,n_P2_re);
title('PRESSURE VS CRANK ANGLE (CYL 2)');
xlabel('CAD (deg)');
ylabel('PRESSURE(kPa)');
axis([0 720 0 6000]);
grid on;
print('-dpng','-r150','F:\Final Data Kohler
LH690\ACAP\12152016\images\img20.png')

figure(21)
plot(ki_cyl_2);
title('CALCULATED KNOCK INTENSITY');
xlabel('CYCLE');
ylabel('INTENSITY(bar)');
axis([0 300 0 200]);
grid on;
print('-dpng','-r150','F:\Final Data Kohler
LH690\ACAP\12152016\images\img21.png')

%% ADD IMAGES TO SLIDES WITH TITLES
% Note: Change the image file full path names to where you save them
Image1 = Slide1.Shapes.AddPicture('F:\Final Data Kohler
LH690\ACAP\12152016\images\img1.png','msoFalse','msoTrue',50,20,900,500);
Image2 = Slide2.Shapes.AddPicture('F:\Final Data Kohler
LH690\ACAP\12152016\images\img2.png','msoFalse','msoTrue',50,20,900,500);
Image3 = Slide3.Shapes.AddPicture('F:\Final Data Kohler
LH690\ACAP\12152016\images\img3.png','msoFalse','msoTrue',50,20,900,500);
Image4 = Slide4.Shapes.AddPicture('F:\Final Data Kohler
LH690\ACAP\12152016\images\img4.png','msoFalse','msoTrue',50,20,900,500);
Image5 = Slide5.Shapes.AddPicture('F:\Final Data Kohler
LH690\ACAP\12152016\images\img5.png','msoFalse','msoTrue',50,20,900,500);
Image6 = Slide6.Shapes.AddPicture('F:\Final Data Kohler
LH690\ACAP\12152016\images\img6.png','msoFalse','msoTrue',50,20,900,500);
Image7 = Slide7.Shapes.AddPicture('F:\Final Data Kohler
LH690\ACAP\12152016\images\img7.png','msoFalse','msoTrue',50,20,900,500);
Image8 = Slide8.Shapes.AddPicture('F:\Final Data Kohler
LH690\ACAP\12152016\images\img8.png','msoFalse','msoTrue',50,20,900,500);
Image9 = Slide9.Shapes.AddPicture('F:\Final Data Kohler
LH690\ACAP\12152016\images\img9.png','msoFalse','msoTrue',50,20,900,500);
Image10 = Slide10.Shapes.AddPicture('F:\Final Data Kohler
LH690\ACAP\12152016\images\img10.png','msoFalse','msoTrue',50,20,900,500);
Image11 = Slide11.Shapes.AddPicture('F:\Final Data Kohler
LH690\ACAP\12152016\images\img11.png','msoFalse','msoTrue',50,20,900,500);
Image12 = Slide12.Shapes.AddPicture('F:\Final Data Kohler
LH690\ACAP\12152016\images\img12.png','msoFalse','msoTrue',50,20,900,500);
Image13 = Slide13.Shapes.AddPicture('F:\Final Data Kohler
LH690\ACAP\12152016\images\img13.png','msoFalse','msoTrue',50,20,900,500);
Image14 = Slide14.Shapes.AddPicture('F:\Final Data Kohler
LH690\ACAP\12152016\images\img14.png','msoFalse','msoTrue',50,20,900,500);
Image15 = Slide15.Shapes.AddPicture('F:\Final Data Kohler
LH690\ACAP\12152016\images\img15.png','msoFalse','msoTrue',50,20,900,500);
```

```
Image16 = Slide16.Shapes.AddPicture('F:\Final Data Kohler
LH690\ACAP\12152016\images\img16.png','msoFalse','msoTrue',50,20,900,500);
Image17 = Slide17.Shapes.AddPicture('F:\Final Data Kohler
LH690\ACAP\12152016\images\img17.png','msoFalse','msoTrue',50,20,900,500);
Image18 = Slide18.Shapes.AddPicture('F:\Final Data Kohler
LH690\ACAP\12152016\images\img18.png','msoFalse','msoTrue',50,20,900,500);
Image19 = Slide19.Shapes.AddPicture('F:\Final Data Kohler
LH690\ACAP\12152016\images\img19.png','msoFalse','msoTrue',50,20,900,500);
Image20= Slide20.Shapes.AddPicture('F:\Final Data Kohler
LH690\ACAP\12152016\images\img20.png','msoFalse','msoTrue',50,20,900,500);
Image21= Slide21.Shapes.AddPicture('F:\Final Data Kohler
LH690\ACAP\12152016\images\img21.png','msoFalse','msoTrue',50,20,900,500);
```

7.4 EES code for adiabatic flame temperature calculation

```
T=2190
P=1
h1=enthalpy(CarbonDioxide,T=T,P=P)
h2=enthalpy(Steam,T=T,P=P)
h3=enthalpy(Nitrogen,T=T,P=P)
h4=enthalpy(CarbonMonoxide,T=T,P=P)


(5.106*h1)+(8.1*h2)+(37.89*h3)+(1.994*h4)=a
```